THESIS ON NATURAL AND EXACT SCIENCES B128

Operational Forecasting in Estonian Marine Waters

PRIIDIK LAGEMAA

TUT PRESS

TALLINN UNIVERSITY OF TECHNOLOGY
Marine Systems Institute

Dissertation was accepted for the commencement of the degree of Doctor of Philosophy in Earth Sciences on February 9, 2012

Supervisor: Prof. Jüri Elken, Marine Systems Institute at Tallinn University of Technology

Opponents: PhD Frank Janssen

PhD Aarne Männik

Defence of the thesis: April 25, 2012 at the Marine Systems Institute at Tallinn University of Technology, Akadeemia tee 15a, Tallinn, Estonia

Declaration:
Hereby I declare that this doctoral thesis, my original investigation and achievement, submitted for the doctoral degree at Tallinn University of Technology has not been submitted for any academic degree.

Priidik Lagemaa

ISSN 1406-4723
ISBN 978-9949-23-261-1(publication)
ISBN 978-9949-23-262-8 (PDF)

LOODUS- JA TÄPPISTEADUSED B128

Operatiivne prognoos Eesti merealadel

PRIIDIK LAGEMAA

TTÜ
KIRJASTUS

CONTENTS

LIST OF PUBLICATIONS

This thesis is based on the following papers, which will be referred to in the text by their Roman numerals.

I. Lagemaa, P., Elken, J. and Kõuts, T. 2011. Operational sea level forecasting in Estonia. *Estonian Journal of Engineering*, 17(4), 301–331.

II. Lagemaa, P., Suhhova, I., Nõmm, M., Pavelson, J. and Elken, J. 2010. Comparison of current simulations by the state-of-the-art operational models in the Gulf of Finland with ADCP measurements. In *IEEE/OES Baltic 2010 International Symposium: IEEE/OES Baltic 2010 International Symposium, 25–27 August 2010, Riga.* IEEE Conference Proceedings, 1–11.

III. Elken, J., Nõmm, M. and Lagemaa, P. 2011. Circulation patterns in the Gulf of Finland derived from the EOF analysis of model results. *Boreal Environment Research*, 16 (suppl. A), 84–102.

AUTHOR'S CONTRIBUTION

The author has the main role in setting up and configuration of the first state-of-art 3D operational marine forecasting system in Estonia, based mostly on the HIROMB model results and observations. The local model HIROMB-EST setup has been implemented on the parallel computer clusters with a sufficient number of pre- and post-processing tools developed by the author. This contribution was an indispensable part of the papers presented in this thesis. The author has actively carried out his own research and has contributed to the calibration and validation studies by his colleagues regarding the HIROMB model. He has also acted a consultant in the field of HIROMB specifics in Estonia. His contribution to writing papers I, II and III besides setting up the models is as follows:

paper I. The author was responsible for data extraction, processing and visualization as well as for writing the first draft and editing the paper. Jüri Elken supervised the work and helped in writing. Tarmo Kõuts wrote the description of the observation system network and assisted in supervising the paper.

paper II. The author was responsible for data extraction, processing and visualization as well as for writing the first draft and editing the paper. The paper was presented by the author at an international symposium. Jüri Elken supervised the work, performed an empirical orthogonal function (EOF) analysis and helped in writing. Juss Pavelson described the observations and assisted in supervising the paper. Irina Suhhova helped to visualize and analyse the current and wind rose figures.

paper III. The author made model data available and participated in the analysis of model results (mean circulation and horizontal EOF modes). He also assisted in the interpretation of the results and in writing the model description. Marden Nõmm participated in the analysis of EOF modes on vertical cross-gulf sections. Jüri Elken supervised the work and wrote the main parts of the paper.

ABBREVIATIONS

BOOS	Baltic Operational Oceanographic System
BSH	Bundesamt für Seeschifffahrt und Hydrographie (Federal Maritime and Hydrographic Agency of Germany)
BSHcmod	Circulation model developed at BSH
DMI	Danish Meteorological Institute
EMHI	Estonian Meteorological and Hydrological Institute
EOF	Empirical Orthogonal Function
EU	European Union
GMES	Global Monitoring for Environment and Security
HBM	HIROMB-BOOS Model
HBV	Hydrologiska Byråns Vattenbalansavdelning (hydrology model)
HELCOM	Helsinki Commission
HIRLAM	High-Resolution Limited Area Model
HIROMB	High-Resolution Operational Model for the Baltic Sea
MARNET	Marine Environmental Network of BSH
MSI	Marine Systems Institute at Tallinn University of Technology
NM	nautical mile
NOAMOD	North Atlantic model
OAAS	Oleg Andrejev & Alexander Sokolov model
PAL	Paldiski station
PAR	Pärnu station
RMSD	Root mean square deviation (equivalent to RMSE)
RMSE	Root mean square error (equivalent to RMSD)
SMHI	Swedish Meteorological and Hydrological Institute
TAL	Tallinn station

1. INTRODUCTION

1.1. Background

Operational oceanography for short-term marine environment forecasts in marginal seas and coastal areas is a continuous issue of oceanographic research and technological developments. Compared to the earlier semi-empirical forecast methods, a new revolutionary approach, numerical modelling based on two-dimensional (2D) shallow-water equations, was proposed for sea level modelling and forecasts in the 1950s (Hansen 1956, Uusitalo 1960). However, the first practical realizations of numerical modelling in everyday forecast services started only in the 1980s (Peeck *et al.* 1982). Following the experience of operational numerical forecasting based on 2D shallow-water equations, the Federal Maritime and Hydrographic Agency of Germany (BSH) implemented a three-dimensional (3D) baroclinic forecast model BSHcmod at the beginning of the 1990s (Kleine 1994). That model became the core of the family of operational models, run in addition to BSH also at the Swedish Meteorological and Hydrological Institute (SMHI) and Danish Meteorological Institute (DMI). An overview of different model versions and setup features has been given by Gästgifvars *et al.* (2008). The model developments are coordinated by the HIROMB (short for High-Resolution Operational Model for the Baltic Sea) consortium. A broader Baltic-wide cooperation frame in operational oceanography is provided by the Baltic Operational Oceanographic System (BOOS) (Buch *et al.* 2006) which takes care, among many other activities, of online exchange of observational and modelled data and dissemination of oceanographic operational products. Further development of the Baltic marine forecasting is presently going on within the MyOcean project (Development and pre-operational validation of upgraded GMES Marine Core Services and capabilities) funded by the European Union (EU). It schedules merging the best features of different model versions into one state-of-art harmonized operational model system HIROMB-BOOS Model (HBM), including assimilation of the real-time observational data and launching the forecast component for biochemical state variables.

The importance of operational forecasting was underestimated in official service level in Estonia until the highest known storm surge occurred in January 2005 at the western coast of Estonia (Elken *et al.* 2006, Suursaar *et al.* 2006). The operational sea level gauge at Pärnu recorded the highest sea level of +275 cm, observed since the beginning of instrumental observations in 1923. The coastal towns of Pärnu and Haapsalu were heavily flooded, which caused considerable damages and economic loss. The Estonian Ministry of Environment initiated an implementation of numerical ocean forecasting and related observational services in Estonia in cooperation with the Marine Systems Institute (MSI) at Tallinn University of Technology and the Estonian

Meteorological and Hydrological Institute (EMHI). The primary goal was considerable reduction of errors in short-term forecasting of extreme sea levels (both the high sea levels causing floods in the coastal areas and low sea levels stopping the ship traffic between the Estonian mainland and the western larger islands). Numerical sea forecasts are also needed for resolving many other practical problems like harmful algal blooms, drift of surface and subsurface substances and objects, or ice conditions. The north-eastern Baltic, including the Gulfs of Finland and Riga, is a region with an increasing use of marine resources; therefore, more detailed oceanographic predictions throughout the water column are needed. Climate change and eutrophication studies focus on the seasonal and long-term changes in stratification and large-scale transport patterns (Eilola *et al.* 2010, Myrberg *et al.* 2010). Growing human activities like building submarine gas pipelines and power cables, offshore windfarms, etc. (Otremba and Andrulewicz 2008, Koivurova and Pölvnen 2010) require now- and forecasts of layered subsurface currents in a spatial range from a few to tens of kilometres in a time span from hours to months and years. Operational oceanographic models, combined with observational data, are straightforward tools to provide such information.

Taking into account all the reasons discussed above it was decided to implement an advanced 3D forecast system in Estonia. Among the Baltic-wide oceanographic service providers, the SMHI was chosen as a core provider for Estonia, since their operational model HIROMB has the highest horizontal grid resolution (1 nautical mile (NM)). Recent validation study of six 3D models against more than 300 vertical profiles of temperature and salinity measured in the Gulf of Finland (Myrberg *et al.* 2010) concluded that HIROMB was the best model, although no model was the best/worst in all cases. Another study (Elken *et al.* 2008) has shown that, on average, during the warm season HIROMB produces too high surface salinity gradients and too low vertical stratification compared to the observational data. Sea level validation (Elken *et al.* 2008, Gästgifvars *et al.* 2008) revealed that root mean square errors of 1–24 h sea level forecasts at different coastal stations of the Gulf of Finland are 5–10 cm. Unfortunately, model comparisons with current observations are quite rare. Gästgifvars *et al.* (2006) concluded that during the rapidly changing weather conditions drift trajectories, calculated using the HIROMB-based system Seatrack Web, followed well the observed drifter trajectories in the central part of the Gulf of Finland. The Estonian coastline is very fragmented, with numerous small bays, peninsulas and islands, therefore, high horizontal resolution is very important for producing detailed information on sea level, currents, temperature, salinity and ice conditions. The numerical sea level forecasts in Estonia started in autumn 2005 and the forecast system is presently in a quite mature state. Nevertheless, gradual developments towards the next-generation forecast system are progressing on the national, Baltic-wide and European levels.

The Baltic Sea is a multi-basin estuarine sea with a wide range of oceanographic variability. The mean surface circulation in the sub-basins is cyclonic (Palmen 1930). On shorter time scales (less than a few months) currents and stratification are modified by the fluctuating forcing, due to the weather patterns and variable water exchange on the outer boundary of the basin (Matthäus and Schinke 1999). The fluctuating circulation components may include propagation of long gravity waves of tidal and/or storm surge origin (Jönsson *et al.* 2008), Ekman transport of the upper layer and compensating deeper flows (Krauss and Brügge 1991), their evolution into upwelling/downwelling patterns (Lehmann and Myrberg 2008) and/or quasi-steady wind circulation patterns characteristic of lakes and channels without lateral density gradients. Adjustment to the changed forcing is governed by generation and decay of inertial waves (Nerheim 2004) and barotropic/baroclinic Kelvin waves (Lass and Talpsepp 1993). There is also a mesoscale component not always directly related to the forcing fields, comprised mainly of frontal excursions and mesoscale eddies (Reissmann *et al.* 2009).

The oceanographic predictability of the Gulf of Finland is complicated due to significant bottom roughness (compared to other Baltic regions as shown by the recent Nord Stream study (The Nord Stream Project 2009)) combined with strong vertical and horizontal density gradients. The baroclinic Rossby radius is only 2–4 km (Alenius *et al.* 2003). It means that, besides high-frequency motions (with periods up to the seiche period of 27 h), low-frequency mesoscale motions play an important role. While upwelling/downwelling and associated coastal jets are directly related to the wind forcing (Laanemets *et al.* 2009), numerous open sea fronts (Pavelson *et al.* 1996) and mesoscale eddies are generated by the internal non-linear ocean dynamics. Unfortunately, no observational subsurface data are available to perform full mesoscale data assimilation and/or initialization of models; therefore, location and phases of the fronts and eddies may quite often be modelled with significant shifts. It means that assimilation of current observations at single points does not necessarily improve the predictions in a distance larger than the mesoscale correlation scale, usually a few times the Rossby radius.

The Gulf of Riga is a sub-basin of the Baltic Sea, bordering the western coast of the Estonian mainland and the southern coast of Saaremaa Island. Due to the morphometry of the basin and dominating cyclone tracks, the coastline of western Estonia is under continuous flooding hazard (Suursaar *et al.* 2006), which is especially high for the town of Pärnu city located at Pärnu Bay. The Estonian mainland and larger islands are connected with ferry traffic across the straits of the Väinameri which lies north of the Gulf of Riga. Due to the small depths of the Väinameri, low sea level is often critical to the ferry traffic. Therefore, high flooding risk combined with the risks to the ferry traffic in case of low sea level events makes a reliable sea level forecasting for this sea area rather important.

1.2. Main objectives of the thesis

This thesis is aimed to study the operational oceanography and its applications in Estonia. The current status is described in detail and further developments are discussed in the light of state-of-art operational oceanography trends in Europe. At the beginning of the work the description of the operation model HIROMB is given with the comprehensive overview of model setups that are in operational use in Estonia.

The main objectives of this thesis are:

- to estimate and analyse the accuracy of the sea level forecasting system in Estonia (paper I),
- to analyse the stability and reliability of the sea level forecasting system (paper I),
- to discuss the future developments of the sea level forecasting system,
- to validate the subsurface currents in two model setups in different conditions against observations (paper II),
- to describe the circulation scheme and basic variability patterns of the Gulf of Finland simulated with the HIROMB model (paper III).

The main part of the thesis is concentrated on the sea level forecasting system which is the most popular application of operational oceanography today. It is followed by the validation study of simulated subsurface currents and the discussion on the circulation scheme of the Gulf of Finland based on the HIROMB model results.

2. OPERATIONAL MODELS

The operational oceanographic forecast models, belonging to the HIROMB consortium, have been running for the Baltic Sea since the 1990s with the primary purpose of giving short-term (up to 60 h) predictions of the sea conditions, in order to handle oil spills, storm surges, support navigation, etc. The core of the model system is a 3D baroclinic eddy-resolving circulation model, based on the original BSHcmod (Kleine 1994) that calculates currents, temperature and salinity in the water column, and sea level. The model contains also a sea ice module. A model code called HIROMB developed by the SMHI is in operational use in Estonia and therefore used within this investigation. Two different setups of the HIROMB model are considered: HIROMB-SMHI, a setup with the 1 nautical mile horizontal resolution grid and HIROMB-EST, a setup with the 0.5 nautical mile horizontal grid step.

Several model code upgrades, starting from version 3.0 to 4.2 have been done during the period from November 2005 to November 2011. The main parameters of the operational versions of the models are presented in Table 1 in paper I. The sea surface wind stress is calculated by the common quadratic

formulation from the corresponding 10-m height wind speed components W_λ and W_φ as $\tau_\lambda = \rho_a c_D W_\lambda \sqrt{W_\lambda^2 + W_\varphi^2}$, $\tau_\varphi = \rho_a c_D W_\varphi \sqrt{W_\lambda^2 + W_\varphi^2}$, where λ and φ are longitude and latitude, respectively, τ_λ and τ_φ are the wind stress components, ρ_a is the air density and c_D is the surface drag coefficient. The model has mixing modules based on the *κ-ω* approach (Umlauf *et al.* 2003) for vertical mixing and Smagorinski formulation for horizontal mixing. It has also an extensive ice mechanics and thermodynamics module. The system performs data assimilation, based on different data: remote sensing data of sea surface temperature and sea ice, in-situ observations at MARNET buoys and from ships, including vertical profiles from HELCOM stations and daily Ferrybox surface transect (Tallinn-Helsinki, Lips *et al.* 2008) data for salinity and temperature.

In the model version 3.0 (released on 15 November 2005) the linear formulation was applied to find the surface drag coefficient c_D as $c_D = (0.7 + 0.09 W_{10}) \times 10^{-3}$ where $W_{10} = \sqrt{W_\lambda^2 + W_\varphi^2}$ is the wind speed in m/s. The bottom friction coefficient *r* was defined as constant. In the course of model development, improved descriptions were introduced for vertical turbulence and drag coefficients on the surface and on the bottom (Axell 2006, Gästgifvars *et al.* 2008, HIROMB Scientific Plan 2010).

Starting from the operational model version 3.3 (released at 18.09.2007) the breaking surface waves, the water-ice roughness parameter and the variable surface drag coefficient were introduced. The surface drag formulation was changed to take the atmospheric stability into account. Actually, the improved surface drag formulation was introduced already in model version 3.1, but this version never got operational and the new formulation was delivered to the users with version 3.3. To improve the surface current velocities, the neutral surface drag was defined as $c_D = 1.3 \times 10^{-3}$ at $W_{10} < 8$ m/s and $c_D = (0.84 + 0.058 W_{10}) \times 10^{-3}$ in case of higher values of W_{10}. The drag coefficient was then slightly modified, according to the stability of the atmosphere, as calculated by the air-water temperature difference. The bottom friction coefficient, grid resolution and forcing (i.e. atmospheric, open sea boundary, rivers) parameters remained unchanged.

The model code version 4.0 was released on December 2009. The formulation of the surface drag coefficient was not changed, but the local bottom drag coefficient formulation was introduced to calculate the momentum transfer from water to bottom, now enabling the calculation of the local drag coefficient $c_{D,bottom}$ from the local thickness of the bottom cell h_b and the bottom roughness parameter $z_{0,b}$. Also the corrected air-ice stress and the improved ice-ocean stress were introduced and the Successive Corrections data assimilation scheme for temperature and salinity was replaced by the Optimal Interpolation method.

2.1. HIROMB-SMHI setup

The SMHI version of the HIROMB model is called HIROMB-SMHI. It has been running since 1995, first in a pre-operational mode, and since 1999 as fully operational (Funquist 2001). During the development some changes have been made in the operational setup, which are described in the following.

At the beginning of the operational runs the model was run in three nested grids: NS12, NB03 and BS01, with the 12 NM, 3 NM and 1 NM horizontal resolutions, respectively. The model domain of the highest resolution covers the entire Baltic Sea area with grid steps of 1′ by latitude and 5/3′ by longitude (Fig. 1a). The model presented the Baltic Sea by 16 vertical layers, with 4 m thickness in the upper 12 m and increasing values towards greater depths. The model was forced mainly by the atmospheric circulation model SMHI-HIRLAM with horizontal resolution of 22 km with a 1 h time step. For freshwater inflow, daily data from the river runoff model HBV were used. At the outer open ocean boundaries a storm surge model (NOAMOD) is used for the water levels together with tides, climatologic salinity and temperature data. The value of the constant bottom friction coefficient r was 0.0028. The model was run two times per day with restart hours 00 h and 12 h. Starting from 9 July 2008 the model run frequency was increased from two to four times per day, i.e. the model was re-run every 6th hour but all the model parameters remained unchanged.

With the new model code version 4.0 release the vertical resolution of the HIROMB-SMHI setup improved significantly, and the coastline was also improved in some regions (e.g. the Poland shoreline). This changed setup is in operational use also today. Now the model presents the Baltic Sea by 50 vertical layers, with a thickness of 4 m in the upper 80 m, and slowly increasing thicknesses towards greater depths. The earlier 12 NM grid is not used anymore and the 3 NM grid boundaries have been extended to 65°53′30″N, 4°9′10″W, resulting nearly in the same coverage as the earlier 12 NM grid. The coverage of the 1 NM grid remained unchanged. Although the possibility of a variable bottom friction coefficient was introduced into the model code, the coefficient was kept constant in the operational runs.

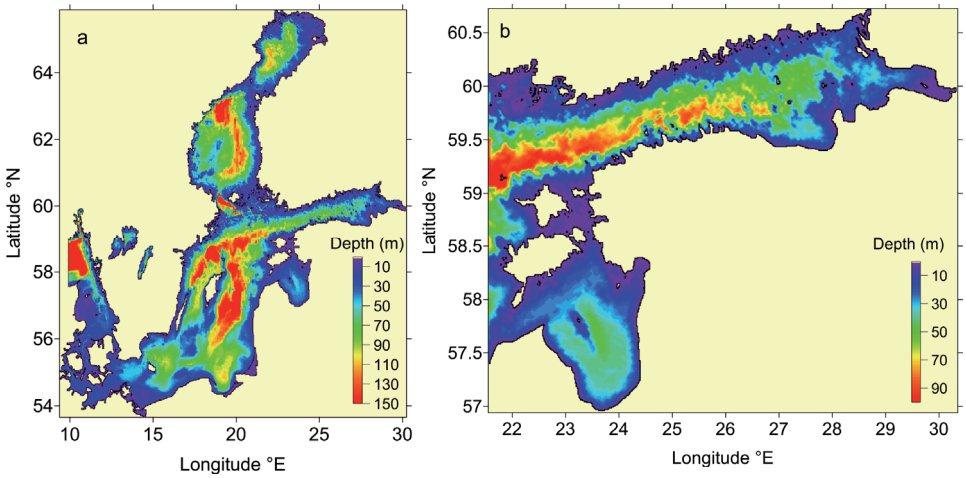

Figure 1. Maps of the HIROMB-SMHI BS01 model grid depths (m) for the entire Baltic Sea (a) and the HIROMB-EST grid for the Estonian sea areas (b).

Starting from 15 September 2010 the official version of HIROMB is 4.2. In this version no new parameterizations affecting the sea level were made. Changes in HIROMB have been continued. From 20 May 2011 the 11 km horizontal resolution HIRLAM forcing was taken into use, forecast length was increased from 48 to 60 h and the amount of data used in data assimilation was increased.

2.2. HIROMB-EST setup

The model setup called HIROMB-EST is operated by the MSI and it has been in operational use since the May 2009. The setup has no nested grids and the horizontal resolution is 0.5 NM. It has 529×455 horizontal grid points and covers mostly Estonian coastal waters, including the entire Gulf of Finland and the Gulf of Riga (Fig. 1b). The setup was initialized from the HIROMB-SMHI 1 NM model and since then the model has been running independently, using only the open sea boundary, river inflow and atmospheric forcing data. The vertical resolution of the model is 3 m from the surface down to 90 m, and 5 m between 90 and 135 m. Atmospheric forcing is taken from the HIRLAM model with an 11 km horizontal resolution which is run at the EMHI. Open sea boundary conditions along the western boundary (21.55°E) of the region are taken from the 1 NM HIROMB-SMHI model results. For freshwater inflow, climatic mean river runoff is used and no data are assimilated into the model. The forecast is initiated once per day starting from midnight and calculating a 48 h forecast with a 1 h time step. The daily forecasts are freely available at open access website http://emhi.ee/?ide=19,1304, presenting forecasts of the sea level, sea surface temperature, sea surface salinity and also ice parameters. Today the HIROMB-EST setup uses model code version 4.0, but in other aspects it has not changed since the beginning of the operational runs.

3. OPERATIONAL SEA LEVEL FORECASTING IN ESTONIA

Sea level variations around the decadal mean values are of great importance for the coastal population. The eastern Baltic Sea has very weak tides but strong and quite often damaging storm surges, together with other types of sea level variation. Variable isostatic Earth crust vertical motion pattern over the region (Ekman 1996), combined with global eustatic sea level change (Ekman 1999), results in long-term trends in sea level, yielding maximum decrease of –8.2 mm/yr in the northern part of the Bothnian Bay (Johansson *et al.* 2003), a slight decrease from –0.5 to –2.8 mm/yr in Estonia (Suursaar and Sooäär 2007) and a slight increase in the southern part of the sea (Dailidiene *et al.* 2006).

Due to the limited transport capacity of the Danish Straits, the variability of the Baltic Sea level can be generally decomposed (Samuelsson and Stigebrandt 1996) into a external variations, due to change in the mean sea level of the basins, forced by the outside Kattegat water level and the basins freshwater budget, and internal variations around the mean state, dominated by wind-driven long rotational gravity waves, influenced by the complex coastline and topography. The internal component has also smaller contributions from saline and freshwater pulses and variations in water density and air pressure. Although the external sea level component is in principle oscillatory (the "harbour" or semi-open bay mode (Miles 1974)), at time scales of forcing weather patterns (periods less than a month) the Baltic sea level response is damped and delayed (Samuelsson and Stigebrandt 1996). The observed sea levels are well correlated along the coastline (Raudsepp *et al.* 1999). Stronger westerly winds and related larger inflows occur usually in autumn and winter. As an example, during the major inflow in January 1993 (Matthäus and Lass 1995), 310 km^3 of North Sea water entered the Baltic in 21 days, raising the mean sea level by 70 cm. Such rapid increases in the sea volume during storms contribute also to actual storm surges (Suursaar *et al.* 2003).

Internal sea level variations are influenced by the semi-isolated seiche systems, Belt Sea–Baltic Proper–Gulf of Finland (passing the Gulf of Bothnia) and Belt Sea–Baltic Proper–Gulf of Bothnia, with the self-oscillation periods of about 25–27 h and 31–39 h (Wübber and Krauss 1979). However, due to the complicated multi-basin topography, the seiches do not have high contribution in the sea level power spectrum (Johansson *et al.* 2001). According to Jönsson *et al.* (2008), instead of full-basin seiches, internal sea level variability is dominated by weakly coupled semi-open bay modes. For the Gulf of Riga, such an open bay mode results in persistent 24-h current oscillations in the Irbe Strait (Lilover *et al.* 1998, Otsmann *et al.* 2001), while the internal (closed bay) seiche period is about 5 h (Suursaar *et al.* 2003).

After the highest known storm surge that occurred in Estonia in January 2005, the implementation of the 3D operational sea level forecasting system was initiated. In August 2005 the first version of the sea level forecasting system was

set up in an operational regime. Following the stage of algorithm developments and forecast validations, since 2007 the sea level forecasts together with observations have been available for the public in the open access Sea Level Information System web page, http://on-line.msi.ttu.ee/kaart.php?en (Fig. 2).

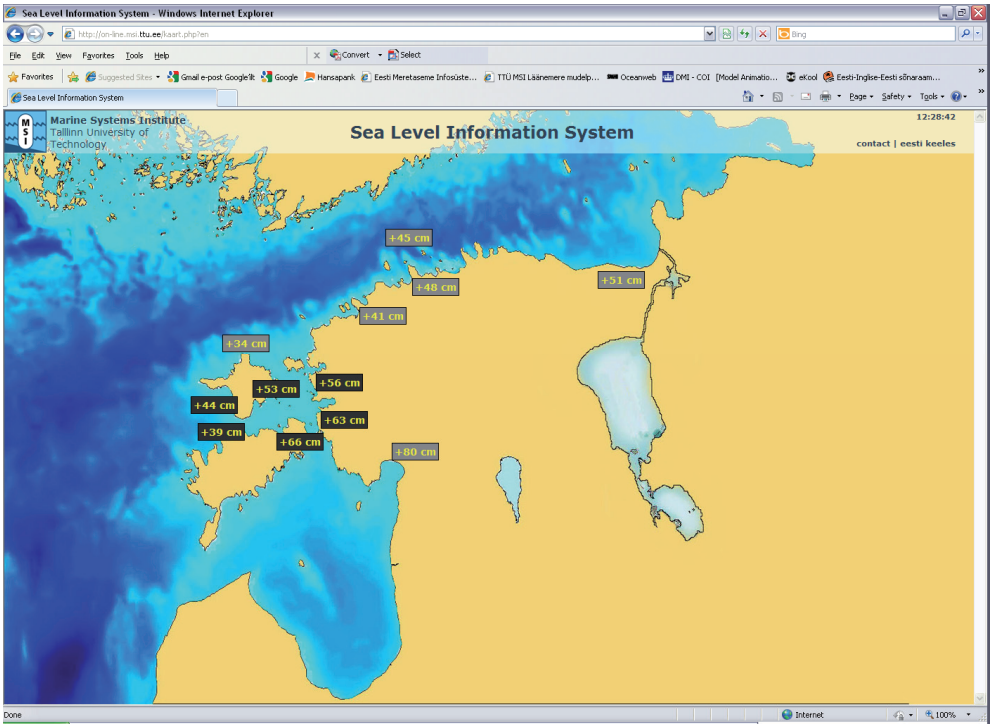

Figure 2. The sea level observation stations presented at the Sea Level Information System web page (http://on-line.msi.ttu.ee/kaart.php?en).

In a normal situation, when the sea level is around 0 cm, the number of clicks in the system per day is about 1000, but during storms it increases about 1000 and even 10 000 times, resulting in about 10 million clicks per day. The users of the system are mainly the people living in coastal areas, but also larger institutions like the Estonian Rescue Service. This system has been used for issuing warnings about high sea level in the Estonian coastal sea, and by national and local authorities for decision-making. The company that operates ferries between the Estonian mainland and islands relies on the sea level forecasts in case of critically low sea level. The skill assessment study and comprehensive description of the operational forecasting system are given in paper I.

3.1. Development of the sea level forecasting system

The sea level forecasting system is aimed to produce as accurate sea level forecasts as possible using any data and methods available. The model is only one component of the forecasting system. While in model development the

computing algorithms are sourced from natural physics, the forecasting system may have purely statistical algorithms as far as these improve the accuracy of the forecast. Therefore, the forecasting system should be interpreted as a post-processing tool for the model to turn the model data into an official forecast. The sea level forecasting system was set up to use 1 NM model data from HIROMB-SMHI in the year 2005 and this has remained unchanged. The reasons for that are discussed later in this section.

Two main components are mandatory for the operation of the forecasting system: the model and the observations. Since the year 2005 both components have undergone several changes like the forecasting system itself and the development is continuing (paper I). The model code has had four releases (the details are given in Section 2), the number of sea level observation stations has increased from 3 to 12 and the functionality of the forecasting system has grown including, e.g., automatic low-frequency error correction and high/low sea level warning messaging function. Despite the increased functionality and larger data capacities, the speed and stability of the system has increased significantly. One good example of the progress is the mean forecast production time, which has decreased from 2.5 h in the year 2006 to 0.5 h in the year 2011. Regarding the stability, the mean uptime of the forecasting system was found to be 96%, which is above the institutional goal. However, the amount of major data gaps (i.e. data missing over two weeks in a row) should be decreased to fulfill another goal, stating that there should not be longer data gaps than 48 h.

The sea level observational network has developed considerably since 2005 and presently comprises of 12 online stations (Fig. 2). A typical configuration of the automatic sea level station consists of a staff gauge as the installation platform and a submerged piezoresistive pressure sensor at the zero level of the staff. Automatic temperature (resolution 0.1°C) and air pressure compensation gain an accuracy of 1 cm in terms of the water column above the sensor. The pressure sensor is connected with the data logging, processing and transmitting device, which calculates sea level as 30 s average water column height, as well as the basic wave parameters locally at the station, and sends data with 5 min intervals over the GPRS communication protocol to the ftp server at the MSI. It was found in paper I that the mean uptime of the observation station is above 97% without taking the major sensor failures into account. The major sensor errors are defined as long-term (over two weeks) failures that are caused by the breakdown of the observation station. On the one hand these major failures are not the direct malfunction of the forecasting system since the users are notified and aware about the missing forecast. On the other hand, although the users do not expect any forecast from the broken station (because of the notification), they still would like to have the forecast as soon as possible. So, the station replacement procedure needs improving as mentioned in paper I.

At the beginning the forecasting system became operational with the forecast update interval $L = 24\,\mathrm{h}$ and forecast length $M = 48\,\mathrm{h}$. The system was then continuously monitored and developed to improve its stability and reliability. At

first the system was set up on Windows Server PC, using the batch scripts, Fortran codes and task scheduler. However, due to the properties of the operating system, the stability and working speed of the system were rather poor and quite often required manual administration. On the other hand, the stability was better than usually expected for systems with similar architecture and the forecasting system was able to produce some forecasts automatically, which was a significant improvement compared to earlier used manual forecasting. Nevertheless, after the 17 December 2008, when the new Linux computational cluster was purchased, the forecasting system was fully re-coded for the Linux environment. At the same time the forecast update interval was decreased to $L = 6\,\mathrm{h}$, gaining an 8% increase in forecast accuracy (paper I). Besides the stability and accuracy increase, the new Linux environment gave possibilities for simpler error handling procedures which were implemented into the forecasting system.

In a few months after the forecasting system was installed on the Linux cluster the automated high/low sea level warning system was implemented. Critical values for the sea level station were defined (paper I, table 3), and when the forecast is out of the defined limits, an automated high/low sea level warning message is sent to the users of the forecasting system. The skill of the high and low sea level forecast and warning system was evaluated. It was found that none of the significant high/low sea level events was missed by the forecasting system. In general, the frequency of high sea levels within the period from 2009 to 2011 was low and no coastal flood was observed, but there were several low sea level events which actually influenced the ship traffic between the small islands and mainland. Most of the high/low sea level events were alerted properly, but still 18% of them were slightly (up to 5 cm) underestimated by the forecast and the warning message was not sent.

One of the main functions of the forecasting system is the variable low-frequency error calculation. A modelled sea level η_{mod} has always a bias relative to a geodetic reference system. After some months of running the initial sea level forecasting system, visual inspection of the time series of the raw model output η_{mod} and the observed sea level η_{obs} revealed that the model error had a low-frequency part that varied from location to location and was slowly changing in time. It is obvious, that such a distortion of the forecast should be removed, or at least suppressed. The initial system running period was too short for comprehensive statistical analysis, therefore a simple method for backward moving average (not centred, since future observations are not known during the forecast) of the model errors over seven days was applied to correcting the low-frequency errors. Although this procedure has already been in operational use for a long time, a proper mathematical formulation of the method was presented only recently in paper I. The effectiveness of the method was further analysed as well. The analysis of autocorrelation of the model error $d(n,1) = \eta_{mod}(n,1) - \eta_{obs}(n)$ time series over the 2–year period (from February

2006 to March 2008) at the Pärnu station showed that the error properties were far from the ideal white noise (Fig. 3). The correlations above 0.2 appear in a quite long (up to 4000 h) time lag, indicating some systematic error component.

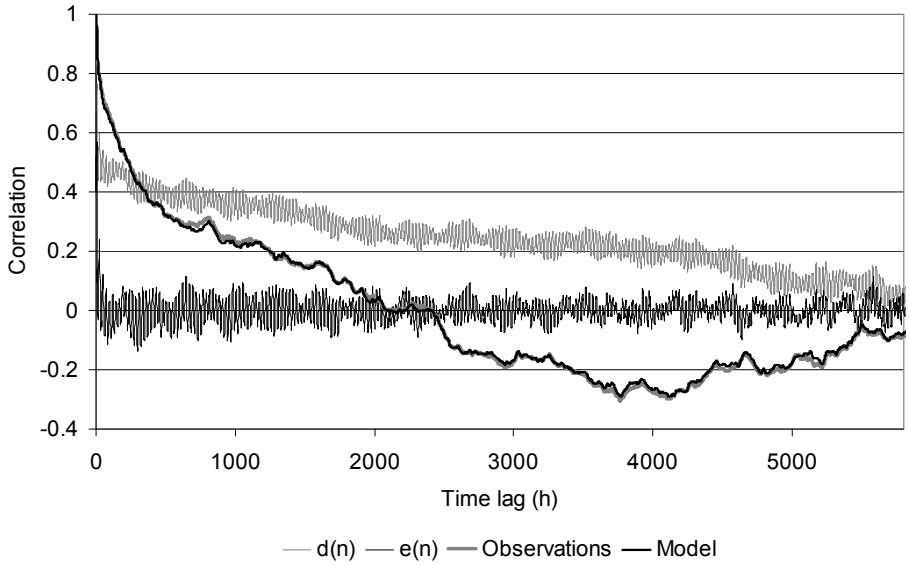

Figure 3. The autocorrelation of observations, corrected sea level forecast, raw model error $d(n)$ and forecast error $e(n)$ at the Pärnu station.

To suppress the systematic error component, a method similar to the autoregressive moving average method was introduced in paper I (formulas (1)–(4)). An analysis revealed the best low-frequency filter length $K = 168$ h in the Estonian coastal sea. It was found that using the specified filter length lowered the root mean square error (RMSE) of the forecast by up to 30% compared to the simple "last-forecast-error" (i.e. filter length $K = 0$) method (Fig. 4). The method given with formulas (1)–(4) in paper I can (besides operational practice) also be used for future calibration of the forecasting system. The recalibration of the forecasting system with the given method is straightforward and simple and can be done each time the model code has changed. In fact, the forecasting system validation study for the period 2009–2011 has shown that the behaviour of the low-frequency error has probably changed compared to the time period from 2006 to 2008 for which the low-frequency suppression method has been calibrated (figs 7 and 8 in paper I). It is obvious that besides further investigation of the changed behaviour of the low-frequency error, the recalibration of the sea level forecasting system should be performed with more recent data. As already mentioned, the calibration method given in paper I provides a good ground for the recalibration.

Although the local setup of HIROMB (0.5 NM setup) has switched into the operational mode and a pre-operational sea level forecast system using the higher resolution model data has already been set up, the official forecasting

system still uses the 1 NM model data to produce sea level forecasts. Several reasons can be pointed out, starting from the need for comprehensive validation of the sea level forecasts based on the HIROMB-EST model. Another issue is extra time needed for running local the model and an increase in possible failure sources affecting the system. In addition to the current possible malfunction sources, the 0.5 NM based sea level forecast will also require an operation of the local HIROMB and HIRLAM models and the transfer of data from all these models between the different systems. So, three considerable malfunction sources are introduced into the system, which means that the increase in the accuracy of the forecast should be significant to weight up the decreased reliability (or the redundancy costs to keep the reliability at the current level) of the operational system. However, considering the quite high accuracy of the current system, such an increase in accuracy is not likely in the near future.

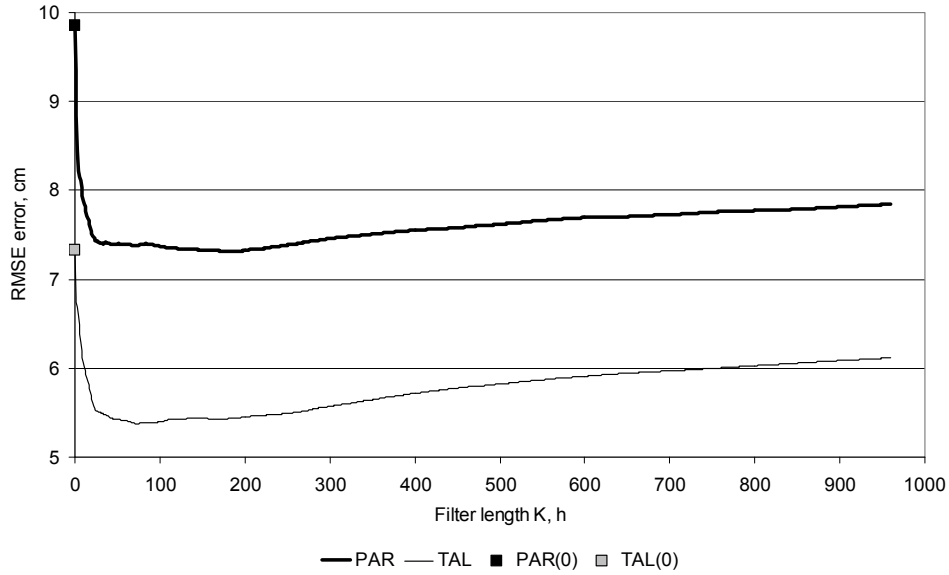

Figure 4. The RMSE dependence on the backward moving average filter length K. PAR–Pärnu station, TAL–Tallinn station.

3.2. The accuracy of the forecasting system

The accuracy of the sea level forecasting system was evaluated in paper I mainly on the basis of data from the period from 2009 to 2011. Standard statistical methods were used, including the root mean square error (RMSE), standard deviation, mean error and correlation analysis. The Taylor diagrams were used as the skill illustrator and the dependence of forecast accuracy on forecast length was presented. An innovative sea level sub-ranges method for finding more objective accuracy of the forecasting system was applied.

The general accuracy of the sea level forecasting system is presented in Figure 5a. The figure shows the centred pattern root mean square deviations

(RMSDs) and correlations found for the whole dataset from 2009–2011. The forecast is the most accurate at the Paldiski station yielding the RMSD below 4 cm and correlation above 98%. The most inaccurate forecast was obtained for the Pärnu station, with the RMSD near 7 cm and correlation near 97%. Although the 7 cm forecast error may seem insignificant for sea level forecasts, caution must be taken in interpreting it. The centred pattern RMSD is the accuracy illustrator most often presented in many investigations, since it combines standard deviation of forecasts and correlation between observations and forecasts. It also has a clear statistical meaning. As the centred pattern RMSD is equivalent to standard deviation of the forecast error (in case of normal distribution), it can be interpreted as the absolute error level within the 68% probability level. Therefore, the RMSD found for the one-year dataset means that the forecast error is lower than the given RMSD on $365 \times 68\% \approx 248$ days, whereas on the remaining 117 days (i.e. approx four months in one year) the error of the forecast is actually higher. It is clear that there is less than four months of stormy days in one year, so for example the given 7 cm RMSD found at the Pärnu station actually describes the non-stormy days when nobody cares about the accuracy of the forecasting system. A two-year study has revealed a maximum of 521 high sea level hours for the period from 2009 to 2011 (Table 6 in paper I), giving on average 11 days of high sea levels per year when the accuracy of the forecast is under an increased interest. To have a more practical accuracy estimate of the forecast, the RMSD value must by multiplied by factor 3, raising the confidence level to 99.7% and therefore leaving approximately one day in a year when the accuracy of the forecast is lower than three times the RMSD. Therefore, stating that the RMSD is below 7 cm at the Pärnu station could mean that the error is below 21 cm on stormy days, but at the same time other uncertainties are left unexplained, for example the conditions when this error might appear.

To get a more detailed error estimation of the forecast during the stormy periods, the sea level was divided into three sub-ranges (high, medium and low) in paper I. Using the mean absolute error relation to sea level forecast, it was found that the mean absolute error starts to increase from certain sea level at each station (fig. 10 in paper I). The limits for high and low sub-range sea levels were determined for the Estonian coast, showing that a different accuracy estimate could be used if the sea level is on average lower than –50 cm or higher than +40 cm. The statistics for these sub-ranges are presented in paper I. It was established that for the high sea level sub-range the RMSDs varied from 5 cm at the Heltermaa station to 13 cm at the Pärnu station (Table 6 in paper I). This means that in case of high sea level (over +50 cm) the 13 cm RMSD value should be preferred at the Pärnu station, since it was obtained using only the 123 h high sea level sub-range data in an about one–year period (the explanation of Table 6 in paper I). To reach the one–day exclusion limit, we have to move to the 80% confidence level (coefficient 1.28) and we get the error estimation 17

cm. So, the error is lower, than the 21 cm error estimation found from the whole data series analysis.

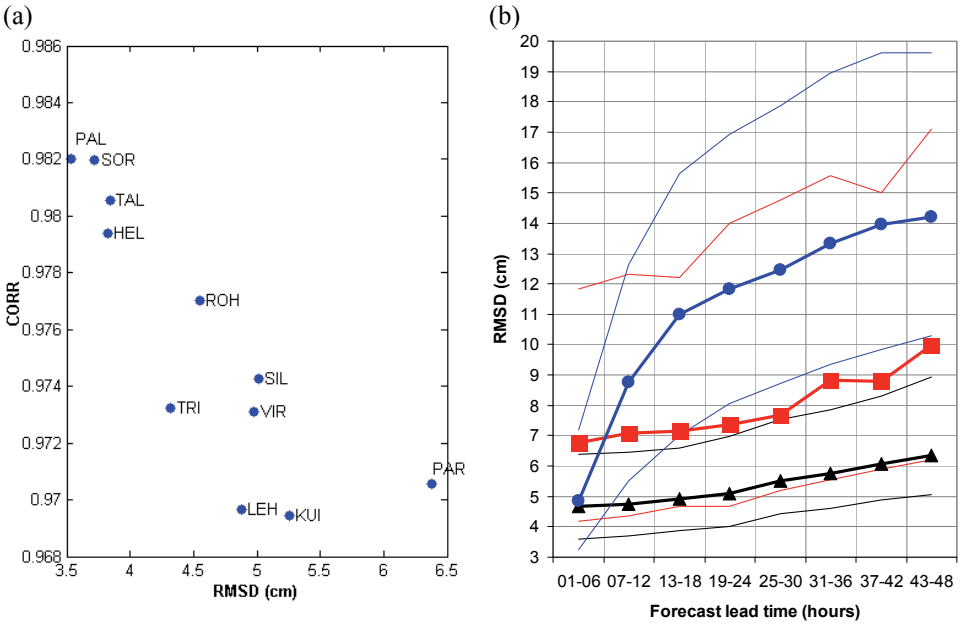

Figure 5. The sea level forecast correlation and RMSD with respect to observation for the whole dataset (a) and RMSD dependence on the forecast length for different data ranges (b). The black, red and blue bold lines on (b) show the mean RMSD over all stations of the whole dataset, high sub-range and persistency forecast respectively. Thin lines with the corresponding colour show the minimal and the maximal individual curve at the most accurate and least accurate station, respectively. The sea level forecast is most accurate at the Paldiski (PAL) station and least accurate at the Pärnu (PAR) station. Abbreviations on (a) note different observation stations.

To investigate the dependence of forecast accuracy on forecast length, the RMSD was calculated for each forecast lead time range and for each station. The results for the whole dataset are presented in Fig. 5b with black lines, including the arithmetic mean of the RMSD at all stations and the minimal (Paldiski station) and maximal (Pärnu station) individual RMSD curves over all stations, to describe the boundaries of the station-wise RMSD dependence, i.e. curves of all other nine stations were within these boundaries. The mean accuracy of the forecast (red bold line in Fig. 5b) decreases only up to 2 cm for the 48 h forecast length, and the maximal error for the 48 h forecast (higher black line in Fig. 5b) is up to 2.5 cm higher than the best available forecast error. The dependence of the mean high sub-range forecast error on forecast length is marked with the red bold line with filled rectangles in Fig. 5b. Again, the boundaries are denoted by the thin red lines to describe the distribution of the curves over individual stations. The results show that the high sub-range forecast depends slightly more on the forecast lead time than on the mean accuracy of the whole dataset. The 48

h forecast accuracy is up to 5 cm lower than the RMSD of the best available forecast, but on average the 6 h forecast is 3 cm more accurate than the 48 h forecast.

As the forecast system skill illustrator, the persistency forecasts were carried out, using observational data available, and compared with the results of the operational forecast. The persistency forecast is one of the most primitive forecast methods. It is based on the assumption that the last observed situation will continue over the entire forecast period. For example, in the 1–6 h persistency forecast it is assumed that the most recent observed sea level is constant over the next 6 h. The simulated persistency forecasts are shown in Fig. 5b with blue lines, similar to the whole dataset. The accuracy of the persistency forecast is close to the accuracy of the forecasting system forecast up to 6 h, but in longer lead times, up to 48 h, the advantage of the forecast system is clearly evident.

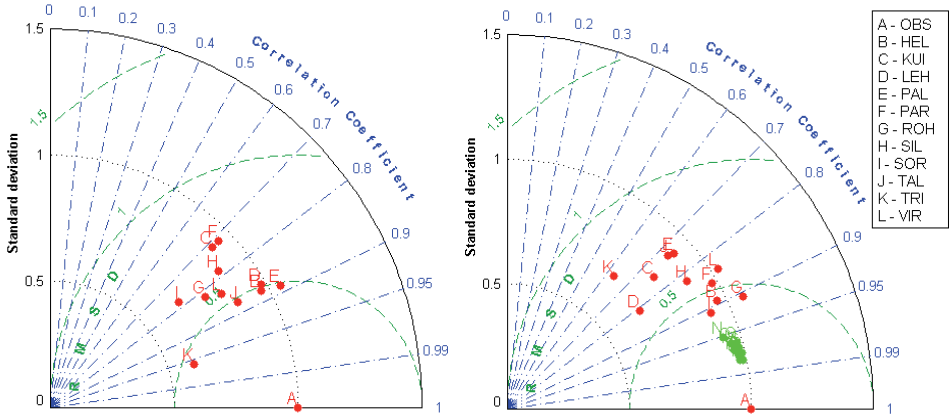

Figure 6. Normalized Taylor diagram for low (left) and high (right) sea level sub-range forecast. The green dots in the high mode Taylor diagram represent the medium sub-range forecast and are shown to illustrate differences between high/low and medium sub-range forecasts. Data for each station are normalized with the standard deviation of corresponding observations. The letter A indicates sea level observations.

The low, medium and high sub-range statistics are summarized in normalized Taylor diagrams (Fig. 6). In general, the low and high sub-range statistics show similar patterns, while the medium sub-range statistics are much better. The standard deviation is underestimated nearly at all stations in all sub-ranges, pointing to problems with the underestimated variance of the forecasted sea level. In low and high sub-ranges both the variance and the phasing contribute to the increase in the RMSD, giving no evidence of a specific source of an increased error, while in high sub-range data the decreased correlation seems to be dominating. Since the storm surges can change the sea level very rapidly, the 1 h temporal error in sea level forecast could cause a high forecast error (up to 50 cm) and lower the correlation rate.

3.3. The outlook of the sea level forecasting system

The development of the sea level forecasting system is an ongoing process showing several new trends. As an improvement to the forecasting system it is planned to use more observational stations, especially the stations operated by the EMHI. The work is already in progress. There are nine new sea level stations, which will be merged into the system soon after the test period is finished. The coverage of the Estonian coastal sea with sea level measurement sites with the addition of new stations. Nevertheless, some more efforts are needed to harmonize the measurement methods, which are somewhat non-uniform today. The current forecast system has already displayed good performance, but the improved online measurement station network should raise the accuracy of the system towards better representation of local peculiarities and features, which in turn are very important in storm cases in certain parts of the coast.

The ensemble forecasts are becoming more and more popular around the Baltic Sea. Today, in case of sensitive forecast (for example before releasing the high sea level warning), the forecasts of different models and different sources are analysed manually. The purpose of ensemble forecasting is to automate this analysis or at least gather all data into one ensemble forecasting system, so all the information can be found in one place (e.g. on a single web page). The exact methods for producing ensemble forecasts for different products are still insufficiently known. It is clear that different weight functions should be found for each model and each product (i.e. sea level, sea surface temperature and salinity etc.) for the calibration of the ensemble forecast, although these weight functions are obviously not too straightforward and need further investigation.

Several discussions have been held during the last decade concerning the low-frequency forecast errors of the sea level. The actual origin of such a dynamic bias is still not clear and should be further investigated. It may have several reasons like distortions in the boundary conditions provided by the "outer" storm surge model NOAMOD, density inaccuracies in the model response, inaccurate volume changes of the Baltic Sea and its sub-basins due to the errors in volume transports in the straits, errors in the freshwater budget, etc. During the validation study of the sea level forecasting system, an attempt was made to find the dependence between the low-frequency error and the Baltic Sea volume change for the optimization of the low-frequency error calculation method. The Baltic-wide mean sea level time series were found and compared with the dynamic sea level bias time series at different stations (fig. 5 in paper I). Although several variations in low-frequency errors and horizontally mean sea level occur at the same time, their phases vary significantly and the statistical correlation is practically absent. Therefore, the forecast of horizontally mean sea level cannot be used for prediction of the low-frequency error component in operational sea level forecasting.

Today, at six online stations out of 11 main wave parameters are experimentally estimated on the basis of the pressure data, and broadcasted to the Sea Level Information System (http://on-line.msi.ttu.ee/kaart.php?en). This system has been running already for 1.5 years and the wave data are used as background information for high-resolution sea level measurements. As indicated by the analysis of the extreme storm surge, the occurrence of critical and above critical sea levels is the weakest point in the forecast system. The role of waves in forming extreme sea levels seems to be quite obvious and some statistics based on the existing time series are already available. As a first step the correction factors for extreme sea levels, taking into account the local wave pattern in actual wind conditions, could improve the performance of the forecast system. A reliable forecast of extreme sea levels accompanied by flood risk is probably the most important task at all.

4. CURRENT SIMULATIONS AND COMPARISONS WITH ADCP OBSERVATIONS

The surface currents that are primarily caused by direct wind forcing can be predicted quite well (Gästifvars *et al.* 2006). Comparisons of subsurface current predictions are quite rare and they mainly come from the strait areas where the flow has essential topographic constrictions. Burchard *et al.* (2009) have shown that adjustment of the model topography may be helpful in improving the quality of predictions.

Current velocity measurements were compared with the 1 NM and 0.5 NM model simulations at four observation sites with different topographic and hydrographic background and in different seasons: Lohusalu (L), Vaindloo1 (V1), Vaindloo2 (V2) and Kunda (K) (Fig. 7). Site L (59.4500°N, 24.1667°E) is located in the western part of the Gulf of Finland on the southern coastal slope. This site near the Lohusalu Peninsula is 6 km from the coast, where the depth is 50 m. The observation data were gathered during the spring and early summer period (13 March to 30 June 2009). Sites V1 (59.8683°N, 26.4300°E) and V2 (59.8500°N, 26.2700°E) about 9 km apart are located in the central part of the gulf in a deeper passage around the small Vaindloo Island. The sites lie approximately 30 km from the southern coast of the gulf, where the depths are 68 m (V1) and 75 m (V2). The measurements were performed in late fall (29 October to 25 November 2009). Site K (59.7017°N, 26.4033°E) is located about 15 km southwards from sites V1 and V2 in the south-eastward extension of the deep basin towards Kunda Bay. The depth of the site is 66 m; the data were collected in winter and early spring (12 January to 27 April 2010).

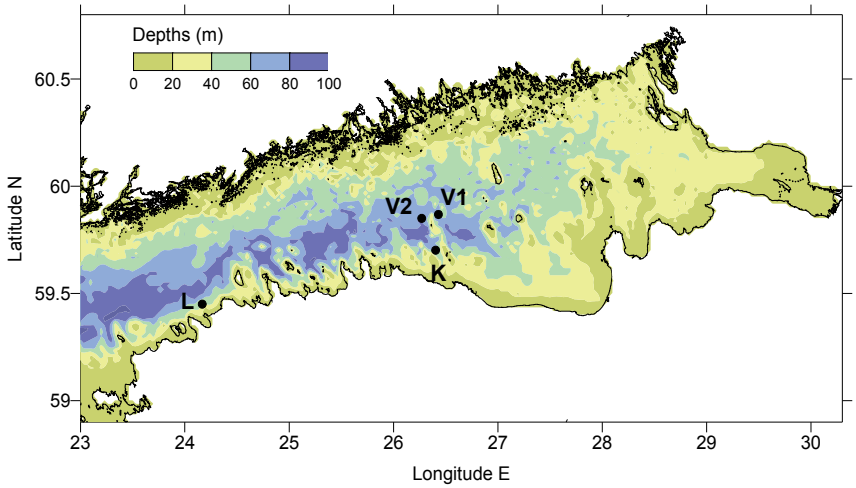

Figure 7. Map of the Gulf of Finland. Locations of ADCP measurements are given by dots and corresponding labels.

At all sites bottom-mounted 307.2 kHz broad-band acoustic doppler current profiler (ADCP) (RDInstruments) was used. The instruments measured current velocities over 2 m depth bins with the sampling interval of 10 min (average of 50 pings). Due to surface side lobe effect the data of two bins from the surface were contaminated and therefore not used, i.e. the upper reliable bin was centred at a depth of 5 m. The first bin available above the instrument was centred at 5 m from the bottom. The quality of the data series at each depth bin was checked using the procedure which is based on certain criteria for the internal control parameters (signal correlation, percentage of good and error velocity) of the ADCP (Book *et al.* 2007). Relying on this analysis, bad data were replaced using linear interpolation of the series.

The simulated currents were validated against observations at depths where the maximal current speeds were registered in the measurement series. These depths were 10 m at observation sites L1 and K and 50 m at observation sites V1 and V2. After analysing the current roses the low- and high-frequency current components were analysed separately. Low-frequency time series of horizontal current components were obtained by using the 36 h moving average procedure. High-frequency current components were obtained by subtracting the corresponding low-frequency series from the raw series.

The analysis of current roses (fig. 2 in paper II) at site L showed more pronounced westward alongshore flow in both models than in measurements. The speed of dominating currents (20–25 cm/s in the 0.5 NM model and 10–15 cm/s in the 1 NM model) was overestimated and the direction (230º–250º and 235º–255º, respectively) was more unidirectional following the recently published general circulation scheme of the Gulf of Finland (fig. 2 in paper III). The observations showed a more varied distribution of current directions

probably due to switching between upwelling and downwelling regimes that was not modelled so well.

At sites V1 and V2 the maximum current speeds were found at a depth of about 50 m. According to the temperature and salinity profiles measured during the ADCP installation, this was approximately the depth of the halocline and the depth of maximum vertical density gradients. The flow directions appeared strongly constrained in specific sectors, both in the measurements and the model results. Significant differences occurred between the 1 NM and 0.5 NM model results at V1, obviously due to the differences in the resolution and gridded bathymetry of the models. Vaindloo Island, located close to the observation sites, is relatively small and poorly described by the 1 NM model (actually absent in the surface layer). Therefore, the 1 NM model predicted an eastward flow spread more widely at site V1 with dominating current speeds of 5–10 cm/s. The results of the 0.5 NM model showed dominating current speeds exceeding 20 cm/s directed mainly south. The observations revealed a south-eastward flow but the dominating current speeds were nearly the same as in the 0.5 NM model. The differences in dominating directions between the 0.5 NM model and the observations may have been caused by the problems of bathymetry in the model domain, namely the unrealistic gridded presentation of the island slopes, submarine hills and deep passages.

Since the modelled low-frequency current time series were often strongly biased, an attempt was made to interpret the model results by possible biases in model bathymetry. When comparing the time series of current components the good correlation is not the most important parameter. The biased mean current components could cause much bigger problems because of a possible change in the direction of the mean current, often resulting in the opposite flow in models compared to observations. The bottom layers at site V1, characterized by well-constrained current roses (fig. 2 in paper II), were chosen for such an analysis. The current rose of the 0.5 NM model clearly indicates that the dominant flow direction is deflected by approximately 40º clockwise from the dominant direction of the ADCP current. As argued before, this could easily be due to the biased bathymetry in the model domain. To follow the direction of local isobaths on the slope of deep passage better, the modelled current vectors were rotated (using classical axis rotation) 40º counter-clockwise to match the dominating direction of the observed current (presumably along-slope). Next, since the depth of the sea at site V1 was greater than the local depth of the model bathymetry, the model depth was scaled accordingly. This means that the data from the 55 m horizon in the model domain were compared with ADCP measurements at a depth of 63 m (both nearest to the bottom). The results of such a transformation are presented in Fig. 8. It is evident that the model results can be significantly improved by a simple transformation when knowing the actual bottom topography at a certain location. It also indicates that the flow in bottom layers is highly dependent on topography.

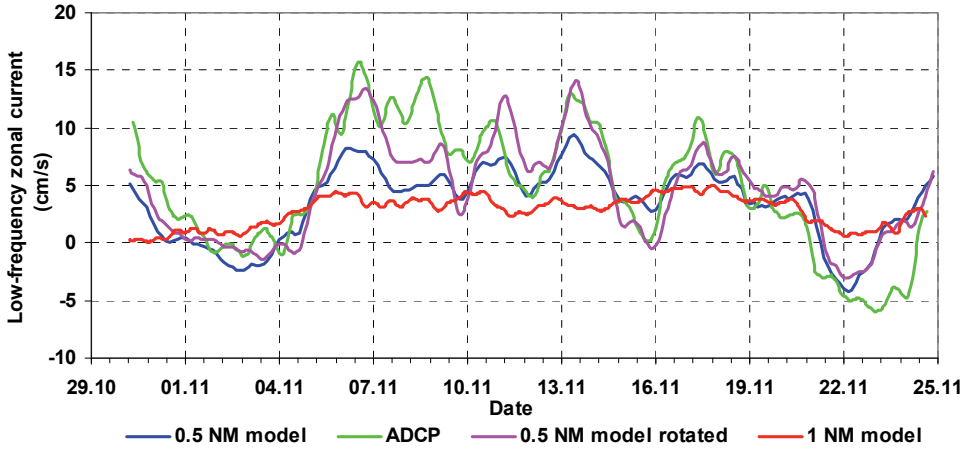

Figure 8. Low-frequency zonal current component time series in bottom layers of the Vaindloo1 site. ADCP at a depth of 63 m, 1 NM model at 55 m and 0.5 NM model at 55 m (i.e. all at depths nearest to the bottom). Note that rotation of the 0.5 NM model currents by 40º gives a better match with measurements.

Unlike other observations, the observations at site K were performed mainly in wintertime. This gave a possibility of validating the model currents in ice conditions although the ice concentration in models was not perfectly simulated. The measured time series of both low-frequency current components contained sharp peaks indicating rapid changes in currents, which were not recorded at other observation sites. Such short-term high-speed currents were observed mainly from 28 January to 11 March. In models these rapid changes in low-frequency currents were not evident probably due to overestimation of the ice coverage. High-frequency currents at observation site K were modified by sea ice even more than low-frequency currents. In the time series graphs of the high-frequency current (Fig. 9) some amplitude increase episodes like around 28 January and 20 February took place right after the ice had disappeared from the observation site. Although not shown here, the same principle applies to low-frequency currents. While in the low-frequency domain the influence of ice was not so clearly visible in bottom layers, high-frequency currents seem to be influenced by ice from the surface down to the bottom. However, there are also some smaller bursts in currents in other time spans, indicating some other source of high-frequency variability. These bursts appear simultaneously with rapid sea level changes (over 20 cm per day). Therefore, local currents are also influenced by large-scale wind events, sometimes in remote areas, resulting in sea level changes. Such sea level related bursts (e.g. from 18 to 27 February, combined with the ice drift events, and from 17 to 21 April) are better simulated by the models than the bursts related to ice movement. As ice cover is also partially related to a rapid change in sea level gradients, it can also be assumed that the bursts seen in high-frequency current time series of model results may be caused by sea level changes. This is another example of the need of accurate sea level in

the model domain. However, both models predicted the high-frequency current bursts related to rapid sea level changes relatively well.

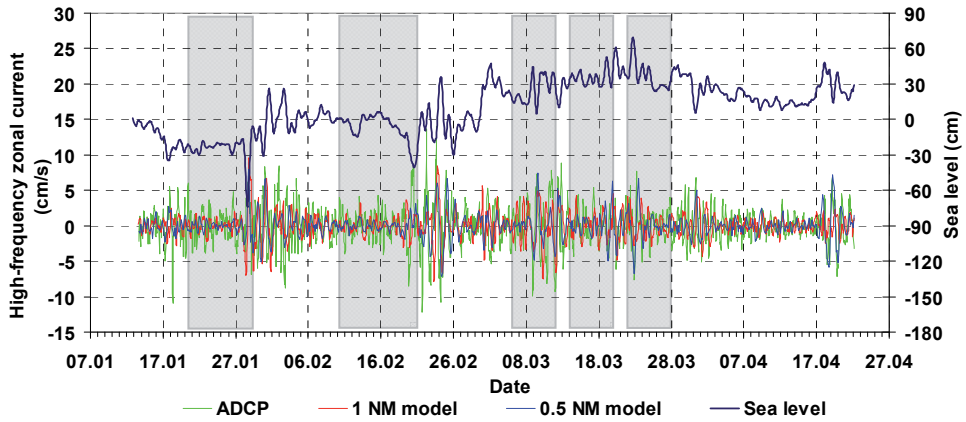

Figure 9. High-frequency zonal current components at a depth of 46 m and modelled sea level time series at the Kunda site. Shaded areas show the ice coverage periods.

5. CIRCULATION AND VARIABILITY PATTERNS IN THE GULF OF FINLAND

5.1. Mean circulation

The Gulf of Finland is an estuarine basin of the Baltic Sea, which has a specific circulation regime and variability patterns. It has the highest specific freshwater discharge (per unit area and unit volume of the basin) among other Baltic Sea sub-basins (Bergström and Carlsson 1994). Since in the west the gulf is connected to the Baltic Proper without a topographical constriction and/or sill, the salinity and density fields exhibit some features of a partially mixed estuary (Pitkänen *et al.* 2008). The mean horizontal circulation is cyclonic – with average inflow of more saline waters close to the southern, Estonian coast and outflow of less saline waters along the northern, Finnish coast. Speeds of the mean circulation have been estimated to be a few cm/s. However, the circulation is modified by several factors. Instantaneous currents may reach 20–30 cm/s or even more (Alenius *et al.* 1998).

Over the seasons, changes in stratification and wind forcing create different mean patterns of circulation in the Gulf of Finland, as described already by Witting (1912) and Palmen (1930) (see the review by Alenius *et al.* 1998). Instrumental observations give reliable estimates of the variability of currents, but unfortunately are limited either in time or space to give estimates of the current patterns and their variations. Present circulation estimates are largely based on the model results.

Multiannual model studies (Lehmann *et al.* 2002, Andrejev *et al.* 2004, Meier 2005) have confirmed the observational arguments of the mean cyclonic

circulation. The results of these model studies give further insight into the problem of persistency of the current direction, i.e. which fraction forms the speed of the vector-mean current from the scalar-mean current speed (Palmen 1930). Within the limits of model performance, Andrejev *et al.* (2004) renewed the earlier observation-based indications by the concepts of high-stability current belts where persistency above 0.5 is concentrated in the outflow region, to the north from the central axis of the gulf.

In the present work, the circulation patterns of the Gulf of Finland were studied using HIROMB 1 NM resolution model data. Daily forecasts from the period 2006–2008 were assembled into one time series and mean circulation was found. The investigation period included the HIROMB model code release from 3.0 to 3.1 in September 2007 when the neutral-stability wind components were introduced into the model code. The period 2006–2008 was characterized by mild to moderate winters and normal wind regime. The mean wind vector, based on the forcing data in the central part of the gulf, was about 2 m/s from 240°–250° as within the longer period. However, several significant meteorological and oceanographic events took place. Intensive upwelling occurred along the southern coast in July–August 2006 (Lips *et al.* 2009), due to the unusually persistent easterly winds. Stormy periods in October–November 2006 and January 2007 caused high sea levels in the gulf due to the south-westerly winds (Elken *et al.* 2008).

The mean current fields (fig. 2 in paper III) exhibit the known cyclonic circulation. The currents in the most stable layer of 4–8 m, just below the drift-influenced surface layer, reveal the maximum outflow of less saline water near the Finnish coast in the Finnish Coastal Current (Stipa 2004). As compared to the earlier results by Andrejev *et al.* (2004), who used the Oleg Andrejev & Alexander Sokolov (OAAS) model, the mean outflow in 1987–1992 was closer to the main axis of the gulf. The shift can be explained by differences in the specific forcing events (e.g. different stratification in an open sea, etc.) during different periods (although the mean wind vectors were the same), and the specific features in the response of the two models under the same forcing (Myrberg *et al.* 2010). Both the HIROMB-SMHI model (present study) and the OAAS model (Andrejev *et al.* 2004) revealed some other interesting circulation features. The southward recirculation loop, detaching from the Finnish Coastal Current and feeding the southern eastward currents, is located just east of the Tallinn–Helsinki connection line. There is also a second southward loop of the Finnish Coastal Current near 26°E (fig. 2 in paper III). In the eastern part of the gulf, from 26.5°E to 27.7°E, the currents near the southern coast are oriented in the reverse, westward direction. This loop is also presented in the results of Soomere *et al.* (2011), especially in calm wind periods in 1987–1991. A formerly not described circulation feature appears in the western part of the southern coast, west of 24.4°E (fig. 2 in paper III). Namely, the coastal currents are directed westwards and the inflow of more saline open Baltic Sea waters takes place offshore, in the deepest parts of the Gulf. This feature was

qualitatively confirmed with the ADCP observations at the Lohusalu site (paper II). However, it was found that the models tend to overestimate the magnitude of the currents in this area possibly due to up- and downwelling jets which were not well modelled.

Vertical structure of the mean currents in the section along longitude 24.4°E (fig. 3 in paper III) exhibits the outflow on the northern slopes of the gulf, some 10–15 km offshore, at depths of 10–20 m. Inflow takes place in the deepest part of the gulf in two depth ranges, close to the surface and in the halocline within the depths from 40 to 60 m. The mean sea level drops by 2–3 cm from north to south, forcing the outflow of surface waters in accordance with the geostrophic relations. Towards greater depths, the density gradients oppose the sea level drop, resulting in the decrease in pressure gradients and along-channel flow.

5.2. Horizontal variability patterns

To study the variability patterns, the deviations of currents, density, sea level and wind from the three-year mean fields were decomposed into the spatial modes (fixed over the time period) with time-dependent amplitudes, using the well-known Empirical Orthogonal Function (EOF) method (e.g. von Storch and Zwiers 1999), which is a Principal Component Analysis. This technique allows estimating the variance ("energy") contribution of individual spatial modes to the overall variability. The time-dependent amplitudes show how different spatial patterns are amplified or damped in specific events. Details of the application of the EOF method in the current study are given in paper III. The variability patterns were studied between the longitudes 23.65°E and 27.93°E (Fig. 1b in paper III).

First, the deviations from the mean fields of wind vectors were studied. The first two wind vector modes comprise 93% of the wind field variance. The EOF modes are almost uniform horizontally: the relative standard deviation of vector magnitudes is only 3% and the standard deviation of directions is less than 2° (for small relative vector magnitudes the direction is quite uncertain, but this is not the case here). It means that on average "physical" wind vectors of the first two EOF modes are geometrically almost orthogonal (perpendicular) at each horizontal grid point. Note that individual modes are exactly orthogonal in terms of the EOF eigenvector scalar product over the whole domain, not necessarily the "physical" vectors at each grid point. Within this analysis, 53% of the wind variance (1st mode) is oriented along the direction 226° (SW–NE) or 46° (according to the EOF sign determination options) and 40% (2nd mode) along 316° (NW–SE) or 136°. This result justifies common usage of the horizontally uniform, only time-dependent wind field in modelling studies of sub-regions, whose extent is much smaller than the baroclinic Rossby radius of the atmosphere (about 1000 km, Gill 1982).

Wind-driven surface currents are generally known to follow the wind stress, but they are deflected from the wind direction due to the Earth's rotation. The

first two current modes (deviations from the mean fields, Fig. 10) comprise together 60% of the variance. They also exhibit horizontally quasi-uniform patterns like the wind modes, but the spatial variability of the vector magnitudes is somewhat higher. Still, the directional variation study is justified and the standard deviation is 18°–20°. Main variations in the surface current direction take place in the coastal areas and between the western and eastern parts of the calculation area. Within the sign determination freedom of EOF modes, the mean direction is 104° or 284° for the 1st mode and 16° or 196° for the 2nd mode. It means that on average the 1st and 2nd surface current modes are geometrically perpendicular within ±2° accuracy.

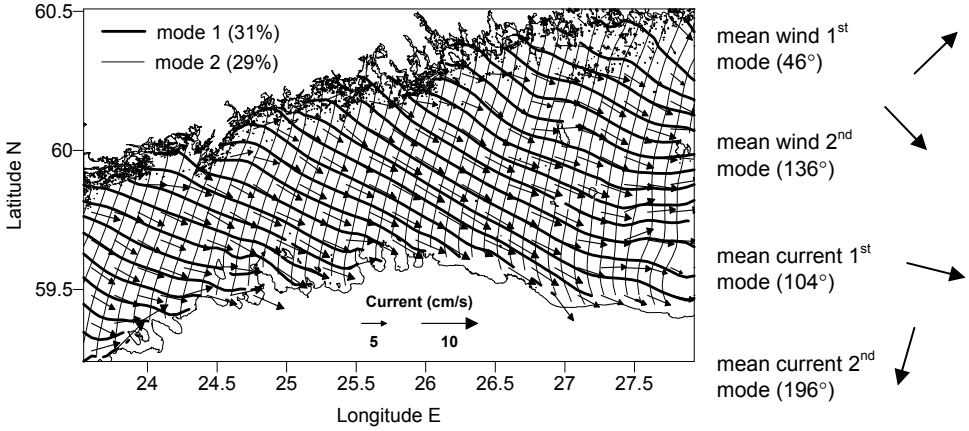

Figure 10. Horizontal EOF mode patterns of the surface current 1st and 2nd modes. The vector patterns of modes are visualized by the streamlines and actual vectors of the 1st mode are also drawn.

In order to investigate the relation between currents and wind, the amplitudes of the first two modes of surface currents A_{u1} and A_{u2} and the amplitudes of wind modes A_{W1} and A_{W2} were found. Since the surface currents have notable energy near the inertial period of 14 h as obtained from the spectral analysis of A_{u1} and A_{u2}, a 3-point filter $\tilde{\psi}(t) = 0.25[\psi(t - T/2) + 2\psi(t) + \psi(t + T/2)]$ was used for their suppression (here ψ and $\tilde{\psi}$ are original and filtered variables, T is the period to be damped). The amplitudes A_{u1} and A_{u2} of the first two current modes correlate well with the wind stress functions $A_{W1}\sqrt{A_{W1}^2 + A_{W2}^2}$ and $A_{W2}\sqrt{A_{W1}^2 + A_{W2}^2}$ of the amplitudes of the first two wind modes A_{W1} and A_{W2}, if the physical vectors of wind stress amplitudes are projected to a proper angle. The best correlations ($R^2 = 0.71$) with both A_{u1} and A_{u2} were obtained when wind amplitudes A_{W1} and A_{W2} were rotated as horizontal vector components (with respect to EOF mode mean directions 46°

and 136°, respectively) clockwise by 20°. This means that the current component A_{u1} towards 104° correlates with the wind stress towards 66° (i.e. 46° + 20°) and component A_{W1} towards 196° correlates with the wind stress towards 156° (136° + 20°). A conclusion from the above is that 60% of the surface current variance is explained by the following relation: the speed of the surface currents is proportional to the wind stress (wind speed squared) (because it is defined this way in the model) and the currents are deflected on average 40° to the right from the wind direction. It is interesting to note that scatter plots of amplitudes of wind stress functions and surface currents revealed two distinct clusters during 2006–2008. These clusters correspond to the older model version 3.0 with linear drag coefficient dependence on the wind speed, and to the new version 3.1 with the stability-dependent wind stress drag coefficient. The values of R^2 were 0.84-0.86 for the old version and 0.77 for the new version. From old to new version, the mean wind-to-current transfer coefficient decreased by about two times. Note that these relation changes reflect only the revision of model features, not the circulation physics. The 40° deflection angle of the current anomalies (from the mean fields) relative to the wind anomalies is the same for both model versions. According to earlier studies, based on observations at specific locations, the deflection angle (including the mean fields) could be up to 60° (Gästgifvars *et al.* 2006).

Sea level variability is heavily (98.6% of variance) dominated by the flat 1st mode, where the difference between the minimal and maximal values is only 2% of the mean value of the mode (Fig. 11). This mode thus presents storage variations (filling and emptying) of the whole gulf, with negligible spatial gradients. Quite expectedly, the amplitudes of this mode are not correlated with local wind amplitudes, since the storage variations of the particular gulf depend on the mean sea level of the entire Baltic Sea and the large-scale air pressure and wind fields over the whole sea area (Lehmann and Hinrichsen 2001, Lehmann *et al.* 2002). Spatial gradients of sea level are dominated by along-channel (2nd mode, 1.0%) and cross-channel (3rd mode, 0.2%) variations. These modes represent the sea level states where the local wind is the dominating forcing factor. The 4th mode (0.03%) reveals high levels in the central part of the Gulf and low levels near the coast, or vice versa, depending on the sign of the amplitude. This mode therefore represents amplification or decay of the mean cyclonic circulation. Sea level gradients significantly depend on wind direction. Along-channel gradients (2nd mode) are amplified by the wind stress projected to 275° ($R^2 = 0.77$) and cross-channel gradients (3rd mode) by wind stress projected to 195° ($R^2 = 0.49$). In other words, sea level rises in the eastern end of the gulf by the westerly wind stress component and on the northern shore by the southerly (slightly south-westerly) wind stress component. The 4th mode of the sea level gradients is excited by the westerly wind stress component (direction $285°, R^2 = 0.39$) and the amplitudes correlate with the 3rd "circulation" mode of the surface currents ($R^2 = 0.55$). To conclude, over a

longer period (several years) the sea level variation is mostly determined by the mean sea level of the whole of the Baltic Sea and only 1.4% of the sea level energy is determined by the local wind above the gulf.

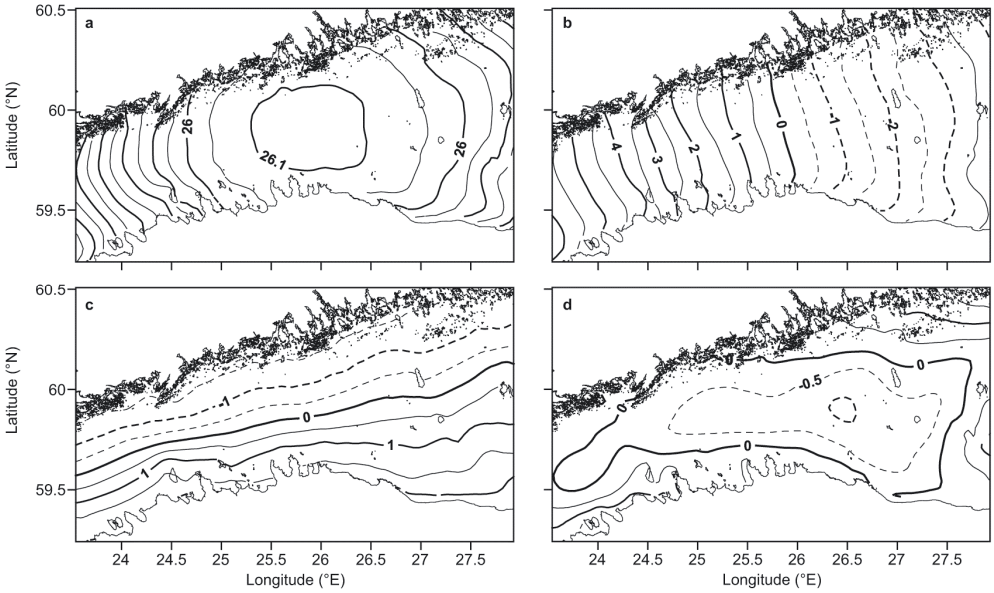

Figure 11. Horizontal EOF mode patterns of sea level. Modes: (a) mode 1 (98.6%), CI = 0.05 cm; (b) mode 2 (1.0%), CI = 0.5 cm; (c) mode 3 (0.2%), CI = 0.5 cm; and (d) mode 4 (0.03%), CI = 0.5 cm. The mode patterns are dimensional (cm), scaled by the square root of the variance of each mode. Note the smaller contour interval (CI) for the flat 1st mode.

5.3. Discussion on mean circulation

In the following, some results concerning the circulation in the Gulf of Finland are presented further for the period until the end of 2011, not included in the published papers. Recent studies have provided the contradictory results. For example, Maljutenko *et al.* (2010) calculated 10-year mean surface currents of the gulf in the period 1997–2006 and found no Finnish Coastal Current in the northern coast of the gulf at all. Although they calculated the circulation for the surface layer, some parts of stable circulation currents should still be represented there. Similar (contradictory) results were obtained by Soomere *et al.* (2011), showing mean surface currents for the period 1987–1991 (same period as in Andrejev *et al.* 2004) at the northern slope of the gulf rather opposite directed to those generally expected by the known circulation scheme. Andrejev *et al.* (2011) investigated the role of the spatial resolution of the model in the mean circulation and concluded that the mean circulation is not dependent on model resolution in a few years scale.

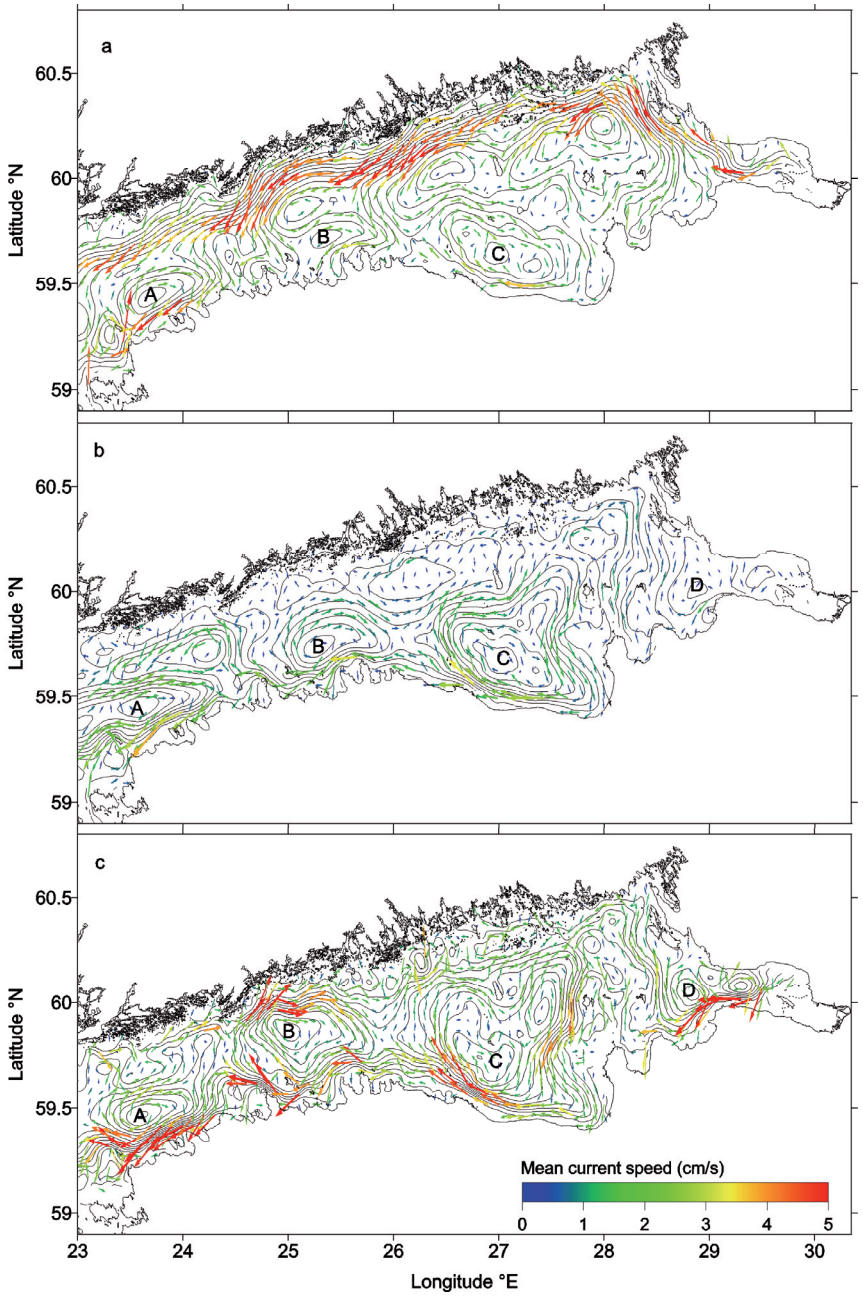

Figure 12. Mean circulation in the Gulf of Finland of the period 2006–2008 found from the 1 NM model setup (a) (redrawn from paper III); of the period 2010–2011 found from the 1 NM model setup (b) and 0.5 NM model setup (c). For the 1 NM model the 4–8 m layer and every 4th vector are presented. For the 0.5 NM model the 6–9 m layer and every 6th vector are presented.

However, recent ferrybox measurements along the Tallinn–Helsinki line have quite often shown that the less saline water occurs in the middle of the gulf, not at the northern slope as expected (Kikas *et al.* 2010, Lips *et al.* 2011). The author determined the mean circulation from the 0.5 NM HIROMB model for the period 1 January 2010–31 December 2011 (Fig. 12c) at different model layers but the results were again "non-traditional". The mean currents found from the 1 NM model for the same period as from the 0.5 NM model confirm the results of the 0.5 NM model. At the same time, as discussed before, the results presented in paper III follow the general circulation scheme rather well. All these results lead to discussions to clarify the reasons for the different circulation patterns.

The mean circulation patterns for the period 2010–2011 show significant differences compared to the period 2006–2008 (Fig. 12). The major difference between these periods is that the Finnish Coastal Current is virtually absent in 2010–2011. Four circulation loops were established: A, B, C and D. Anticyclonic loops A and C (A was already mentioned as an "unexplained" circulation feature in paper III) are present in both 2006–2008 and 2010–2011. These seem to be quite persistent, although the scale of eddy C is smaller in the period 2006–2008. However, loop B differs significantly between the periods. The mean surface currents for the years 2010–2011 show rather anticyclonic currents in this area, which is also the case in Soomere *et al.* (2011). The mean circulation is also slightly different at the eastern end of the gulf. In 2006–2008 the fresh water originating from the Neva River flows out of the bay following the overall cyclonic pattern. In the period 2010–2011 a small anticyclonic curve D forms just before less saline water enters the wide part of the gulf. This is explained by the upward entrainment of saline water in the narrow estuary introducing an anticyclonic character into the flow (Fujiwara *et al*. 1997). In case of stronger winds the anticyclonic circulation cell E is forced into Neva Bay.

The quadratic wind stress analysis was made for the period 1981–2011 based on the observations at the Kalbadagrund meteorological station. The purpose of the analysis was to qualitatively find the differences in wind regimes in different periods (Fig. 13). Therefore, data from raw observations (performed approximately at 30 m height) were used without converting them into 10 m height winds as it is in model forcing. The mean wind stresses along the dominating wind direction were found. The 1st of August (start of the transition period from calm to windy conditions) was chosen as the beginning of the averaging year (e.g. the year 2010 in Fig. 13 means the period from 1 August 2009 to 31 July 2010). The wind stress components were rotated 34° to follow the dominating wind direction and minimize the mean orthogonal component of the wind stress. The results (Fig. 13) show a significant difference in the mean wind stress between 2006–2008 and 2010–2011, whereas the mean 34° wind stress components over these periods were 0.034 and 0.004, respectively. Therefore, the westerly wind stress component was very low in the years 2010–2011 compared to normal wind stress in period 2006–2008. However, the other

investigation periods mentioned above have a similar mean wind stress to each other.

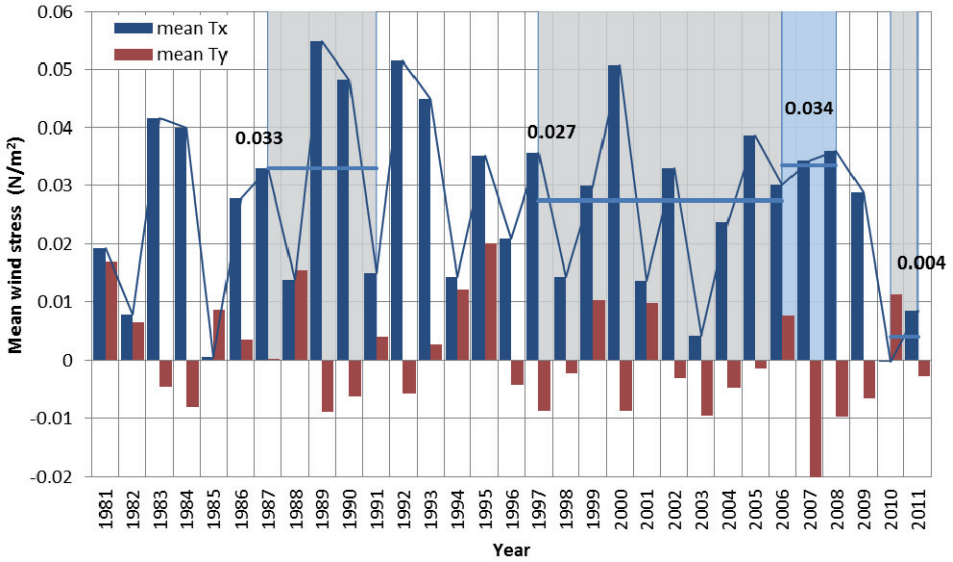

Figure 13. Yearly mean wind stress components in 34° rotated coordinates. The averaging year starts from 1 August. The shaded regions with the corresponding mean values for each shaded region show the periods where circulation studies have been carried out.

It is obvious that different wind regimes produce different current regimes, which stresses again that an inaccurate atmospheric forcing in the hydrodynamic model could cause large-scale misleading results. However, it is out of the scope of this study to find quantitative explanations to the problem and further investigation is needed.

6. CONCLUSIONS

After the storm surge in January 2005 it was decided to implement the operational 3D marine forecasting system in Estonia. Among many other reasons like harmful algae blooms or drift of surface substances the primary goal of the operational forecasting system was to increase the accuracy of sea level forecasts. Considering the validation studies available at the time, the state-of-art operational model HIROMB was chosen as a basis for the operational forecasting in Estonia. The sea level forecasting system was made operational already in August 2005 based on the 1 NM HIROMB-SMHI model results, after which the work towards a local high-resolution model setup was started. The operational runs of the 0.5 NM HIROMB setup operated by the MSI were initiated in May 2009.

The sea level forecasting system is in continuous development and both mandatory components of the forecasting system (model and observations) have had spectacular progress. As the model code has had four new releases, the sea level observation network includes today already 12 observation stations, some of them performing also wave measurements. The core of the sea level forecasting system has gone through serious stability and reliability improvements in the course of development, resulting in five times quicker forecast production and the mean uptime of the system 96%.

High sub-range sea level analysis revealed that the RMSE of the sea level forecast is below 13 cm and correlation greater than 63%. The increase in the sea level forecast RMSE in connection with forecast length was below 3 cm per 48 h when taking the whole (2009–2011) dataset into account. The advantage of the sea level forecasting system compared to the primitive persistency forecast method was clearly revealed.

The validation of high- and low-frequency sub-surface currents in the 0.5 and 1 NM models showed reasonable match with the currents recorded during four different ADCP current observations in the Gulf of Finland. In general the models tend to underestimate the current variability in both the high- and low-frequency domains and the currents are more unidirectional compared to observations. Near-bottom and coastal currents are highly constrained by topography. When knowing the actual bottom topography, the modelled near-bottom currents can be simply transformed to present more realistic results.

The investigation of the circulation scheme of the Gulf of Finland based on the HIROMB model results showed reasonable accordance with general knowledge. The mean horizontal circulation is cyclonic, with the outflow of the less saline water originating from the Neva River along the Finnish coast. Compared to the earlier results, the Finnish Coastal Current was found to be closer to the Finnish coast. The inflow of more saline water from the Baltic Proper to the gulf takes place in the deepest part of the entrance to the gulf in the surface and also at the depths from 40–60 m.

The main conclusions of the thesis are:

- The application of a low-frequency filter, developed for suppressing the systematic error component in the modelled sea level, increased the accuracy of the sea level forecasting system by up to 30%. The best low-frequency filter length is K = 168 h in the Estonian coastal sea.
- Analysis of the high sea level events for the period from 2006 to 2008 showed the ±25 cm accuracy of storm surge forecasts, when taking into account the ±3 h time shift between the observations and the forecast. The statistical analysis of the whole data domain in sea level forecasts in 2009–2011 revealed the RMSE less than 7 cm and correlations above 97%.
- High current speeds (above 20 cm/s) were measured in the deep layers of the rough-bottom area around a small island. Such currents were in general well simulated by the 0.5 NM model, only slightly biased with regard to the dominating direction. The correlation between currents in the model and observations is higher in the bottom layers of the water column.
- The high-frequency variations in currents caused by rapid sea level variations are well predicted by the models. It was found that the rapid mean sea level variations influence the currents in the whole water column from the surface down to the bottom.
- The study of the circulation patterns in the Gulf of Finland revealed several smaller anticyclonic loops at the Estonian coast.
- On the sea surface, quasi-uniform drift currents of the Gulf of Finland are deflected on average by 40° to the right from the wind direction and cover 60% of the circulation variance.
- Sea level variability in the Gulf of Finland is heavily (98%) dominated by almost uniform changes due to the water storage variations of the gulf.

Although much more developments are foreseen, the operational oceanography in Estonia has made significant progress within the last seven years in both scientific and operational aspects. Despite huge differences in resources, long steps have been taken to be a competitive operational oceanography centre in the community of high-level marine forecasting centres community. In addition to the scientific studies presented in this thesis, more studies are using the HIROMB model results as comparative data giving valuable information to scientists. The operational sea level forecast has already become a natural part of the weather forecast today, but it is only the beginning in the course of bringing the importance and value of marine environment forecasts to the public.

REFERENCES

Alenius, P., Myrberg, K. and Nekrasov, A. 1998. The physical oceanography of the Gulf of Finland: A review. *Boreal Environment Research*, 3, 97–125.

Alenius, P., Nekrasov, A. and Myrberg, K. 2003. Variability of the baroclinic Rossby radius in the Gulf of Finland. *Continental Shelf Research*, 23, 563–573.

Andrejev, O., Myrberg, K., Alenius, P. and Lundberg, P.A. 2004. Mean circulation and water exchange in the Gulf of Finland – A study based on three-dimensional modelling. *Boreal Environment Research*, 9, 1–16.

Andrejev, O., Soomere,T., Sokolov, A. and Myrberg, K. 2011. The role of the spatial resolution of a three-dimensional hydrodynamic model for marine transport risk assessment. *Oceanologia*, 53, 309–334.

Axell, L. *Weaker Surface Currents in HIROMB 3.1*., 9th HIROMB Scientific Workshop 28–31 August 2006, SMHI, Gothenburg, 25 slides, www.environment.fi/syke/hiromb, 16.10.2011.

Bergström, S. and Carlsson, B. 1994. River Runoff to the Baltic Sea. *Ambio*, 23, 280–287.

Book, J.W., Perkins, H., Signell, R.P. and Wimbush, M. 2007. *The Adriatic Circulation Experiment winter 2002/2003 mooring data report: A case study in ADCP data processing.* Memo. Rep. NRL/MR/7330-07-8999, U.S. Naval Research Laboratory, Stennis Space Center, Miss., 50 pp.

Buch, E., Elken, J., Gajewski, J., Håkansson, B., Kahma, K. and Soetje, K. 2006. Present status of the Baltic Operational Oceanographic System. In *Proceedings of the Fourth International Conference on EuroGOOS, Brest, France, 2006* (Dahlin, H., Flemming, N.C., Marchand, P. and Petersson, S.E., eds). Office of Official Publications of the European Communities, 276–280.

Burchard, H., Janssen, F., Bolding, K., Umlauf, L. and Rennau, H. 2009. Model simulations of dense bottom currents in the Western Baltic Sea. *Continental Shelf Research*, 29, 205–220.

Chant, R.J., Geyer, W.R., Houghton, R., Hunter, E. and Lerczak, J. 2007. Estuarine boundary layer mixing processes: Insights from dye experiments. *Journal of Physical Oceanography*, 37, 1859–1877.

Dailidiene, I., Davuliene, L., Tilickis, B., Stankevicius, A. and Myrberg, K. 2006. Sea level variability at the Lithuanian coast of the Baltic Sea. *Boreal Environment Research*, 11, 109–121.

Eilola, K., Gustafson, B.G., Hordoir, R., Höglund, A., Kuznetsov, I., Meier, H.E. M., Neumann, T. and Savchuk, O.P. 2010. Quality assessment of state-of-the-art coupled physical-biogeochemical models in hind cast simulations 1970–2005. *SMHI Oceanografi*, nr. 101, 21 pp.

Ekman, M. 1996. A consistent map of the postglacial uplift of Fennoscandia, *Terra Nova*, 8(2), 158–165.

Ekman, M. 1999. Climate changes detected through the world's longest sea level series. *Global and Planetary Change*, 21, 215–224

Elken, J., Kõuts, T., Raudsepp, U., Laanemets, J. and Lagemaa, P. 2006. BOOS/HIROMB-based marine forecasts in Estonia: problems, experiences and challenges. In *Proceedings of US/EU-Baltic International Symposium, May 23–25, Klaipeda, Lithuania*. 1–22.

Elken, J., Kõuts, T., Lagemaa, P., Lips, U., Raudsepp, U. and Väli, G. 2008. Sub-regional observing and forecast system for the NE Baltic: Needs and first results. In *US/EU-Baltic International Symposium, 2008 IEEE/OES: US/EU-Baltic Symposium "Ocean Observations, Ecosystem-Based Management & Forecasting", Tallinn, 27–29 May, 2008*. IEEE Conference Proceedings, 1–9.

Funkquist, L. 2001. HIROMB, an operational eddy-resolving model for the Baltic Sea. *Bulletin of the Maritime Institute in Gdansk*, 28, 7–16.

Gästgifvars, M., Lauri, H., Sarkanen, A., Myrberg, K., Andrejev, O. and Ambjörn, C. 2006. Modeling surface drifting of buoys during a rapidly-moving weather front in the Gulf of Finland, Baltic Sea. *Estuarine, Coastal and Shelf Science*, 70, 567–576.

Gästgifvars, M., Müller-Navarra, S., Funkquist, L. and Huess, V. 2008. Performance of operational systems with respect to water level forecasts in the Gulf of Finland. *Ocean Dynamics*, 58, 139–153.

Gill, A. 1982. *Atmosphere-Ocean Dynamics*. Academic Press, 662 pp.

Hansen, W. 1956. Theorie zur Errechnung des Wasserstandes und der Strömungen in Randmeeren nebst Anwendungen, *Tellus*, 8, 287–300.

HIROMB Scientific Plan 2009–2013, ver. May 2010. (4 April 2012, ftp://ftp.dmi.dk/pub/Users/Nicolai.Kliem/BOOS_HIROMB_annual_meeting/HIROMB_May_12/HIROMB_Scientific_Plan_May-2010.doc)

Johansson, M., Boman, H., Kahma, K.K. and Launiainen, J. 2001. Trends in sea level variability in the Baltic Sea. *Boreal Environment Research*, 6, 159–179.

Johansson, M., Kahma, K. and Boman, H. 2003. An improved estimate for the long-term mean sea level on the Finnish Coast. *Geophysica*, 39(1–2), 51–73.

Jönsson, B., Döös, K., Nycander, J. and Lundberg, P. 2008. Standing waves in the Gulf of Finland and their relationship to the basin-wide Baltic seiches. *Journal of Geophysical Research*, 113, C03004.

Kikas, V., Norit, N., Meerits, A., Kuvaldina, N., Lips, I. and Lips, U. 2010. High-resolution monitoring of environmental state variables in the surface layer of the Gulf of Finland (during a dynamic spring bloom in March–May 2010). In *4th IEEE/OES Baltic Symposium, Riga, 24–27 August 2010*, 1–9.

Kleine, E. 1994. *Das Operationelle Modell des BSH für Nordsee und Ostsee. Konzeption und Übersicht, Bundesamt für Seeschifffahrt und Hydrographie* (manuscript report).

Koivurova, T. and Pölvnen, I. 2010. Transboundary environmental impact assessment in the case of the Baltic Sea gas pipeline. *International Journal of Marine and Coastal Law*, 25, 151–181.

Krauss, W. and Brügge, B. 1991. Wind-produced water exchange between the deep basins of the Baltic Sea. *Journal of Physical Oceanography*, 21, 373–384.

Laanemets, J., Zhurbas, V., Elken, J. and Vahtera, E. 2009. Dependence of upwelling mediated nutrient transport on wind forcing, bottom topography and stratification in the Gulf of Finland: Model experiments. *Boreal Environment Research*, 14, 213–225.

Lass, H.U. and Talpsepp, L. 1993. Observations of coastal jets in the Southern Baltic. *Continental Shelf Research*, 13(2–3), 189–203.

Lehmann, A., Krauss, W. and Hinrichsen, H.H. 2002. Effects of remote and local atmospheric forcing on circulation and upwelling in the Baltic Sea. *Tellus*, 54A, 299–316.

Lehmann, A. and Myrberg, K. 2008. Upwelling in the Baltic Sea – A review. *Journal of Marine Systems*, 74, S3–S12.

Lilover, M.-J., Lips, U., Laanearu, J. and Liljebladh, B. 1998. Flow regime on the Irbe Strait. *Aquatic Sciences*, 60, 253–265.

Lips, U., Lips, I., Kikas, V. and Kuvaldina, N. 2008. Ferrybox measurements: a tool to study meso-scale processes in the Gulf of Finland (Baltic Sea). In *US/EU-Baltic Symposium "Ocean Observations, Ecosystem-Based Management & Forecasting", Tallinn, 27–29 May, 2008.* IEEE Conference Proceedings, 1–6.

Lips, I., Lips, U. and Liblik, T. 2009. Consequences of coastal upwelling events on physical and chemical patterns in the central Gulf of Finland (Baltic Sea). *Continental Shelf Research*, 29, 1836–1847.

Lips, U., Lips, I., Liblik, T., Kikas, V., Altoja, K., Buhhalko, N. and Rünk, N. 2011. Vertical dynamics of summer phytoplankton in a stratified estuary (Gulf of Finland, Baltic Sea). *Ocean Dynamics*, 61, 903–915.

Maljutenko, I., Laanemets, J. and Raudsepp, U. 2010. Long-term high-resolution hydrodynamical model simulation in the Gulf of Finland. In *IEEE/OES Baltic 2010 International Symposium: IEEE/OES Baltic 2010 International Symposium, 25–27 August 2010, Riga*. IEEE Conference Proceedings, 1–7.

Matthäus, W. and Lass, H.-U. 1995. The recent salt inflow into the Baltic Sea. *Journal of Physical Oceanography*, 25(2), 280–286.

Matthäus, W. and Schinke, H. 1999. The influence of river runoff on deep water conditions of the Baltic Sea. *Hydrobiologia*, 393, 1–10.

Meier, H.E.M. 2005. Modeling the age of Baltic Sea water masses: Quantification and steady state sensitivity experiments. *Journal of Geophysical Research*, 110, C02006.

Miles, J.W. 1974. Harbor seiching. *Annual Review of Fluid Mechanichs*, 6, 17–35.

Myrberg, K., Ryabchenko, V., Isaev, A., Vankevich, R., Andrejev, O., Bendtsen, J., Erichsen, A., Funkquist, L., Inkala, A., Neelov, I., Rasmus, K., Rodriguez Medina, M., Raudsepp, U., Passenko, J., Söderkvist, J., Sokolov, A., Kuosa, H., Anderson, T. R., Lehmann, A. and Skogen, M. D. 2010. Validation of

three-dimensional hydrodynamic models of the Gulf of Finland. *Boreal Environment Research*, 15, 453–479.
Nerheim, S. 2004. Shear-generating motions at various length scales and frequencies in the Baltic Sea – an attempt to narrow down the problem of horizontal dispersion. *Oceanologia*, 46, 477–503.
Otremba, Z. and Andrulewicz, E. 2008. Environmental concerns related to existing and planned technical installations in the Baltic Sea. *Polish Journal of Environmental Studies*, 17, 173–179.
Otsmann, M., Suursaar, Ü. and Kullas, T. 2001. The oscillatory nature of the flows in the system of straits and small semienclosed basins of the Baltic Sea. *Continental Shelf Research*, 21, 1577–1603.
Palmen, E. 1930. Untersuchungen über die Strömungen in den Finnland umgebenden Meeren. *Societas Scientiarum Fennica, Commentationes Physico-Mathematicae*, 12, 1–94.
Pavelson, J., Laanemets, J., Kononen, K. and Nõmmann, S. 1996. Quasi-permanent density front at the entrance to the Gulf of Finland: response to wind forcing. *Continental Shelf Research*, 17, 253–265.
Peeck, H.H., Proctor, R. and Brockmann, C. 1982. Operational storm surge models for the North Sea. *Continental Shelf Research*, 2(4), 317–329.
Pitkänen, H., Lehtoranta, J. and Peltonen, H. 2008. The Gulf of Finland. In *Ecology of Baltic Coastal Waters* (Schiewer, U., ed.), Ecological Studies, 197, 2, II.C, 285–308.
Raudsepp, U., Toompuu, A. and Kõuts, T. 1999. A stochastic model for the sea level in the Estonian coastal area. *Journal of Marine Systems*, 22, 69–87.
Reissmann, J.H., Burchard, H., Feistel, R., Hagen, E., Lass, H.U., Mohrholtz, V., Nausch, G., Umlauf, L. and Wieczorek, G. 2009. Vertical mixing in the Baltic Sea and consequences for eutrophication – A review. *Progress in Oceanography*, 82, 47–80.
Samuelsson, M. and Stigebrandt, A. 1996. Main characteristics of the long-term sea level variability in the Baltic Sea. *Tellus*, 48A, 672–683.
Soomere, T., Delpeche, N., Viikmäe, B., Quak, E., Meier, M.H.E. and Döös, K. 2011. Patterns of current-induced transport in the surface layer of the Gulf of Finland. *Boreal Environment Research*, 16(Suppl A), 49–63.
Stipa, T. 2004. Baroclinic adjustment in the Finnish coastal current. *Tellus*, 56, 79–87.
Suursaar, Ü. and Sooäär, J. 2007. Decadal variations in mean and extreme sea level values along the Estonian coast of the Baltic Sea. *Tellus*, 59A, 249–260.
Suursaar, Ü., Kullas, T., Otsmann, M. and Kõuts, T. 2003. Extreme sea level events in the coastal waters of West Estonia. *Journal of Sea Research*, 49, 295–303.
Suursaar, Ü., Kullas, T., Otsmann, M., Saaremäe, I., Kuik, J. and Merilain, M. 2006. Cyclone Gudrun in January 2005 and modelling its consequences in the Estonian coastal waters. *Boreal Environment Research*, 11, 143–159.

The Nord Stream Project. 2009. *Nord Stream Environmental Impact Assessment Documentation for Consultation under the Espoo Convention. Key Issue Paper, Seabed Intervention: Works and Anchor Handling.* February 2009, 53 pp.

Umlauf, L., Burchard, H. and Hutter, K. 2003. Extending the κ-ω turbulence model towards oceanic applications. *Ocean Modelling*, 5, 195–218.

Uusitalo, S. 1960. The numerical calculation of wind effect on sea level elevations. *Tellus*, 12(4), 427–435.

von Storch, H. and Zwiers, F.W. 1999. *Statistical Analysis in Climate Research.* Cambridge University Press, Cambridge, 484 pp.

Witting, R. 1912. Zusammenfassende Übersicht der Hydrographie des Bottnischen und Finnischen Meerbusens und der Nördlichen Ostsee. *Finn. Hydrogr.-biol. Unters.*, No. 7.

Wübber, C. and Krauss, W. 1979. The two-dimensional seiches of the Baltic Sea. *Oceanologica Acta*, 2, 435– 446.

ABSTRACT

The operational oceanography in Estonia is reviewed in this thesis by describing the current status of the forecasting models and systems as well as by giving an overview of the validation studies of the products. Two setups of HIROMB models, with 1 NM and 0.5 NM horizontal grid resolutions, are operationally used in forecasting the marine environment of Estonia. The sea level forecasting system is the main topic of this work. The accuracy of the forecasting system is evaluated in two periods: 2006–2008 and 2009–2011. The forecast error of critically high sea level events is estimated to ±25 cm within the time window of ±3 h between the observed and forecasted maxima. Taylor skill assessment procedures are applied to more recent data, revealing the root mean square error of the sea level forecast lower than 7 cm and correlation higher than 97%.

The validation study of subsurface currents shows that near-bottom and coastal currents are highly constrained by topography. High current speeds (above 20 cm/s) were measured in the deep layers of the rough-bottom area around a small island. Such currents were in general well simulated by the 0.5 NM model, only slightly biased by the dominating direction. The modelled near-bottom currents are easy to transform into more realistic results if proper topography is taken into account.

The study of the circulation scheme of the Gulf of Finland shows interesting smaller loops near the Estonian coastline, compromising at the same time the general cyclonic circulation of the gulf. On the sea surface quasi-uniform drift currents are deflected on average by 40° to the right from the wind direction and they cover 60% of the circulation variance. Sea level variability is heavily (98%) dominated by nearly uniform changes, which are caused by the water storage variations in the gulf.

RESÜMEE

Peale 2005 aasta jaanuaritormi Pärnus hakati Eestis arendama kolmemõõtmelist operatiivset mereprognooside süsteemi peamise eesmärgiga luua usaldusväärne veetaseme prognoosisüsteem. Operatiivse prognoosimudeli käivitamiseks oli ka palju muid põhjuseid nagu näiteks reostusainete triivi operatiivne hindamine ja vetikate õitsengute prognoos. Tuginedes sel ajal kättesaadavatele valideerimisandmetele valiti Eesti prognoosimudeliks HIROMB. Veetaseme prognoosisüsteem käivitati operatiivselt 2005. aasta augustis ja see põhines 1 meremiilise horisontaalse võrgusammuga mudelil HIROMB-SMHI. Peale seda alustati tööd lokaalse kõrgresolutsiooniga mudeli käivitamiseks, mille tulemusel valmis 2009. aasta mais 0.5 meremiilise võrgusammuga operatiivne lokaalne mudel HIROMB-EST. Tänaseks kasutatakse Eestis operatiivselt endiselt nii 1 kui ka 0.5 meremiilise sammuga mudelit paralleelselt. Käesolevas töös on esitatud detailne kirjeldus Eestis kasutatavatest operatiivsetest meremudelitest ja nende tulemusi valideeritud. Veetaseme prognoosisüsteemi täpsust hinnati kahel erineval ajavahemikul: 2006–2008 ja 2009–2011. Kriitiliselt kõrge veetaseme prognoositäpsuseks hinnati ±25 cm ruumilist ja ±3 h ajalist viga. Kasutades Taylori mudeli osavuse hindamise meetodit leiti et veetaseme prognoosi ruutkeskmine hälve on väiksem kui 7 cm ja korrelatsioon kõrgem kui 97%.

Mudelitega simuleeritud hoovuste valideerimine ADCP mõõtmistega näitab, et põhja- ja rannikulähedased hoovused on topograafia poolt tugevalt mõjutatud. Mõõtmised karedapõhjalise merepõhja kohal väikse saare ümbruses näitavad, et hoovuste kiirused võivad kohati olla suured (üle 20 cm/s). Poole meremiiline mudel suutis selliseid hoovuseid küllaltki hästi simuleerida kuigi domineeriv hoovuse suund oli väikeses nihkes. Uuring näitas, et teades täpsemat põhja topograafiat on põhjalähedasi mudeli hoovuseid on võimalik lihtsate transformatsioonidega muuta palju täpsemaks.

Soome lahe keskmise tsirkulatsiooni arvutused näitasid küllaltki hästi üldist tsüklonaalset soome lahe tsirkulatsiooni tuues samal ajal välja huvitavaid väiksemaid tsirkulatsioonipesasid eesti rannikumeres. EOF analüüs näitas, et veepinnal on 60% hoovuste muutlikkusest jagunenud ühtlaselt suundudes keskmiselt 40° paremale domineeriva tuule suunast. Veetase muutub peamiselt (98%) ühtlaselt mis näitab et Soome Lahe veetaset mõjutab peamiselt üldine veebilansi muutus lahes, mis on tingitud kogu läänemere keskmisest veetasemest.

ACKNOWLEDGEMENTS

I express my deepest thanks to my supervisor Prof. Jüri Elken for the knowledge and interest in marine science he has kindly given to me. His friendly patience in supervising me through all years of my studies is highly appreciated.

I also thank PhD Urmas Raudsepp and PhD Tarmo Kõuts for interesting discussions on operational oceanography.

Special thanks are due to Lars Axell from the SMHI for friendly communication and helpful guidance. The importance of his contribution cannot be overestimated.

My gratitude goes to all my colleagues in the MSI as well as in other institutes belonging to the HIROMB consortium. The discussions and workshops with them have been a pleasure. Useful remarks and notes of the referees have been of great help.

The work was financially supported by the Environmental Investment Centre, Estonian Meteorological and Hydrological Institute, Estonian Science Foundation grant 7328, the European Social Fund's Doctoral Studies and Internalization Programme DoRa.

I thank my family for continuous support and understanding for the time that the studies have kept me away from them. Huge emotional support by my daughter Grete was a crucial stimulus for writing this thesis.

ELULOOKIRJELDUS

1. Isikuandmed

Ees- ja perekonnanimi	Priidik Lagemaa
Sünniaeg ja -koht	26.12.1980, Tallinn
Kodakondsus	Eesti

2. Kontaktandmed

Aadress	Akadeemia tee 15a, 12618 Tallinn, Estonia
E-posti aadress	priidik26@gmail.com

3. Hariduskäik

Õppeasutus	Lõpetamise aeg	Haridus (eriala/kraad)
Tallinna Tehnikaülikool	2005	Tehniline füüsika/MSc

4. Keelteoskus (alg-, kesk- või kõrgtase)

Keel	Tase
eesti	emakeel
inglise	kesktase
vene	algtase

5. Täiendusõpe

Õppimise aeg	Täiendusõppe läbiviija nimetus

6. Teenistuskäik

Töötamise aeg	Tööandja nimetus	Ametikoht
2006–…	Tallinna Tehnikaülikooli Meresüsteemide instituut	Insener

7. Teadustegevus

Lagemaa, P., Elken, J. and Kõuts, T. 2011. Operational sea level forecasting in Estonia. *Estonian Journal of Engineering*, 17(4), 301–331.

Elken, J., Nõmm, M. and Lagemaa, P. 2011. Circulation patterns in the Gulf of Finland derived from the EOF analysis of model results. *Boreal Environment Research*, 16 (suppl. A), 84–102.

Lagemaa, P., Suhhova, I., Nõmm, M., Pavelson, J. and Elken, J. 2010. Comparison of current simulations by the state-of-the-art operational models in the Gulf of Finland with ADCP measurements. In *IEEE/OES Baltic 2010 International Symposium: IEEE/OES Baltic 2010 International Symposium, 25–27 August 2010, Riga.* IEEE Conference Proceedings, 1–11.

Raudsepp, U., Uiboupin, R., Sipelgas, L., Lagemaa, P., Kõuts, T. and Lips, U. 2010. Use of Earth observation data and numerical modeling in the development of marine downstream services in Estonia. In *IEEE/OES Baltic 2010 International Symposium: IEEE/OES Baltic 2010 International Symposium, 25–27 August 2010, Riga.* IEEE Conference Proceedings, 1–11.

Kõuts, T., Verjovkina, S., Lagemaa, P. and Raudsepp, U. 2010. Use of lightweight on-line GPS drifters for surface current and ice drift observations. In *IEEE/OES Baltic 2010 International Symposium: IEEE/OES Baltic 2010 International Symposium, 25–27 August 2010, Riga.* IEEE Conference Proceedings, 1–11.

Erm, A., Elken, J., Pavelson, J., Kask, J., Voll, M., Kört, M., Roots, O., Liblik, T., Lagemaa, P. and Buschmann, F. 2010. Observation of high-speed deep currents and resuspension of soft sediments in the central part of the Gulf of Finland. In *The Baltic Sea Geology-10. The 10-th International Marine Geological Conference. 24–28 August 2010, VSEGEI, St. Petersburg, Russia. Abstract volume.* SPb. Press VSEGEI, 25–26.

Liiv, T. and Lagemaa, P. 2008. The variation of the velocity and turbulent kinetic energy field in the wave in the vicinity of the breaking point. *Estonian Journal of Engineering*, 14, 42–64.

Elken, J., Kõuts, T., Lagemaa, P., Lips, U., Raudsepp, U. and Väli, G. 2008 Sub-regional observing and forecast system for the NE Baltic: Needs and first results. In *US/EU-Baltic International Symposium, 2008 IEEE/OES: US/EU-Baltic Symposium "Ocean Observations, Ecosystem-Based Management & Forecasting", Tallinn, 27–29 May, 2008.* IEEE Conference Proceedings, 1–9.

Elken, J., Kõuts, T., Lips, U., Raudsepp, U., Lagemaa, P. and Liblik, T. 2007. Performance of the operational HIROMB model in relation to the oceanographic extreme events and seasonal fluxes in the Gulfs of Finland and Riga. In *Fifth Study Conference on BALTEX, Kuressaare, Saaremaa, Estonia, 4–8 June 2007* (Isemer, H.-J., ed.). Geesthacht: International BALTEX Secretariat, 77–78.

Raudsepp, U., Elken, J., Kõuts, T., Liblik, T., Kikas, V., Lagemaa, P. and Uiboupin, R. 2007. Forecasting skills of the HIROMB in the Gulf of Finland. In *Geophysical Research Abstracts: EGU General Assembly, 2007.* European Geosciences Union, 10617.

Elken, J., Kõuts, T., Raudsepp, U., Laanemets, J. and Lagemaa, P. 2006. BOOS/HIROMB-based marine forecasts in Estonia: problems, experiences and challenges. In *Proceedings of the US/EU Baltic International Symposium "Integrated Ocean Observation Systems for Managing Global & Regional Ecosystems Using Marine Research, Monitoring & Technologies", Klaipeda, May 23–25, 2006.* Center of Marine Research, Klaipeda, 1–22.

8. Kaitstud lõputööd

Magistrikraad (teaduskraad), 2005, Sukelduva murdlaine eksperimentaalne uurimine välimises rannaalas, Tallinna Tehnikaülikool, Ehitusteaduskond, Mehaanikainstituut

9. Teadustöö põhisuunad

Operatiivokeanograafia, numbriline modelleerimine, tsirkulatsioon

10. Teised uurimisprojektid

Operatiivse mereprognooside mudelsüsteemi rakendused Läänemere suuremastaabiliste ja mesomastaapsete tsirkulatsioonimustrite uurimiseks, 2008–2011

Läänemere vee- ja ainevahetusprotsessid muutuvates kliimatingimustes. Rannikumere dünaamika ja optika, 2003–2007

Läänemere vee- ja ainevahetusprotsessid muutuvate välismõjude tingimustes, 2008–2013

Läänemere tsirkulatsiooni aastakümnete skaalaga muutused ja nende deskriptorid, 2012–2015

Development and pre-operational validation of upgraded GMES Marine Core Services and capabilities (MyOcean), 2009–2012

Mereprognooside süsteemi HIROMB arendamine, 2006–2008

Mereprognooside süsteemi HIROMB tööle rakendamine EMHIs, 2007–2010

SNOOP – Shipping-induced NOx and SOx emissions - OPerational monitoring network, 2009–2012

CURRICULUM VITAE

1. Personal data

Name	Priidik Lagemaa
Date and place of birth	26 December 1980, Tallinn

2. Contact information

Address	Akadeemia tee 15a, 12618 Tallinn, Estonia
E-mail	priidik26@gmail.com

3. Education

Educational institution	Graduation year	Education (field of study/degree)
Tallinn University of Technology	2005	Physics/MSc

4. Language competence/skills (fluent; average, basic skills)

Language	Level
Estonian	native
English	average
Russian	basic skills

5. Special courses

Period	Educational or other organisation

6. Professional employment

Period	Organisation	Position
2006–to date	Marine Systems Institute at Tallinn University of Technology	Engineer

7. Scientific work

Lagemaa, P., Elken, J. and Kõuts, T. 2011. Operational sea level forecasting in Estonia. *Estonian Journal of Engineering*, 17(4), 301–331.

Elken, J., Nõmm, M. and Lagemaa, P. 2011. Circulation patterns in the Gulf of Finland derived from the EOF analysis of model results. *Boreal Environment Research*, 16 (suppl. A), 84–102.

Lagemaa, P., Suhhova, I., Nõmm, M., Pavelson, J. and Elken, J. 2010. Comparison of current simulations by the state-of-the-art operational models in the Gulf of Finland with ADCP measurements. In *IEEE/OES Baltic 2010 International Symposium: IEEE/OES Baltic 2010 International Symposium, 25–27 August 2010, Riga.* IEEE Conference Proceedings, 1–11.

Raudsepp, U., Uiboupin, R., Sipelgas, L., Lagemaa, P., Kõuts, T. and Lips, U. 2010. Use of Earth observation data and numerical modeling in the development of marine downstream services in Estonia. In *IEEE/OES Baltic 2010 International Symposium: IEEE/OES Baltic 2010 International Symposium, 25–27 August 2010, Riga.* IEEE Conference Proceedings, 1–11.

Kõuts, T., Verjovkina, S., Lagemaa, P. and Raudsepp, U. 2010. Use of lightweight on-line GPS drifters for surface current and ice drift observations. In *IEEE/OES Baltic 2010 International Symposium: IEEE/OES Baltic 2010 International Symposium, 25–27 August 2010, Riga.* IEEE Conference Proceedings, 1–11.

Erm, A., Elken, J., Pavelson, J., Kask, J., Voll, M., Kört, M., Roots, O., Liblik, T., Lagemaa, P. and Buschmann, F. 2010. Observation of high-speed deep currents and resuspension of soft sediments in the central part of the Gulf of Finland. In *The Baltic Sea Geology-10. The 10-th International Marine Geological Conference. 24–28 August 2010, VSEGEI, St. Petersburg, Russia. Abstract volume.* SPb. Press VSEGEI, 25–26.

Liiv, T. and Lagemaa, P. 2008. The variation of the velocity and turbulent kinetic energy field in the wave in the vicinity of the breaking point. *Estonian Journal of Engineering*, 14, 42–64.

Elken, J., Kõuts, T., Lagemaa, P., Lips, U., Raudsepp, U. and Väli, G. 2008 Sub-regional observing and forecast system for the NE Baltic: Needs and first results. In *US/EU-Baltic International Symposium, 2008 IEEE/OES: US/EU-Baltic Symposium "Ocean Observations, Ecosystem-Based Management & Forecasting", Tallinn, 27–29 May, 2008.* IEEE Conference Proceedings, 1–9.

Elken, J., Kõuts, T., Lips, U., Raudsepp, U., Lagemaa, P. and Liblik, T. 2007. Performance of the operational HIROMB model in relation to the oceanographic extreme events and seasonal fluxes in the Gulfs of Finland and Riga. In *Fifth Study Conference on BALTEX, Kuressaare, Saaremaa, Estonia, 4–8 June 2007* (Isemer, H.-J., ed.). Geesthacht: International BALTEX Secretariat, 77–78.

Raudsepp, U., Elken, J., Kõuts, T., Liblik, T., Kikas, V., Lagemaa, P. and Uiboupin, R. 2007. Forecasting skills of the HIROMB in the Gulf of Finland.

In *Geophysical Research Abstracts: EGU General Assembly, 2007*. European Geosciences Union, 10617.

Elken, J., Kõuts, T., Raudsepp, U., Laanemets, J. and Lagemaa, P. 2006. BOOS/HIROMB-based marine forecasts in Estonia: problems, experiences and challenges. In *Proceedings of the US/EU Baltic International Symposium "Integrated Ocean Observation Systems for Managing Global & Regional Ecosystems Using Marine Research, Monitoring & Technologies", Klaipeda, May 23–25, 2006.* Center of Marine Research, Klaipeda, 1–22.

8. Defended theses

Master's thesis, 2005, Experimental Investigation of Plunging Breaking Waves in Outer Surf Zone, Tallinn University of Technology, Faculty of Civil Engineering, Department of Mechanics

9. Main areas of scientific work/Current research topics

Operational oceanography, numerical modelling, circulation

10. Other research projects

Application of an operational oceanographic model system to study the Baltic Sea large- and mesoscale circulation patterns, 2008–2011

Baltic Sea water and material exchange processes in changing climatic conditions. Dynamical and optical processes in coastal sea areas, 2003–2007

Baltic Sea water and matter exchange processes in conditions of changing external forcing, 2008–2013

Decadal changes and descriptors of Baltic Sea circulation, 2012–2015

Development and pre-operational validation of upgraded GMES Marine Core Services and capabilities (MyOcean), 2009–2012

Development of HIROMB marine forecast system, 2006–2008

Installation of operational marine forecast system at EMHI, 2007–2010

SNOOP – Shipping-induced NOx and SOx emissions - OPerational monitoring network, 2009–2012

Paper I

Lagemaa, P., Elken, J. and Kõuts, T. 2011. Operational sea level forecasting in Estonia. *Estonian Journal of Engineering*, 17(4), 301–331.

Estonian Journal of Engineering, 2011, **17**, 4, 301–331 doi: 10.3176/eng.2011.4.03

Operational sea level forecasting in Estonia

Priidik Lagemaa, Jüri Elken and Tarmo Kõuts

Marine Systems Institute at Tallinn University of Technology, Akadeemia tee 15a, 12618 Tallinn, Estonia; priidik26@gmail.com

Received 4 May 2011, in revised form 17 October 2011

Abstract. The operational sea level forecasting system in Estonia, based on the HIROMB model forecasts and on 11 online sea level observation stations, is described and validated. The system is operational since 08.08.2005. Statistical analysis for the period 2006–2008 data is performed to investigate the properties of low-frequency sea level error and error estimation of high sea level events. A 7-day backwards moving average filter is the most appropriate for Estonian waters to correct the raw sea level forecast. For the time period 2006–2008 the forecast error of critically high sea level events is ±25 cm within ±3 h between the observed and forecasted maxima. Taylor skill assessment procedures are applied to the data, covering the period 2009–2011. The data is divided into three forecast sub-ranges (low, medium and high sea level), to investigate the possibilities of the online error estimation. Smaller errors are present for medium and low sub-range and larger errors for the high sub-range. The necessities for further development are outlined.

Key words: sea level, water level, modelling, HIROMB, Baltic Sea, Estonia, operational forecasting.

1. INTRODUCTION

Sea level variations around the decadal mean values are of great importance for the coastal population. The eastern Baltic Sea has very weak tides but strong and quite often damaging storm surges, combined with other types of sea level variation. Variable isostatic Earth crust vertical motion pattern over the region [1], combined with the global eustatic sea level change [2] results in long-term trends of observed sea level, yielding a maximum decrease –8.2 mm yr^{-1} in the northern part of the Bothnian Bay [3], a slight decrease from –0.5 to –2.8 mm yr^{-1} in Estonia [4] and a slight increase in the southern part of the sea [5].

Due to the limited transport capacity of the Danish Straits, the variability of the Baltic sea level can be generally decomposed [6] into the external variations,

due to the change in mean sea level of the basins, forced by the outside Kattegat sea level and the basins freshwater budget, and into the internal variations around the mean state, dominated by wind-driven long rotational gravity waves, influenced by the complex coastline and topography. The internal component has also smaller contributions from saline and freshwater pulses and variations in water density and air pressure. Although the external sea level component is in principle oscillatory (the "harbor" or semi-open bay mode [7]), at time scales of forcing weather patterns (periods less than a month) the Baltic sea level response is damped and delayed [6]. Observed sea levels are well correlated along the coastline [8]. Stronger westerly winds and related larger inflows occur usually during autumn and winter. As an example, during the major inflow in January 1993 [9], 310 km^3 of North Sea water entered the Baltic in 21 days, raising the mean sea level by 70 cm. Such rapid increases in the sea volume during the storms contribute also to the actual storm surges [10].

Internal sea level variations are influenced by semi-isolated seiche systems, Belt Sea–Baltic Proper–Gulf of Finland (passing the Gulf of Bothnia) and Belt Sea–Baltic Proper–Gulf of Bothnia, with self-oscillation periods about 25–27 h and 31–39 h [11]. However, due to the complicated multi-basin topography, the seiches do not have high contribution to the sea level power spectrum [12]. Jönsson et al. [13] have recently discussed that instead of full-basin seiches, the internal sea level variability is dominated by weakly coupled semi-open bay modes. For the Gulf of Riga, such open bay mode results in persistent 24-h current oscillations in the connecting Irbe Strait [14,15], while the internal (closed bay) seiche period is about 5 h [10].

Short-term prediction of the sea level in marginal seas and coastal areas is a continuous issue of oceanographic research and technological developments. Compared to the earlier semi-empirical forecast methods, a revolutionary approach, numerical modelling based on two-dimensional (2D) shallow water equations, was proposed for sea level modelling and forecasts in the 1950s [16,17]. However, first realizations of numerical modelling in the everyday forecast services started only in the 1980s [18]. Following the experiences of operational numerical sea level forecasting, based on 2D shallow water equations, Germany's Federal Maritime and Hydrographic Agency (BSH) implemented a three-dimensional (3D) baroclinic forecast model BSHcmod at the beginning of 1990s [19]. That model became a core of the family of operational models, run in addition to BSH also at the Swedish Meteorological and Hydrological Institute (SMHI) and Danish Meteorological Institute (DMI). An overview of different model versions and set-up features has been recently given in [20]. The model developments are coordinated by the HIROMB (High-Resolution Operational Model for the Baltic Sea) consortium. A broader Baltic-wide cooperation frame in operational oceanography is provided by the BOOS (Baltic Operational Oceanographic System) [21] that takes care, among many other activities, of on-line exchange of observational and modelled data and dissemination of operational products. Further development of the Baltic marine forecasting is

presently going on within the EU-funded MyOcean (Development and pre-operational validation of upgraded GMES Marine Core Services and capabilities) project. It aims at the merging of the best features of different model versions into one harmonized operational model system HIROMB-BOOS, including assimilation of the real-time observational data and launching the forecast component for biochemical state variables.

Introduction of numerical sea level forecasts in Estonia was delayed in the official service level until the highest known storm surge occurred in January 2005 at the western coast of Estonia [22,23]. Operational sea level gauge at Pärnu recorded highest sea level height of +275 cm, the highest observed so far since the beginning of instrumental observations in 1923. The coastal towns Pärnu and Haapsalu were heavily flooded and considerable damages and economic loss occurred. The Estonian Ministry of Environment initiated an implementation of numerical ocean forecasting and related observational services in Estonia in cooperation with the Marine Systems Institute (MSI) at Tallinn University of Technology and the Estonian Meteorological and Hydrological Institute (EMHI). The primary goal was a considerable reduction of the errors in short-term forecasting of the extreme sea levels (both the high sea levels causing floods in the coastal areas, and low sea levels stopping the ship traffic between the Estonian mainland and the western larger islands). Numerical sea forecasts are needed also for many other practical problems like harmful algal blooms, drift of surface and subsurface substances and objects, or ice conditions. Therefore it was decided to implement an advanced 3D forecast system.

Among the Baltic-wide oceanographic service providers, SMHI was chosen as a core provider for Estonia, since their operational model HIROMB has the highest horizontal grid resolution (1 NM). The Estonian coastline is very fragmented, with numerous small bays, peninsulas and islands, therefore high horizontal resolution is very important for producing detailed information on sea level, currents, temperature, salinity and ice conditions. The numerical sea level forecasts started in autumn 2005 and the forecast system is presently in a quite mature state. Nevertheless, gradual developments towards the next-generation forecast system are progressing on the national, Baltic-wide and European levels.

The aim of the paper is to give an overview of the present Estonian sea level forecasting system, present the practice of applied forecast production methods and estimate the system performance and statistical accuracy. Following the forecast system description, specific aspects of the low-frequency error correction, examples of forecast performance during extreme sea levels and statistical evaluation of the forecast accuracy along the different coastal areas and sea level variation range are analysed in detail. Finally, conclusions and outlook of further investigations and developments are presented.

2. OPERATIONAL FORECASTING SYSTEM DESCRIPTION

2.1. The operational model

The operational oceanographic forecast models, belonging to the HIROMB consortium, have been running for the Baltic Sea since the 1990s with the primary purpose of giving short-term (up to 48 or 60 h) predictions of the sea conditions, in order to handle oil spills, storm surges, support navigation etc. The core of the model system is a 3D baroclinic eddy-resolving circulation model, based on the original BSHcmod [19] that calculates also currents, temperature, salinity and turbulence in the water column. The model contains also a sea ice module.

The SMHI version, HIROMB (or HIROMB-SMHI) has been running since 1995 in a pre-operational mode, and since 1999 the model is fully operational [24]. The model is forced mainly by the data from atmospheric circulation model SMHI-HIRLAM with a horizontal resolution of 22 km and with a 1 h time step. For the freshwater inflow, daily data from the river runoff model HBV is used. At the outer open ocean boundaries a storm surge model (NOAMOD) is used for the water levels together with tides, climatologic salinity and temperature data. The sea surface wind stress is calculated by the common quadratic formulation from the corresponding 10 m height wind speed components W_λ and W_φ as $\tau_\lambda = \rho_a c_D W_\lambda W_{10}$, $\tau_\varphi = \rho_a c_D W_\varphi W_{10}$, where λ and φ are longitude and latitude respectively, τ_λ and τ_φ are the wind stress components, ρ_a is the air density, $W_{10} = \sqrt{W_\lambda^2 + W_\varphi^2}$ is the wind speed, and c_D is the surface drag coefficient.

During the study period, there had been several model code upgrades, starting from version 3.0 to 4.2. The main parameters of the model's operational versions are presented in Table 1. The model version 3.0, started at 15.11.2005, was set up in three nested grids with horizontal resolution of 12, 3 and 1 NM, respectively. The model domain of highest resolution covers the whole Baltic Sea area with grid step 1′ along latitudes and 5/3′ along longitudes (Fig. 1a,b). The model presented the Baltic Sea by 16 vertical layers, with 4 m thickness in the upper 12 m and increasing values towards the greater depths. The linear formulation was used to find the surface drag coefficient $c_D = (0.7 + 0.09 W_{10}) \times 10^{-3}$. The value of bottom friction coefficient r was 0.0028. In the course of the model development, improved descriptions were introduced for vertical turbulence and drag coefficients on the surface and on the bottom [20,25–27].

Starting from the operational model version 3.3 (upgraded at 18.09.2007), the breaking surface waves, the water-ice roughness parameter and the variable surface drag coefficient were introduced. The surface drag formulation was changed to account for the atmospheric stability. Actually, the improved surface drag formulation was introduced already in model version 3.1, but this version never got operational and the new formulation was delivered to the users with version 3.3. To improve the representation of surface current velocities, the neutral surface drag was defined as $c_D = 1.3 \times 10^{-3}$ at $W_{10} < 8$ m/s and $c_D = (0.84 + 0.058 W_{10}) \times 10^{-3}$

Table 1. Operational versions of HIROMB and changes affecting the sea level

Version	3.0	3.3	4.0	4.2
Release date	15.11.2005	18.09.2007	08.12.2009	15.09.2010
Horizontal grid resolution, NM	1; 3; 12		1; 3	
Vertical grid resolution, m	24 layers (3×4, 3×6, 3×10, 2×15, 2×20, 2×30, 2×40, 7×60)		50 layers (20×4, 5×5, 3×6, 2×7, 8, 9, 10, 11, 14, 17, 21, 26, 32, 39, 9×40)	
Bottom friction coefficient	$r = 0.0028$		$c_{D,\text{bottom}} = \dfrac{\kappa^2}{\log^2\left(\dfrac{h_b}{2z_{0,b}}+1\right)}$, $z_{0,b} = 0.01$ m	
Meteorological forcing	HIRLAM (SMHI), horizontal resolution 22 km till 30.05.2011 after that date 11 km.			
Wind drag coefficient formulation	$c_D = (0.7 + 0.09W_{10})\times10^{-3}$		$c_D = 1.3\times10^{-3}$ if $W_{10} < 8$ $c_D = (0.84 + 0.058W_{10})\times10^{-3}$ if $W_{10} \geq 8$	

in case of higher values of W_{10}. The drag coefficient was then slightly modified, according to the stability of the atmosphere, as calculated from the air-water temperature difference. Other modifications in the model code were not relevant to the sea level. The bottom friction coefficient, grid resolution and forcing (i.e. atmospheric, open sea boundary, rivers) parameters remained unchanged.

Starting from 9.07.2008 the model run frequency was increased from 2 to 4 times per day, i.e. the model was re-run every 6th hour whereas all other model parameters remained unchanged. However, the forecasting system still used only the +00 h forecast files until 17.12.2008 when the increased re-run frequency was introduced to the Estonian forecasting system.

With the introduction of version 4.0, upgraded officially on 08.12.2009, the vertical resolution of the model improved significantly and the coastline was also improved at some regions. Now the model presents the Baltic Sea by 50 vertical layers, with the layer's thickness of 4 m in the upper 80 m, and slowly increasing towards the greater depths. The 3 NM grid boundaries were extended to 65°53′30″N, 4°9′10″W, giving nearly the same coverage as the earlier 12 NM grid. The coverage of the 1 NM grid remained unchanged. The formulation of the surface drag coefficient was not changed, but the local bottom drag coefficient formulation was introduced to calculate the momentum transfer from water to bottom, now enabling the calculation of local drag coefficient $c_{D,\text{bottom}}$ from the local thickness of the bottom cell h_b and the bottom roughness parameter $z_{0,b}$. Though, in the operational model the bottom friction coefficient was kept constant (in 1 NM grid $z_{0,b} = 0.01$ m and in 3 NM grid $z_{0,b} = 0.03$ m). Also the

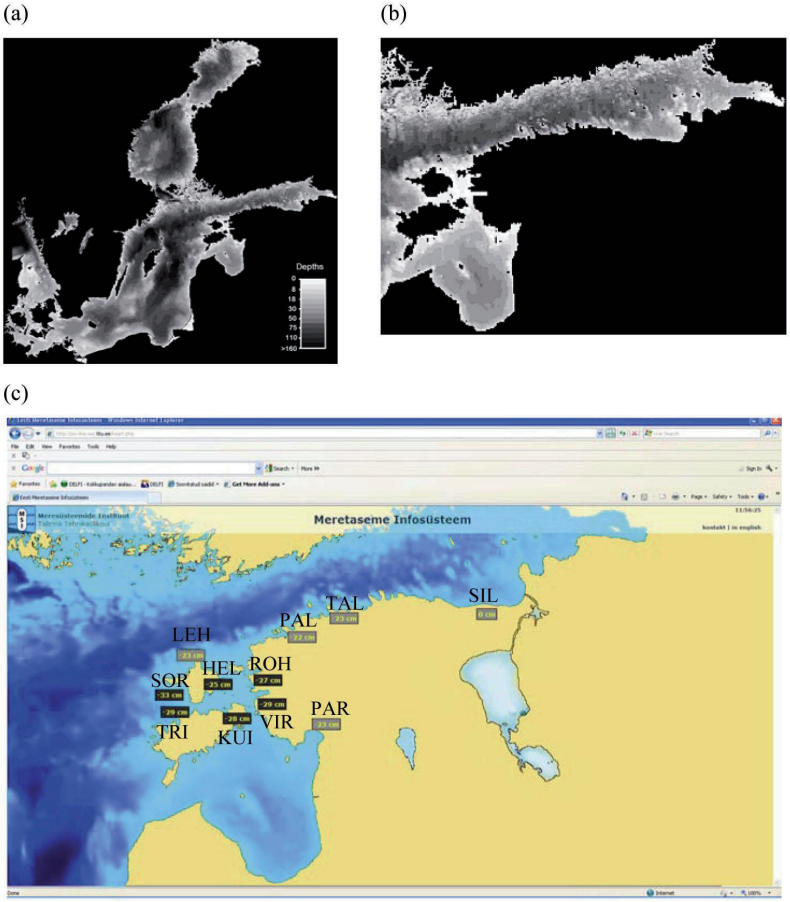

Fig. 1. Maps of the HIROMB-SMHI BS01 model grid for the whole Baltic Sea (a) and zoomed for the Estonian sea areas (b). Coastal on-line stations with used station name abbreviations, added to the web page (http://on-line.msi.ttu.ee/kaart.php) screenshot showing sea level observation results (c).

corrected air-ice stress and improved ice-ocean stress were introduced and the Successive Corrections data assimilation scheme for temperature and salinity was replaced by the Optimal Interpolation method. The Estonian forecasting system started to use version 4.0 model data on 10.12.2009.

Starting from 15.09.2010, the official version of HIROMB is 4.2. That contains no new parameterizations affecting the sea level. The changes in the

HIROMB have been continued. From 20.05.2011 the 11 km horizontal resolution HIRLAM forcing was taken into use, the forecast length was increased from 48 to 60 h and the amount of data used in data assimilation has been increased.

2.2. Online coastal observations

The coastal observational network, run by MSI, has undergone a significant evolution since 2005 and presently consists of 11 on-line stations (Fig. 1c, Table 2). A typical configuration of the automatic sea level station contains a staff gauge as an installation platform and a submerged piezoresistive pressure sensor at zero level of the staff. We use high-precision pressure sensors from Keller Ltd series 36WX and 46X with measuring amplitude of 5 m. Automatic temperature (resolution 0.1 °C) and air pressure compensation ensure an accuracy of 1 cm in terms of water column above the sensor. The pressure sensor is connected via a RS485 interface with the data logging, processing and transmitting device, which calculates sea level as a 30 s average water column height, as well as the basic wave parameters locally at the station, and sends the data with 5 min interval over GPRS communication protocol to a ftp server at MSI. On the server side, on-line data transfer is handled by GPRS Gateway software.

Table 2. Online sea level stations operated by MSI

Station name and acronym	WGS84 position	Sea level sensor	Reference	Last levelling	Zero level on staff gauge, cm	In operation since
Heltermaa HEL	58°52.0′N 23°02.8′E	Keller 36WX pressure sensor	3 m staff gauge	27.05.2010	144	Oct 2008
Kuivastu KUI	58°34.0′N 23°24.0′E	2×Keller 46X pressure sensor	3 m staff gauge	28.05.2010	122	Jan 2010
Lehtma LEH	59°04.1′N 22°41.8′E	HMS-1820 sea level station	3 m staff gauge	17.04.2009	107	Jun 2007
Paldiski PAL	59°20.1′N 24°04.8′E	Keller 36WX pressure sensor	3 m staff gauge	05.05.2010	128	Aug 2005
Pärnu PAR	58°23.3′N 24°29.2′E	Aanderaa Data Instruments sea level station	4 m staff gauge	23.04.2010	119	Jul 2000
Rohuküla ROH	58°54.3′N 23°25.5′E	Keller 36WX pressure sensor	3 m staff gauge	27.05.2010	144	Jan 2009
Sillamäe SIL	59°25.4′N 27°44.4′E	Keller 36WX pressure sensor	–	–	–	Jun 2007
Sõru SOR	58°41.5′N 22°31.3′E	2×Keller 46X pressure sensor	3 m staff gauge	27.05.2010	130	Feb 2010
Tallinn TAL	59°26.7′N 24°45.8′E	Keller 36WX pressure sensor	3 m staff gauge	05.05.2010	140	Mar 2004
Triigi TRI	58°35.5′N 22°42.2′E	2×Keller 46X pressure sensor	2.6 m staff gauge	28.05.2010	161	Jan 2010
Virtsu VIR	58°34.6′N 23°30.5′E	Keller 36WX pressure sensor	3 m staff gauge	28.05.2010	121	Jan 2009

Messages, coming from a number of GPRS modems in the field are converted into ASCII files and transmitted to ftp server(s), and also to the ftp box at MSI, from where the international data exchange occurs. After the initial quality control (obvious outliers are removed), the data is automatically fed into the BOOS system. The data is further delivered also to the EU project MyOcean.

Automatic sea level measurements are regularly checked by the readings of the staff gauge. It is a scale with 1 cm resolution for visual observations of the sea level (Fig. 2). The staff gauge is connected with the geodetic height system by means of high precision leveling, which is repeated regularly, typically once per year. The purpose of the comparison of the data from two independent measurements is the analysis of the long term trends in sensor performance and monitoring of local geodetic peculiarities, coming from vertical movements of hydrotechnical constructions, which the sea level station is fixed to.

The sea level sensors work quite reliably, showing only 2%–3% missing data without taking the major failures as powering of the station or sensor break-downs into account. The 97% up-time of the observation station is within the limits of the institutional goal but the procedures for major failures could be improved. Some stations are very old and should be replaced to decrease the amount of major failures. It would be ideal to replace at least the sensor of the station after a 5 years service. Though today, in case of a major failure of the

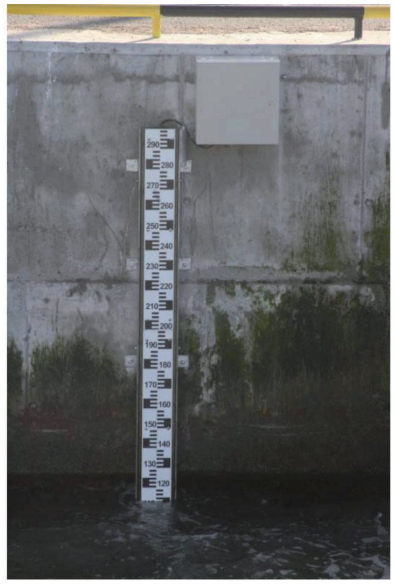

Fig. 2. Typical sea level observation station. The sensors are submerged behind and below the staff gauge and connected by cable to the box of the data handling unit (right above the staff gauge).

station, first the finances are to be found and then the station can be replaced, which takes much time and causes long gaps in measurements. Major sensor failures occurred in SOR, TRI (both from 20.07.2010 to 9.09.2010) and TAL stations (19.10.2009 to 14.11.2009, from 3.04.2010 to 19.04.2010 and from 22.10.2010 to 22.12.2010). In case of failures in the operational data transmission, the data is retrieved for climatological studies from the SD memory cards of on-site data loggers. The redundancy of the system is very much dependent on the sensors performance. In most of the stations there is only one sea level sensor and if it fails, no observation data is recorded. In some stations sensors are duplicated.

2.3. Initial system development, low-frequency error correction

Starting from 08.08.2005, the HIROMB data was downloaded daily, retrieving model results with 48 h forecast length. Shortly after this the first version of the forecasting system became operational with the forecast update interval $L = 24$ h and forecast length $M = 48$ h. The system was then continuously monitored and developed to improve its stability and reliability. After 17.12.2008, the forecast update interval was decreased to 6 h and the analysis was performed for the time period from 2006 to 2008.

A modelled sea level η_{mod} has always a bias relative to a geodetic reference system. After some months of running the forecasting system, a comparison of the time series of the model output η_{mod} and the observed sea level η_{obs} revealed that the model error has a low-frequency part that varies from location to location and is changing slowly in time. As an example, in the PAR station the "zero drift" varied during the three first implementation months (from September to November 2005) up to 25 cm (it dropped from 55 to 30 cm in about a month). It is obvious, that such a distortion of the forecast is inacceptable. The initial system running period was too short for a comprehensive statistical analysis, therefore a simple method for backward moving average (not centered, since future observations are not known during the forecast) of the model errors over 7 days was applied for the correction of the low-frequency errors. The maximum difference between the centered and the backward moving average in PAR was 8 cm, which is still small compared to the sea level variation range (from – 71 to 173 cm in 2006–2008). A statistical analysis for the period from February 2006 to March 2008 confirmed the usefulness of the applied procedure, details of which are presented below.

We have discrete sea level observations $\eta_{obs}(n)$ at the specific point (station) and raw model forecasts $\eta_{mod}(n, p)$ progressing in time, where n is the time index corresponding to a time t and p is the index denoting the forecasts with different lead time. While $\eta_{obs}(n)$ is updated in real time after each time step (in our case 1 h), $\eta_{mod}(n, p)$ is updated incrementally over L time steps (model restart interval, in our case 24 h in period 2006–2008) extending M steps forward (forecast length, in our case $M = 48$). Usually $M > L$ and several

forecasts with different lead time are available for the time n. This way for one observation time series we can assemble $P = \max(p) = M/L$ forecast time series, including the forecasts with the lead time from $(p-1)L+1$ to pL. In our case we have $P = 2$ forecast time series $\eta_{mod}(n,1)$ and $\eta_{mod}(n,2)$, denoted with the forecast indices $p = 1$ and $p = 2$, with the lead times 1–24 and 25–48, respectively. In the operational procedure we have a new forecast after each time step, that starts from the time N and extends to $N+M$. The forecast start time indices $m(n, p)$ are incrementing with a step L and can be found as

$$m(n, p) = L \cdot \lfloor (n-S)/L \rfloor + S - (p-1)L, \tag{1}$$

where the floor brackets denote the down-rounded integer operator and $S \le n$ is the time span between the start time of the model calculations and the last observation taken into account. Note that due to the time, needed for the model calculations (first HIRLAM and then HIROMB) and data transfer, we have an approximately 7 h long time lag in the operational procedure between model calculations start times $L \cdot \lfloor n/L \rfloor$ and the calculation of the forecast. Therefore the time, corresponding to the number of observations N, is usually not the same as model calculations start time $(N \notin L \cdot \lfloor n/L \rfloor)$ and we have more observations to use by the time the forecast is calculated. We have chosen to use $S = 4$ h for stability of the system (not 7, since sometimes the model data is received sooner and/or the observation data is delayed). The model results with the shortest lead time $p = 1$ (also called "best available forecast", the lead time from 1 to L) together with the observations $\eta_{obs}(n)$, $n = M+1, \ldots, N$, $N >> (M, L)$ allow an analysis of the model errors $d(n,1) = \eta_{mod}(n,1) - \eta_{obs}(n)$. The analysis of an autocorrelation of $d(n,1)$ time series over the 2 years period at the PAR station (Fig. 3) shows that the error properties are far from the ideal white noise. The correlations above 0.2 appear in a quite long (up to 4000 h) time lags indicating some systematic error component.

For finding the improved forecast $\eta_{fc}(n, p)$, we apply a correction

$$\eta_{fc}(n, p) = \eta_{mod}(n, p) - b(n, p), \tag{2}$$

where

$$b(n, p) = \frac{1}{K}\sum_{k=1}^{K} d(m-k) = \frac{1}{K}\sum_{k=1}^{K} [\eta_{\mathrm{mod}}(m-k) - \eta_{obs}(m-k)], \tag{3}$$

is the low-frequency part of the model error (or dynamic bias), found using the backward moving average of the initial model error. The indices m should be found according to Eq. (1). In the operational procedure we use only the dynamic bias from the best available forecast $b(N+1,1)$ to correct all the forecasts within the interval $n = (N+1, N+M)$. For the performance optimization, it is necessary to choose the filter length K so that the forecast errors $e(n, p) = \eta_{fc}(n, p) - \eta_{obs}(n)$ twould be minimized. The selected cost function is the least

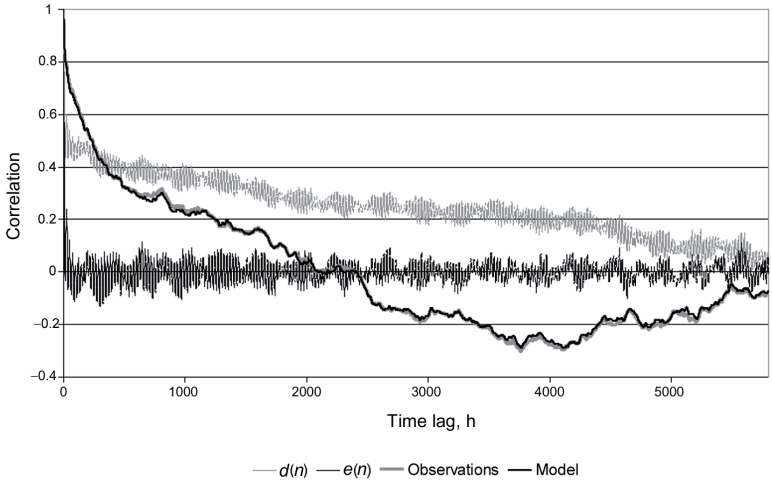

Fig. 3. The autocorrelation of observations, corrected model forecast, raw model error $d(n)$ and forecast error $e(n)$ at PAR station.

mean square error (MSE) estimate and we search for the best K that minimizes the expression

$$E(K) = \frac{1}{N-A}\sum_{n=A}^{N}[\eta_{fc}(n) - \eta_{obs}(n)]^2 = \frac{1}{N-A}\sum_{n=A}^{N}[\eta_{mod}(n) - b(n) - \eta_{obs}(n)]^2$$

$$= \frac{1}{N-A}\sum_{n=A}^{N}\left\langle\left\{\eta_{mod}(n) - \frac{1}{K}\sum_{k=1}^{K}[\eta_{mod}(m-k) - \eta_{obs}(m-k)]\right\} - \eta_{obs}(n)\right\rangle^2$$

$$\rightarrow \min, \qquad (4)$$

where $A = \max(K) + 1$ is the maximum filter length, chosen for the search $(\max(K) << N)$ and m can be found from Eq. (1).

The method (1)–(4) is similar to the autoregressive moving average (ARMA) method, but differs from it by the non-unit increments L and M. Instead of the determination of K from the autocorrelation functions, we used numerical evaluation of Eq. (4) for $K = 1,\ldots,960$ with $L = 24$. Both at the PAR and the TAL stations, the value of $\sqrt{E}$ has a minimum in the band of moving average filter lengths from about 50 to 200 h. Therefore, considering possible data gaps, $K = 168,$ adopted during the system start-up period, is a good choice, decreasing the RMSE by about twice compared to the raw forecast $(K = 0)$. As a result, the autocorrelation of the forecast error $e(n)$ drops rapidly close to zero (Fig. 3) and is much closer to the white noise properties than the autocorrelation of the raw forecast error $d(n)$.

The low-frequency error correction method, described above (and used in the forecasting system), is designed to minimize the errors of the sea level forecast for the operational purposes only. The method is purely statistical, giving a temporary solution until the actual model physics, numerical implementation and forcing data are improved. Regarding more comprehensive correction techniques, there are some test studies for the sea level data assimilation in the North and Baltic Sea region [28], but such assimilation is not yet implemented in the operational practice.

There have been several discussions during the last decade concerning the low-frequency forecast errors of the sea level. The origin of such a dynamic bias is still not clear; there could be several reasons like distortions in the boundary conditions provided by the "outer" storm surge model NOAMOD, density inaccuracies in the model response, inaccurate volume changes in the Baltic Sea and its sub-basins due to the errors in volume transports in the straits, errors in the freshwater budget, etc. Although the analysis of these reasons is out of the scope of this paper, an attempt was made to find the relationship between the dynamic bias and the Baltic Sea volume change during the optimization of the low-frequency error calculation method. The Baltic-wide mean sea level time series were found and compared with the dynamic sea level bias time series in different stations (Fig. 5). Although several variations of $b(n,1)$ and horizontally mean sea level occur at the same time, their phases vary significantly and the statistical correlation is practically absent. Therefore it was found that the forecast of the horizontally mean sea level cannot be used for the prediction of $b(n,1)$.

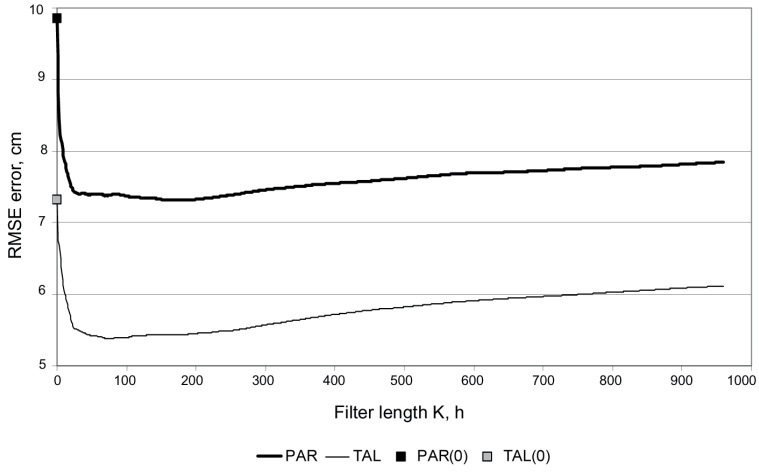

Fig. 4. The RMSE dependence on the backward moving average filter length K.

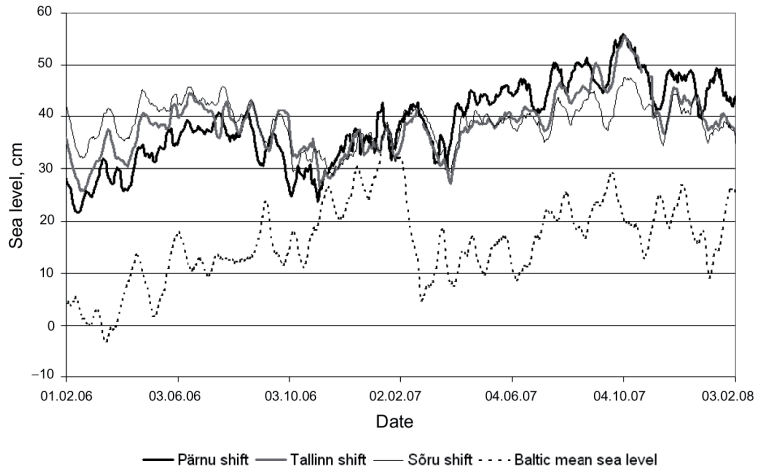

Fig. 5. Time series of low-pass filtered (7 days moving average) sea level difference between model raw output and sea level observations (shift) for Pärnu, Tallinn and Sõru and model raw output for Baltic mean sea level.

The low-frequency error variations at PAL station during a later period (03.2009–03.2011) are presented later. There were two model upgrades during this period, which can be distinguished from the dynamic bias curve. Although the version 4.2 did not introduce any changes, affecting directly sea level, the variability range of the dynamic bias seemingly increased, a feature that requires further investigation.

2.4. Forecast production

Results from the HIROMB-SMHI model with 1 NM resolution (grid BS01) are used in the production of the sea level forecasts for the Estonian coast. The forecasting system is operationally run 4 times per day with cron scheduler in Linux cluster. The system has 4 main steps, all covered with error handling procedures:

1) download the model data;
2) download the observational data;
3) process the model and observation data;
4) publish the forecast and archive the data.

The model data is downloaded from the SMHI ftp server, saved and unzipped. The data is provided in GRIB format, having separate file for each time step and resulting in M model files. Each file is downloaded and checked separately. The system automatically assesses the quality of the file and either re-downloads the file or starts downloading the next file. The re-download is repeated maximum

5 times per file after which the error message is sent to the administrator. The downloading state is the most time consuming and fragile step in the forecasting system due to the size of the 3D files and network stability. However, there has been significant progress in the network stability and speed. Although the file sizes were approximately twice smaller in 2006, the download took about 2 h, while today it completes usually within 10 to 20 min.

The crucial element for the operational forecasting is the sea level observations. New observation is available every 5 min, as described in Section 2.2. The forecasting system, however, only downloads the data with a 1 h interval, assembling separate 1 h interval observations data file, which is not always with the same quality as the data in observational system itself. Similarly with the model data, in case of errors in the observational data the re-download is performed maximum 5 times, after which the data is defined missing for the forecasting system. For example, if the data is too late in the observational ftp, then this data is defined as missing, although files of this data exists in observational system archive. For the offline analysis, the differences between the observational and the forecasting system's data archive could be decreased by creating a direct link between the subsystems, but this has not been implemented yet.

In the data processing step the model data is first extracted from the 3D model data files and appended to the model extractions time series files $\eta_{mod}(n, p)$ for each station. After constructing the model extractions and the observation data, a simple automated quality control is performed: the unreasonable high or low values and data gaps are flagged. However, the manual revision of the data during the current study showed the need for some improvement of this quality control, although only 0.7% of data was considered "bad" during manual revision. Before adding more sophisticated quality controls to the operational forecasting system, these controls have to be well calibrated and validated, to avoid filtering out actual rapid sea level changes, which naturally happen mostly in the areas and periods of high flooding risk.

After the bad quality data has been flagged and removed from further calculations, the low-frequency error $b(N+1,1)$ (from Eq. (3)) and the corrected forecasts are calculated as $\eta_{fc}(n, p) = \eta_{mod}(n, p) - b(N+1,1)$ for each station, where $n = N + (p-1)L + 1, \ldots, N + pL - S$ (the special case of Eq. (2)). Although it is possible to use Eq. (4) operationally for finding the best filter length K for each forecast separately, in order to ensure stability of the long-term statistics the recalculation procedure is not implemented operationally. The processing step continues with gathering the forecasts of all lead times and stations into one forecast file. Due to up to 7 h time span between the start times of the model and the forecast calculations (see also the explanation of Eq. (1)), only the forecast lead times greater than 5 h are written into forecast file, which unfortunately means that only the 6th hour forecast from the "best available" forecast reaches the users.

The data gaps are usually the most problematic in the operational systems. The forecasting system has some simpler redundancy functions in case the model

or observation data is missing. In case the model data is missing for some reason, the data from the previous forecast is used to produce the forecast; so in principle the first L records are deleted from the previous forecast file and used as the new forecast file. This means that the replacement $\eta_{fc}(n, p) = \eta_{fc}(n, p+1)$ is performed and, of course, the forecast length M is decreased by L. If the model data is missing also during the next forecasting system run time, the replacement $\eta_{fc}(n, p) = \eta_{fc}(n, p+2)$ is performed etc., until the model data has been missing for $M = 48$ h in a row. After that period the forecast will be provided with missing value codes and an alert message will be sent to the administrator. Another source for missing forecast is gaps in observations. In case there are less than 48 acceptable observation-forecast pairs in the last 7 days or the observation data has been missing for the last 48 h, the forecast will be again provided with missing value codes.

In connection with the forecast production, an automated high/low sea level checking is done for each forecast. Critical values for every coastal station are defined (Table 3) and when the forecast is out of the defined limits, an automated high/low sea level warning message is sent to the users. The skill of the high and low sea level forecast and warning system was evaluated by comparing the number of high/low sea level events forecasted and observed (Table 3). In general the amount of high sea levels within the period from 2009 to 2011 was low and no coastal flood was observed, but there were several low sea level events which actually influenced the ship traffic between small islands and mainland. Most of the occurred high/low sea level events were alerted properly, but still 18% of high/low events were underestimated by the forecast and the warning message was not sent. The reason behind the missed warning messages was that the sea levels were slightly below the warning limits. Thus it can be concluded that no really important high/low sea level event was missed by the forecasting system. The users can choose how often they want to get the warning message. By default, the maximum warning message frequency is once in 24 h. Without this option the system could send out up to 8 messages for the same

Table 3. Low and high sea level warning limits and the performance of the warning system. If forecast value is outside the limits the warning message will be sent to the users by the system

Station acronym	HEL	KUI	LEH	PAL	PAR	ROH	SIL	SOR	TAL	TRI	VIR
Limit of low sea level warning, cm	−50	−60	−50	−60	−90	−50	−60	−50	−60	−50	−60
Limit of high sea level warning, cm	70	70	50	50	90	70	80	50	70	50	70
Number of low sea level warnings forecasted/observed	1 2	0 0	2 3	3 3	1 1	2 2	3 3	2 2	1 1	0 1	1 3
Number of high sea level warnings forecasted/observed	12 10	8 13	5 7	4 4	2 2	13 13	6 5	3 7	4 4	3 5	9 13

high/low sea level event. Only one warning per one high/low sea level event is recommended for a typical end-user.

As a final step of the forecasting system, all the data is archived and the forecast is published to the users (via ftp and web). Both the measurements of the sea level along the Estonian coast and the forecasts are presented in an open access webpage Sea Level Information System http://on-line.msi.ttu.ee/kaart.php?en. In normal situation, when the sea level is around 0 cm, the number of clicks in the system per day is about 1000, but during storms it increases 1000 and even 10 000 times, resulting in 10 million clicks per day. The users of the system are mainly the people living in the coastal areas, but also larger institutions like Estonian Rescue Service. This system has been used for issuing warnings about high sea level in the Estonian coastal sea, and by national and local authorities for decision-making. The company that operates ferries between the Estonian mainland and islands relies on the forecasts of critically low sea level.

2.5. Analysis methods

Standard statistical methods were used to study the archived operational results of the observations and forecasts. An analysis was made for two different time periods: 01.10.2006–01.03.2008 and 1.03.2009–1.03.2011.

The RMSE minimizing algorithms described above and the autocorrelation function technique were used mainly for the time period 2006–2008 data to find the optimal algorithm for low-frequency error calculations. Storm surge events were analysed to investigate the skill of the forecasting system for predicting the high sea level events. The events were handled separately to find the forecast error with respect to observations. Also the temporal errors of the storm peaks (time span between the maximal sea level in the forecast and in the observations) were found and recorded manually.

Starting from 17.12.2008, the forecasting system was improved to use model data and produce forecast 4 times per day, i.e., after each 6 h. Also the observation network was extended to 11 stations. For the analysis period from 2009 to 2011, different statistics were calculated, mainly for the forecasts with lead time +01 h to +06 h. The time percentage analysis was done to evaluate the forecasting system up-time and different sources of the forecasting system failures. For statistical calculations all data was revised, gaps and corrupted data were removed and the data time series (model, forecast and observation) were trimmed to the same length for each station separately. For example, if the observation data for certain time was missing, then both the forecast and the model data were excluded from the analysis, although one of those could have been quality data. This trimming procedure was essential to find comparable statistics.

Mean absolute error (MAE) was calculated by taking arithmetic mean of the absolute deviations between each observation and forecast and monthly mean absolute error (MMAE), describing seasonal variation of the forecast error, was found as the arithmetic mean of MAE over the one month period. The root mean

square difference (RMSD), standard deviation (STD) and correlation (CORR) were found between forecast and observed data to describe the forecast error, amplitude and phase respectively. Mean error (ME), describing the conformity of the error distribution to the normal distribution, was found as arithmetic mean over the deviations between the observation and the forecast. To evaluate the accuracy of the forecasting system in greater detail, the whole range of sea level variations was divided into three sub-ranges at each station: high, medium and low. The forecasted sea levels were rounded to the nearest integer and sorted with corresponding forecast errors in ascending order. Then MAE was calculated for each forecasted sea level and the sea level sub-ranges were found. Both the whole range and the sub-range statistical characteristics were analysed. Taylor diagram [29] was chosen to summarize the statistical results.

3. RESULTS AND DISCUSSION

3.1. Forecasting high sea levels in 2006–2008

The period 2006–2008 included several storm surges with high sea levels, observed and forecast in many coastal areas. Since these cases were extensively reported in mass media and published partly in [30,31], only a short note is given here. The purpose of including this period here is that the second (2009–2011) dataset does not contain significant storm surges.

Figure 6 presents examples of high sea level events observed during January 2007 at PAR and TAL station. The sea level can increase over 40 cm within an hour (see PAR), which could lead to large instantaneous errors, if there is a time lag between the model and the observations. In case of flood risk, the end-users are interested in maximum sea levels during the risk period, normally about half a day.

High sea levels were found for two stations, PAR and TAL, for the time period 10.2006–03.2008. The criteria for a high sea level event were chosen 130 cm in PAR station and 90 cm in TAL station, with at least a 24 h time span between different high sea level events. There were 5 and 6 such events at PAR and TAL stations, respectively (Table 4). The forecast error was lower than ±25 cm for all these events and the time shift between observed and forecasted sea level maximum was within ±3 h.

3.2. Statistical analysis of sea level forecasts in 2009–2011

Statistical analysis for 11 coastal stations (Table 2) was performed for sea level forecasts within time period 1.03.2009–1.03.2011, although different time periods were available for different stations. A sample plot of forecasts and observations of the whole time period at PAL station is given in Fig. 7. Notice that the forecast is the output of the forecasting system, which is related to the model through the low-frequency error correction (see Eq. (2)).

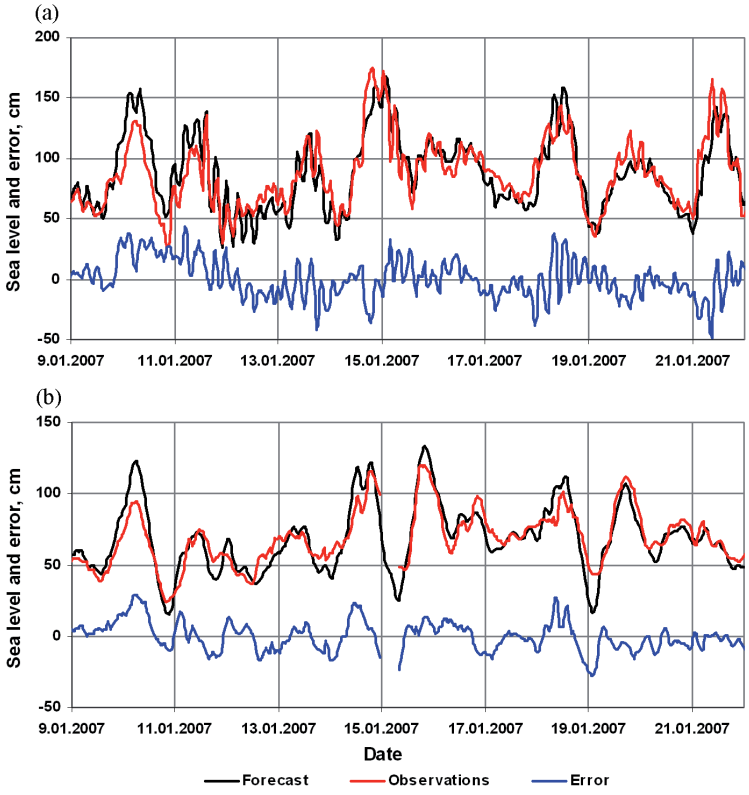

Fig. 6. High sea level events in January 2007 at the stations PAR (a) and TAL (b).

Table 4. Observed high sea level events at stations PAR and TAL within the time period 10.2006–03.2008

Date	Time	Observed sea level, cm	Forecast error, cm	Time shift, h	Station
10.01.2007	10:00	132	24	1	PAR
11.01.2007	18:00	138	–3	0	PAR
15.01.2007	04:00	175	–5	1	PAR
18.01.2007	14:00	144	16	1	PAR
21.01.2007	12:00	166	–19	2	PAR
10.01.2007	09:00	94	25	0	TAL
14.01.2007	22:00	117	6	0	TAL
15.01.2007	23:00	121	14	0	TAL
16.01.2007	23:00	98	–9	0	TAL
18.01.2007	15:00	101	13	1	TAL
19.01.2007	20:00	112	–1	0	TAL

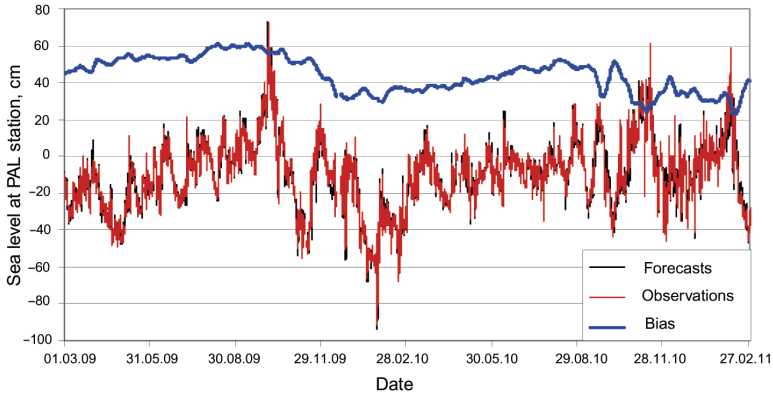

Fig. 7. Sea level observation and output of the forecasting system at the PAL station. The original model data can be found by adding forecast (black) and dynamic bias (blue). Investigation period included one storm surge event (over 65 cm) on 5.10.2009 and one low sea level event (above −80 cm) on 28.01.2010.

3.2.1. The data gaps and the up-time of the forecasting system

Two stations, KUI and TRI went online in Nov 2009 and the PAR observation station broke down on 24.05.2010, so these stations had less data compared to other stations. The observation data at SOR, TAL and TRI contained major data gaps. The stations SOR and TRI were out of order from 20.07.2010 to 9.09.2010 and the station TAL was down from 19.10.2009 to 14.11.2009, from 3.04.2010 to 19.04.2010 and from 22.10.2010 to 22.12.2010. These gaps were taken into account in up-time calculations of the forecasting system.

The percentage of missing data (Table 5) shows the data amount that was actually used in statistical calculations. Notice that the amount of data, actually used in calculations, was lower than the amount of actual forecasts, delivered to the users. The difference comes from the system's ability to forecast sea level even if observation data is not available for a short time. Statistical analysis used needs the data without any gaps, which means that the percentage of missing data amount, not used in the calculations, is higher by short-time (below 48 h) missing observation data.

The data gaps for the best available (forecast lead times from 1 to 6 h) forecast were analysed in greater detail. Three reasons for the forecasting system failures were identified and the amount of these failures was calculated. First, and the most obvious, is that the forecasting system can not run in case of hardware failures (cluster down, no electrical power, etc). This kind of error was found 1% of the time. Secondly, if the model results are missing then the forecasting system fails, which was the case in 2.6% of time. This failure appears mainly due to the network errors. It is also possible that the network is working, but the model data is uploaded to ftp-box too late (for example, the model calculations take too

Table 5. Main statistics for the whole range of data within time period 1.03.2009–1.03.2011. Stations KUI, TRI and PAR have shorter time period, i.e. 6.11.2009–1.03.2011 for KUI and TRI and 01.03.2009–24.05.2010 for PAR

Station acronym	HEL	KUI	LEH	PAL	PAR	ROH	SIL	SOR	TAL	TRI	VIR
Missing data, %	7	7	8	5	11	6	5	11	19	16	6
Long-term missing observation, %	3	1	3	0	9	1	0	7	9	12	2
Forecast down-time for end-user, %	1.4	1	3	1	4	1	1	7	8	11	2
ME, cm	0.08	0.10	0.11	0.05	0.24	0.07	0.08	0.00	0.07	0.25	0.07
MAE, cm	2.92	3.98	3.65	2.69	4.79	3.47	3.85	2.77	2.94	3.32	3.77
Mean dynamic bias, cm	43.25	45.34	37.66	44.30	44.15	42.50	32.09	40.47	41.55	35.83	41.51
STD of observation, cm	18.91	21.44	19.94	18.69	26.35	21.26	22.20	19.69	19.60	18.79	21.59
STD, cm	18.62	20.79	19.14	18.44	26.16	21.21	21.89	19.23	19.17	18.08	21.29
RMSD, cm	3.82	5.26	4.88	3.53	6.37	4.55	5.01	3.72	3.85	4.32	4.98
Normalized STD	0.98	0.97	0.96	0.99	0.99	1.00	0.99	0.98	0.98	0.96	0.99
Normalized RMSD	0.20	0.25	0.24	0.19	0.24	0.21	0.23	0.19	0.20	0.23	0.23
CORR, %	98	97	97	98	97	98	97	98	98	97	97

much time in case of heavy ice conditions), but the forecasting system has to send out the forecast. The percentages in time of the first two failures were obviously equal for every station. The third reason for the failures is long-term missing observations (Table 5). As explained above, the forecast is defined missing in case there are less than 24 successful observations present within the last three days (72 h). At most of the stations this failure was below 3% of time, while at three stations (SOR, TAL, TRI) it was higher. The reason was break-down of the observation station or very long network error between the forecasting system and the observation station. The analysis was made intentionally with the data stored by the forecasting system, to evaluate the performance of the actual forecast that has been delivered to the end-user. To summarize the best available forecast data gaps analysis, the general down-time was about 6%. The down-time of the forecasting system itself would have been about 4%.

The missing observation data was divided into two categories. A missing observation was defined as long-term in case there was less than 24 h not-missing data within the 72 h period, preceding the missing observation under evaluation. All other missing data was defined as short-term. The sub-category of long-term missing data was major data gaps, i.e., the data was missing over 2 weeks in a row. The observation was missing on average 7% of time, of that 4% long-term and 3% short-term.

Due to the forecasting system's ability to restore a forecast from previous forecasts, the up-time of the forecasting system for the end-user is higher than the best available forecast up-time. In case the model data is missing, the forecasting system uses data from the previous model run and delivers 6 h shorter forecast to the end-user. If the model data has been missing for 48 h or more, the forecasting system is "down" for the end-user. The percentage of down-time for end-user is given in Table 5 for every station. Mean down-time of all stations is 4%. If the major data gaps from SOR, TAL, TRI stations are excluded, the mean up-time of the forecasting system for the end-user would be 98%.

The institutional goal for the end-user up-time is to keep it higher than 96% while the forecasting system can not be down longer than 48 h in a row. As described above, the first part of this goal is fulfilled, but there are major data gaps in the observations that should be avoided. The network link from the observation stations to the forecasting system can be improved by software changes (multiple download attempts, other transfer protocols like 3G or satellite communication, etc). The second part needs improved observation stations maintenance routines, which could prevent the breakdown and more effective removing of the failures.

3.2.2. Statistics for the whole dataset

In order to evaluate the dependence of the performance of the forecasting system on the forecast update interval L, the statistics for forecasts, made with $L = 6$ (used operationally since about 2009) and $L = 24$ (used operationally until about 2009) were calculated and compared. The best available forecasts for both update intervals for the period 2009–2011 were used to obtain comparable results, i.e., the $L = 6$ data was obtained from the operational runs and the $L = 24$ data was simulated with 2009–2011 data. The improvement was calculated as the decrease in the mean RMSD and increase in the mean correlation with regards to the increase in the forecast frequency. The mean improvements were found 8% and 0.5% for RMSD and correlations, respectively. Correlation improvement percentage for high and low sea level sub-ranges (see below) was 3.1% and 4.3%, respectively.

As described before, a 7 day filter was used in the forecasting system to correct the low-frequency error. The mean dynamic bias (Table 5), shows a range from 32 to 46 cm. Most of the stations have the mean dynamic bias over 40 cm, the lowest mean dynamic bias is at SIL station, which can be explained by the geographical distance from other stations and closeness to the Neva and Narva rivers, discharging fresh water into that region. Unexpectedly, low values of mean dynamic biases were found also at LEH and TRI stations, which can point to bathymetry inaccuracies in the model domain. The mean forecast errors are near zero at all stations, which shows a rather good performance of the dynamic bias correction algorithm.

Monthly mean absolute errors at different stations are presented in Fig. 8. In general there is no seasonal difference in MMAEs. The MMAE at station PAR is

higher than for the other stations, reaching 6.1 cm in April 2010, while MMAE of the LEH station distinguishes with high variability of MMAE. There is a significant increase in MMAEs, starting from 09.2010, which is the same time as upgrade to HIROMB v. 4.2 (released on 15.09.2010), although there were no changes introduced in v. 4.2, which should influence the sea level. The sea level had also high variance in spring 2010 (Fig. 7), which amplified the increase in MMAEs. Previous upgrade to the model version 4.0 on 10.12.2009 is not so clearly visible, although the MMAEs are slightly increased in that period.

The RMSD is one of the most important statistics for describing the performance and accuracy of the forecasting system. While it combines standard deviation of forecasts and correlation between observations and forecasts, it also has clear statistical meaning. Considering that RMSD is equivalent to a standard deviation of the forecast error (in case of normal distribution), it can be interpreted as the absolute error level within the 68% probability level. The RMSDs of the best available sea level forecasts, varied from 3 cm (PAL) to 7 cm (PAR), giving evidence of rather accurate forecasts.

To summarize the performance of investigated sea level forecasts, RMSD vs. correlation plot (Fig. 9a) was used instead of the commonly used normalized Taylor diagram. The reason is the high similarity of statistics between different stations (notice the scales of Fig. 9a) which would lead to a poorly readable Taylor diagram. Nevertheless, from the values of STDs, normalized with STDs of observations (Table 6) it is concluded that forecasts tend to underestimate the variance of the sea level. The best general performance in the means of RMSD/CORR rate is at PAL station with 98.2% correlation. Correlation is high (over 97%) at all stations, which points to small overall phase errors of the forecasting system.

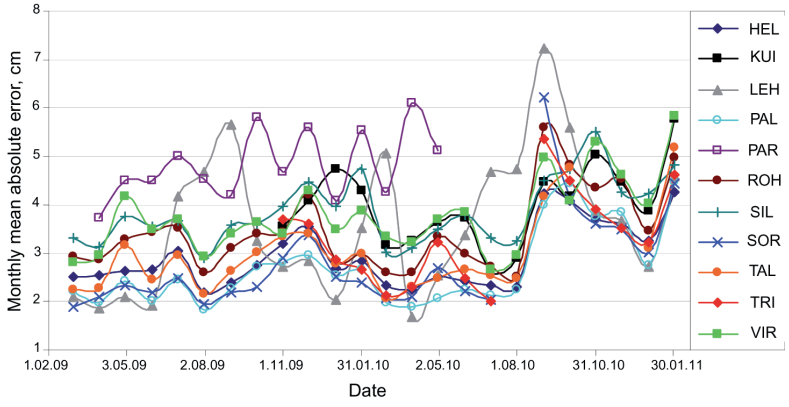

Fig. 8. Monthly mean absolute errors of the forecast at different stations. Mean errors are increased after release of the new HIROMB v. 4.2 on 15.09.2010.

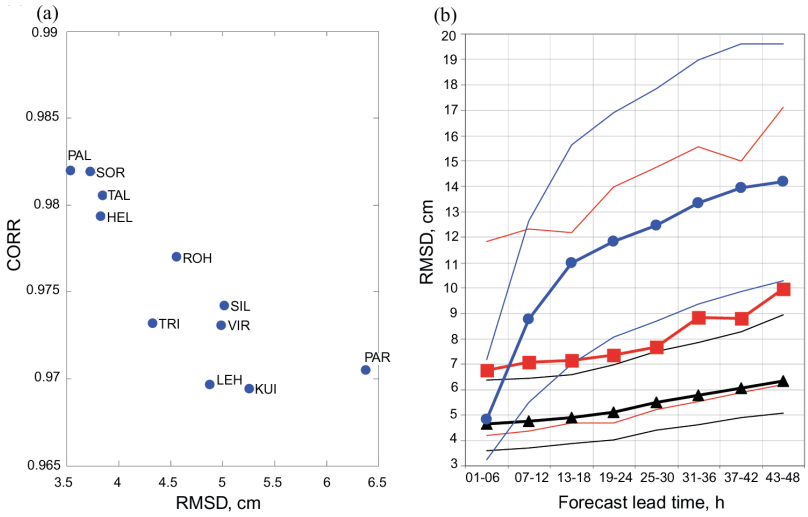

Fig. 9. Forecast correlation and RMSD with respect to observation for the whole dataset (a) and RMSD dependence on forecast length for different data ranges (b). On (b) the black, red and blue bold lines show the mean RMSD over all stations of the whole dataset, high sub-range and persistency forecast, respectively. Thin lines with corresponding color show minimal and maximal individual curve from the most accurate and least accurate station, respectively. Forecast is most accurate at the PAL station and least accurate at the PAR station.

To investigate the forecast accuracy dependence on the forecast length, the RMSD was calculated for each forecast lead time range (from $(p-1)L+1$ to pL) and for each station (Fig. 9b). The minimal boundary is from the station PAL and the maximal boundary from the station PAR as could be expected from Fig. 9a. The mean accuracy of the forecast decreases only up to 2 cm for the 48 h forecast length and the error for the 48 h forecast is up to 2.5 cm higher than the best available forecast error, which is mostly presented in this paper.

As an illustration of the forecast precision, the persistency forecasts were carried out, using available observational data, and compared to the results of the operational forecast. The persistency forecast is one of the most primitive forecast methods and it is based on the assumption that the last observed situation will continue over the forecast period. For example, in 1–6 h persistency forecast it is assumed that the most recent observed sea level is constant over the next 6 h. The accuracy of the persistency forecast (Fig. 9b) is close to the accuracy of the forecasting system forecast up to 6 h, but in longer lead times, up to 48 h, the advantage of the forecast system is clearly evident.

Table 6. Main statistics for low, medium and high sub-ranges within the time period 1.03.2009–1.03.2011. Stations KUI, TRI and PAR have shorter time period, i.e. 6.11.2009–1.03.2011 for KUI and TRI and 01.03.2009–24.05.2010 for PAR

Station acronym	HEL	KUI	LEH	PAL	PAR	ROH	SIL	SOR	TAL	TRI	VIR
Definition of low sea level sub-range, cm	–50	–50	–50	–60	–60	–60	–50	–60	–50	–60	–50
Definition of high sea level sub-range, cm	35	15	35	40	50	40	50	40	50	20	40
Number of low sea levels	307	693	375	50	222	97	150	46	284	46	322
Number of medium sea levels	15 272	9 368	15 273	16 120	8 317	15 754	15 795	14 963	12 962	8 977	15 337
Number of high sea levels	232	521	110	111	123	216	334	144	87	245	310
ME of low sub-range forecast, cm	1.49	1.06	–0.31	2.43	2.61	5.56	0.47	1.31	0.17	0.79	1.21
STD of low sea level observation, cm	7.49	8.74	6.25	9.27	8.78	9.48	14.81	7.00	8.79	8.32	7.79
STD of low sea level, cm	7.26	7.95	6.12	9.69	8.30	7.21	12.82	4.64	7.59	5.01	6.40
RMSD of low sea level, cm	3.65	6.30	3.17	4.51	6.44	5.48	9.31	4.47	4.22	3.78	4.26
Normalized STD of low sea level	0.97	0.91	0.98	1.05	0.95	0.76	0.87	0.66	0.86	0.60	0.82
Normalized RMSD of low sea level	0.49	0.72	0.51	0.49	0.73	0.58	0.63	0.64	0.48	0.45	0.55
CORR of low sea levels, %	88	72	87	89	72	82	78	78	88	96	84
ME of medium sub-range forecast, cm	0.05	0.06	0.11	0.05	0.22	0.07	0.10	0.00	0.07	0.23	0.11
STD of medium sea level observation, cm	16.48	16.17	17.93	17.83	22.92	19.66	19.70	18.62	17.57	17.51	18.80
STD of medium sea level, cm	16.06	15.00	17.06	17.52	22.37	19.40	19.31	18.10	17.07	16.77	18.14
RMSD of medium sea level, cm	3.80	4.96	4.91	3.51	6.23	4.48	4.88	3.71	3.82	4.29	4.85

Table 6. *Continued*

Station acronym	HEL	KUI	LEH	PAL	PAR	ROH	SIL	SOR	TAL	TRI	VIR
Normalized STD of medium sea level	0.97	0.93	0.95	0.98	0.98	0.99	0.98	0.97	0.97	0.96	0.97
Normalized RMSD of medium sea level	0.23	0.31	0.27	0.20	0.27	0.23	0.25	0.20	0.22	0.24	0.26
CORR of medium sea levels, %	97	95	96	98	96	97	97	98	98	97	97
ME of high sub-range forecast, cm	0.10	–0.44	0.37	–0.64	–2.81	–2.32	–0.71	–0.52	–0.88	0.71	–3.39
STD of high sea level observation, cm	11.40	12.05	9.08	7.75	22.80	15.29	13.19	9.85	8.48	7.10	15.87
STD of high sea level, cm	10.95	9.62	6.08	7.14	22.28	16.28	11.82	9.03	7.61	4.89	16.35
RMSD of high sea level, cm	5.18	8.01	5.47	5.42	12.05	6.89	7.57	4.13	5.97	5.52	9.16
Normalized STD of high sea level	0.96	0.80	0.67	0.92	0.98	1.06	0.90	0.92	0.90	0.69	1.03
Normalized RMSD of high sea level	0.45	0.66	0.60	0.70	0.53	0.45	0.57	0.42	0.70	0.78	0.58
CORR of high sea level, %	89	75	81	74	86	91	82	91	73	63	84

3.2.3. Statistics of sub-ranges

Due to the broad range of temporal scales of the sea level variations it is obvious that the statistics of sea level time series greatly depends on the length of the time series and the presence of high/low sea level events. The statistics for mostly medium range sea level fluctuations does not describe extreme events like high and low sea levels sufficiently and can be even misleading, if used in the wrong context. For the end-users, the accuracy of sea level forecast is always much more important during the extreme events than in “normal situations”, therefore evaluation of statistics especially for such events has a great practical relevance.

The relationships between mean absolute errors and the forecast sea levels were found (Fig. 10), to find the statistics, describing in greater detail the extreme events of sea level. Three different sub-ranges were found for every station: low, medium and high sea level sub-ranges (the limits of these sub-ranges should not be confused with high/low sea level warning limits). Limits defining these sub-

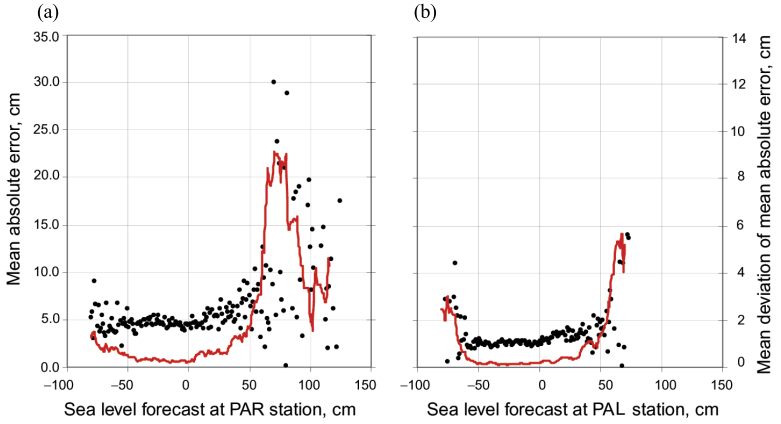

Fig. 10. Mean absolute errors at PAR (a) and PAL (b) stations. Line indicates mean deviation of 10 following mean absolute errors. Three sub-ranges can be distinguished: low, medium and high sea level sub-range. For the PAL station the low sub-range has more contrast than the PAR station.

ranges were found for every station (Table 6). These sub-ranges were different from station to station, although an attempt was made to use more general common sub-range limits.The limits were rounded to the nearest 5 cm. Two values for the low sub-range limit were found: –50 cm for 6 stations and –60 cm for 5 stations. The limits of high sub-range varied from +15 to +50 cm. The graphical presentation of the mean deviation of 10 following data points was used to identify the boundaries of different sub-ranges (not shown here). These three sub-ranges were clearly visible for all stations, indicating a relationship between the forecast sea level and error, and making it possible to estimate forecast error while the forecast value is known. While most of the data fall in the medium sub-range and have the lowest errors, the high and low sub-ranges had less data and errors were higher than medium sub-range sea level forecasts. Also, since most of the data was in the medium sub-range, the statistics of this sub-range was very similar to that of the whole range of data.

The forecasting system has a tendency to show an uneven error distribution in case of low and high sea level sub-ranges, while in the medium sub-range the mean errors were near zero, indicating the conformity to normal distribution and adequate low-frequency error correction. Low sub-range error is shifted to the positive side (low sea levels are predicted higher) and high sub-range to the negative side (high sea levels are predicted lower), which should be taken into account when interpreting RMSD values for corresponding sub-ranges. Such a distortion of low and high sea level forecasts was noted also for the northern coast of the Gulf of Finland [20].

From Fig. 10 it could be expected that RMSD of medium sub-range forecasts are significantly lower than in other sub-ranges. Nevertheless, the RMSDs of medium and low sub-ranges are comparable (which is probably the effect of uneven error distribution), while high sub-range forecasts have a higher RMSDs, as expected. The correlations of low and high sub-range forecasts were lower than in the medium sub-range, indicating certain phasing errors in these sub-ranges. The low sub-range had considerably lower STDs, compared to other sub-ranges.

The mean high sub-range forecast error dependence on the forecast length is presented in Fig. 9b. The high sub-range forecast depends slightly more on the forecast lead time than the mean accuracy of the whole dataset. The 48 h forecast accuracy is up to 5 cm worse than the RMSD of the best available forecast, but on average the 6 h forecast is 3 cm more accurate than the 48 h forecast. It could also be noted that the accuracy of the high sub-range forecast is still better than the accuracy of the persistency forecast.

Normalized Taylor diagrams of high and low sub-range sea level forecasts are presented in Fig. 11. The RMSDs and STDs are normalized with the STD of the observations. To illustrate the differences between medium and high/low forecast sub-ranges, the medium sub-range statistics are presented in the same diagram as the high sub-range statistics. Compared to the medium sub-range (and also to the whole data statistics) the correlations and RMSDs are considerably lower. The distribution of STDs is sparser, although the forecast at most stations underestimates the variance of the sea level, following the same trend as general statistics.

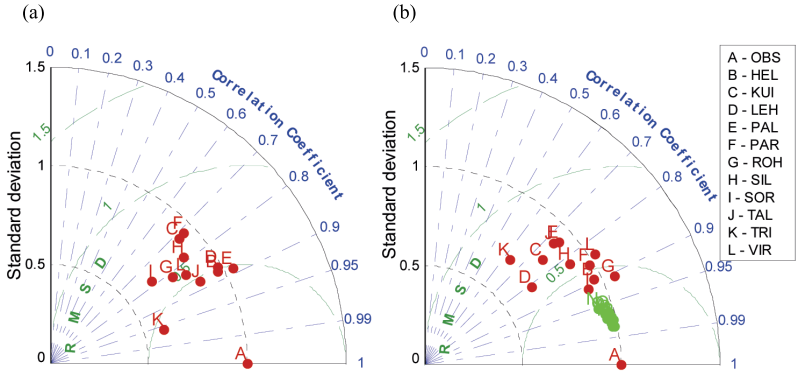

Fig. 11. Normalized Taylor diagram for low (a) and high (b) sea level forecast sub-range. The green dots in high mode Taylor diagram represent medium sub-range forecast and are shown to illustrate differences between high/low and medium sub-range forecast. Data at each station is normalized with standard deviation of corresponding observations; A indicates observations.

4. CONCLUSIONS AND OUTLOOK

The performance of the Estonian sea level forecast system was analysed within two time periods using different statistical methods. The HIROMB BS01 grid model and data from sea level observation stations was used to produce sea level forecast for the Estonian coast. Using the RMSD minimizing algorithms, a 7 day moving average filter was found to be the most accurate for the correction of low-frequency error. Correlation of this error (dynamic bias) with the Baltic Sea volume change was not found. High sea level analysis within the time period of 2006–2008 showed ±25 cm accuracy of storm surge forecasts, taking into account the ±3 h time shift between the observation and forecast.

Today the update frequency of the sea level forecast is 4 times a day (+00, +06, +12 and +18), which gives on average 8% more accurate forecast compared to 24 h update interval with respect to the RMSD. The accuracy of the forecast is slightly related to the forecast length, resulting in up to 2.5 cm higher RMSD for 48 h forecast than the best available forecast (6 h). Although an input data quality control algorithm is applied to the forecasting system, which can remove obvious outliers, there is still a need for further calibration of online quality control to increase the reliability of the system. Statistical analysis of the whole period 2009–2011 revealed a RMSD less than 7 cm and correlations above 97% at all stations.

The data was divided into three sub-ranges (low, medium and high), which were analysed separately. The limits of sub-ranges and statistics were found for every station, which showed the differences especially in the high sub-range, where the maximum RMSD was found up to 13 cm and a correlation down to 63%. This method for estimating forecast errors revealed the possibility of implementation of an automatic on-line error estimation system.

As an improvement for the forecasting system it is planned to use more observational stations, especially the stations operated by EMHI. The work is already in progress. Also the implementation of MyOcean products could improve the forecasting system, enabling the possibility for ensemble forecasts of the sea level, which provides more information and better online error estimates for the forecast and therefore is becoming more and more popular around the Baltic Sea. There are 9 new sea level stations recently installed by EMHI, which will be merged into the system soon after the test period. The coverage of the Estonian coastal sea with sea level measurement sites increases remarkably, when new stations are added. Nevertheless, more efforts are needed in order to harmonize the measurement methods. The current forecast system has already showed good performance. With the improved on-line measurement station network, the accuracy of the system should improve even more towards better representation of local peculiarities and features, which in turn are very important in certain storm cases at certain locations of the coast.

Today, at 6 on-line stations out of 11, basic wave parameters are estimated, based on the pressure data, and broadcast to the Sea Level Information System (http://on-line.msi.ttu.ee/kaart.php?en) already for a period of 1.5 year. The wave data are used as background information for high resolution sea level measure-

ments. As indicated by the analysis of extreme storm surges, the occurrence of critical and above critical sea levels is the weakest point in the forecast system. The role of waves in forming of extreme sea levels is quite obvious and some statistics is already available, based on the existing time series. The HIROMB models do not include a wave module. Thus, taking into account the local wave pattern in actual wind conditions could improve the performance of the forecast system for extreme sea levels.

ACKNOWLEDGEMENTS

We thank the Environmental Investment Centre, Estonian Meteorological and Hydrological Institute, Estonian Science Foundation (grant No. 7328) for financial support for the development and maintenance of the forecasting system.

REFERENCES

1. Ekman, M. A consistent map of the postglacial uplift of Fennoscandia. *Terra Nova*, 1996, **8**, 158–165.
2. Ekman, M. Climate changes detected through the world's longest sea level series. *Global Planet Change*, 1999, **21**, 215–224.
3. Johansson, M., Kahma, K. and Boman, H. An improved estimate for the long-term mean sea level on the Finnish coast. *Geophysica*, 2003, **39**, 51–73.
4. Suursaar, Ü. and Sooäär, J. Decadal variations in mean and extreme sea level values along the Estonian coast of the Baltic Sea. *Tellus*, 2007, **59A**, 249–260.
5. Dailidiene, I., Davuliene, L., Tilickis, B., Stankevicius, A. and Myrberg, K. Sea level variability at the Lithuanian coast of the Baltic Sea. *Boreal Environ. Res.*, 2006, **11**, 109–121.
6. Samuelsson, M. and Stigebrandt, A. Main characteristics of the long-term sea level variability in the Baltic Sea. *Tellus*, 1996, **48A**, 672–683.
7. Miles, J. W. Harbor seiching. *Annu. Rev. Fluid. Mech.*, 1974, **6**, 17–35.
8. Raudsepp, U., Toompuu, A. and Kõuts, T. A stochastic model for the sea level in the Estonian coastal area. *J. Marine Syst.*, 1999, **22**, 69–87.
9. Matthäus, W. and Lass, H.-U. The recent salt inflow into the Baltic Sea. *J. Phys. Oceanogr.*, 1995, **25**, 280–286.
10. Suursaar, Ü., Kullas, T., Otsmann, M. and Kõuts, T. Extreme sea level events in the coastal waters of West Estonia. *J. Sea Res.*, 2003, **49**, 295–303.
11. Wübber, C. and Krauss, W. The two-dimensional seiches of the Baltic Sea. *Oceanol. Acta*, 1979, **2**, 435–446.
12. Johansson, M., Boman, H., Kahma, K. K. and Launiainen, J. Trends in sea level variability in the Baltic Sea. *Boreal Environ. Res.*, 2001, **6**, 159–179.
13. Jönsson, B., Döös, K., Nycander, J. and Lundberg, P. Standing waves in the Gulf of Finland and their relationship to the basin-wide Baltic seiches. *J. Geophys. Res.*, 2008, **113**, C03004.
14. Lilover, M.-J., Lips, U., Laanearu, J. and Liljebladh, B. Flow regime on the Irbe Strait. *Aquatic Sci.*, 1998, **60**, 253–265.
15. Otsmann, M., Suursaar, Ü. and Kullas, T. The oscillatory nature of the flows in the system of straits and small semienclosed basins of the Baltic Sea. *Cont. Shelf Res.*, 2001, **21**, 1577–1603.
16. Hansen, W. Theorie zur Errechnung des Wasserstandes und der Strömungen in Randmeeren nebst Anwendungen. *Tellus*, 1956, **8**, 287–300.

17. Uusitalo, S. The numerical calculation of wind effect on sea level elevations. *Tellus*, 1960, **12**, 427–435.
18. Peeck, H. H., Proctor, R. and Brockmann, C. Operational storm surge models for the North Sea. *Cont. Shelf Res.*, 1982, **2**, 317–329.
19. Kleine, E. Das operationelle Modell des BSH für Nordsee und Ostsee. Konzeption und Übersicht. Bundesamt für Seeschifffahrt und Hydrographie (Manuscript), 1994.
20. Gästgifvars, M., Müller-Navarra, S., Funkquist, L. and Huess, V. Performance of operational systems with respect to water level forecasts in the Gulf of Finland. *Ocean Dynamics*, 2008, **58**, 139–153.
21. Buch, E., Elken, J., Gajewski, J., Håkansson, B., Kahma, K. and Soetje, K. Present status of the Baltic Operational Oceanographic System. In *Proc. Fourth International Conference on EuroGOOS.* Brest, France, 2006 (Dahlin, H., Flemming, N. C., Marchand, P. and Petersson, S. E., eds). Office of Official Publications of the European Communities, 2006, 276–280.
22. Elken, J., Kõuts, T., Raudsepp, U., Laanemets, J. and Lagemaa, P. BOOS/HIROMB-based marine forecasts in Estonia: problems, experiences and challenges. In *Proc. US/EU-Baltic International Symposium*. Klaipeda, Lithuania, 2006, 22.
23. Suursaar, Ü., Kullas, T., Otsmann, M., Saaremäe, I., Kuik, J. and Merilain, M. Cyclone Gudrun in January 2005 and modelling its consequences in the Estonian coastal waters. *Boreal Environ. Res.*, 2006, **11**, 143–159.
24. Funkquist, L. HIROMB, an operational eddy-resolving model for the Baltic Sea. *Bull Mar. Inst.*, Gdańsk, 2001, **28**, 7–16.
25. Elken, J., Nõmm, M. and Lagemaa, P. Circulation patterns in the Gulf of Finland derived from the EOF analysis of model results. *Boreal Environ. Res.*, 2011, **16**, 84–102.
26. Axell, L. Weaker surface currents in HIROMB 3.1. In *9th HIROMB Scientific Workshop*. Gothenburg, 2006. www.environment.fi/syke/hiromb, 16.10.2011.
27. HIROMB Scientific Plan 2009–2013, ver. May 2010. http://balticlagoons.projects.eucc-d.de/plugins/
28. Sørensen, J. V. T., Madsen, H. and Madsen, H. Efficient Kalman filter techniques for the assimilation of tide gauge data in three-dimensional modeling of the North Sea and Baltic Sea system. *J. Geophys. Res.*, 2004, **109**, C03017.
29. Taylor, K. E. Summarizing multiple aspects of model performance in single diagram. *J. Geophys. Res.*, 2001, **106**, 7183–7192.
30. Elken, J., Kõuts, T., Lagemaa, P., Lips, U., Raudsepp, U. and Väli, G. Sub-regional observing and forecast system for the NE Baltic: Needs and first results. In *US/EU-Baltic International Symposium "Ocean Observations, Ecosystem-Based Management & Forecasting"*. Tallinn, 2008. IEEE Confer. Proc., 2008, 421–429.
31. Elken, J. Mereprognooside süsteemi HIROMB arendamine, SA KIK Veekaitseprogrammi projekt nr 36 lõpparuanne. Tallinn, 2008. http://www.msi.ttu.ee/~elken/HIROMB_2008_Lopparuanne_sisuline.pdf, 16.10.2011.

Operatiivne meretaseme prognoosisüsteem Eestis

Priidik Lagemaa, Jüri Elken ja Tarmo Kõuts

On kirjeldatud ja valideeritud operatiivset meretaseme prognoosisüsteemi Eestis. Prognoosisüsteem põhineb HIROMB-mudeli prognoosil ja 11-l reaalajas toimival meretaseme mõõtejaamal. Süsteem töötab alates 08.08.2005. Töös on analüüsitud prognoosisüsteemi efektiivsust aastail 2006–2008 ja 2009–2011. On uuritud madalsagedusliku veetaseme prognoosivea omadusi ja hinnatud prognoosiviga ekstreemsete veeseisude esinemise korral, mille täpne ennustamine on

prognoosisüsteemi põhirakenduseks. Uuring näitab, et 7-päevane tagasiulatuva liikuva keskmisega filter on Eesti rannikul sobivaimaks meetodiks, et prognoosimudeli väljundandmetest madalsageduslikku viga välja filtreerida. Ekstreemsete (üle kriitilise taseme) veetasemete prognoosi täpsus on ±25 cm ja ajaline maksimaalse meretaseme saabumise täpsus ±3 tundi. Värskemate, 2009.–2011. aasta meretaseme prognooside hindamiseks kasutatakse Taylori täpsushindamise meetodit. Reaalajas prognoosivea arvutamise võimalikkuse uurimiseks jagatakse meretaseme prognoosid kolme alamrühma (madal, keskmine ja kõrge). On leitud, et madalamate ja keskmiste veetasemete prognoosid on täpsemad kui kõrgemate veetasemete omad. On vaadeldud prognoosisüsteemi edasiarendamise võimalusi ja põhjendatud vajadust parendada reaalajas toimivat mõõteandmete kvaliteedikontrolli.

Paper II

Lagemaa, P., Suhhova, I., Nõmm, M., Pavelson, J. and Elken, J. 2010. Comparison of current simulations by the state-of-the-art operational models in the Gulf of Finland with ADCP measurements. In *IEEE/OES Baltic 2010 International Symposium: IEEE/OES Baltic 2010 International Symposium, 25–27 August 2010, Riga.* IEEE Conference Proceedings, 1–11.

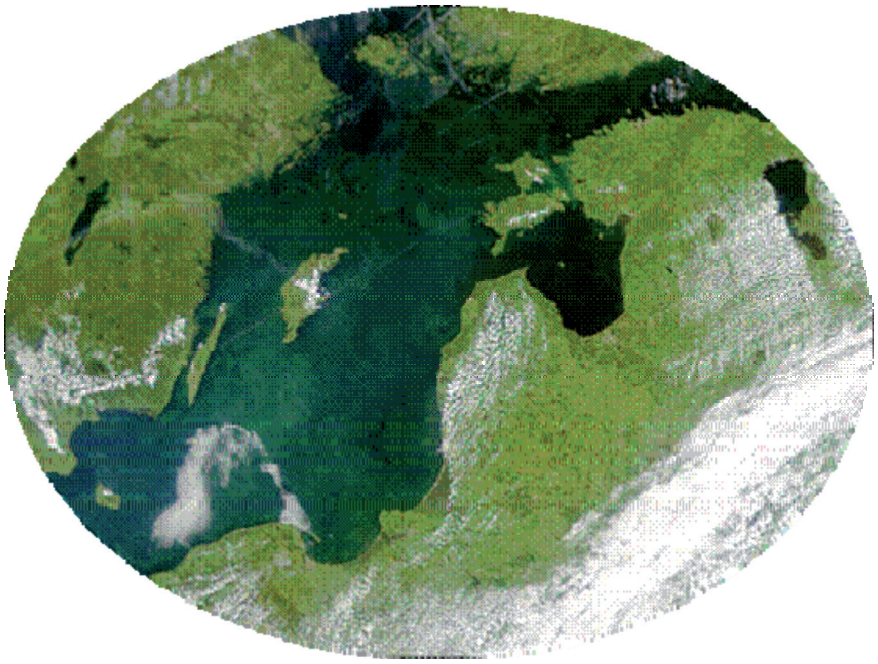

2010 IEEE/OES US/EU Baltic International Symposium (BALTIC)

August 25, 26, 27 2010 - Riga, Latvia

IEEE Catalog Number: CFP10AME-ART
ISBN: 978-1-4244-9227-5/10/$26.00 ©IEEE

Comparison of Current Simulations by the State-of-the-Art Operational Models in the Gulf of Finland with ADCP Measurements

P. Lagemaa, I. Suhhova, M. Nõmm, J. Pavelson and J. Elken
Marine Systems Institute at Tallinn University of Technology
Akadeemia 21, EE12618 Tallinn, Estonia, priidik26@gmail.com

Abstract-**Current modeling results from two operational models (Baltic-wide HIROMB-BS01 with 1 nautical mile resolution and subregional HIROMB-EST with 0.5 mile resolution) were compared with ADCP measurements at four sites of different topographic and hydrographic background in the Gulf of Finland. Both models predict a reasonable match with the observed subsurface currents in most of the cases, although there are no data to carry out the assimilation of mesoscale oceanographic features. The correlations of the modeled currents with the observed counterparts yield quite often the values above 0.5, both in the low-frequency and high-frequency range. In general, the models tend to generate less current variability (smaller standard deviations) than observed. There is also some site-specific bias of mean currents.**

Near-bottom and coastal currents are highly constrained by the topography. High current speeds (above 20 cm/s) were measured in the deep layers of the rough-bottom area around a small island. Such currents were in general well simulated by the 0.5 nm model, only slightly biased by the dominating direction. The modeled near-bottom currents are simply transformable into more realistic results if the correct topography is taken into account. Both the observations and the subregional model results revealed similar halocline-intensified EOF modes of vertical current structure, the amplitudes of which were correlated quite well.

INTRODUCTION

The northeastern Baltic, including the Gulfs of Finland and Riga, is a region with an increasing use of marine resources; therefore more detailed oceanographic predictions throughout the water column are needed. Climate change and eutrophication studies focus on the seasonal and long-term changes of stratification and large-scale transport patterns [1,2]. Growing human activities like building submarine gas pipelines and power cables, offshore windfarms, etc. [3,4] require now- and forecasts of layered subsurface currents in a spatial range from a few to tens of kilometers in a time span from hours to months and years. Operational oceanographic models, combined with observational data, are straightforward tools to provide such information. Development of forecast tools is done within the BOOS and HIROMB consortia with the support from the EU MyOcean project.

The Gulf of Finland is an elongated estuarine basin of the Baltic Sea. By coastline and mean depths the gulf is like a wide channel. However, oceanographic predictability of the gulf is complicated due to the significant bottom roughness (compared to other Baltic regions as shown by the recent Nord Stream study [5]) combined with the strong vertical and horizontal density gradients. The baroclinic Rossby radius is only 2–4 km [6]. It means that besides the high-frequency motions (with periods up to the seiche period of 27 h), low-frequency mesoscale motions play an important role. While upwelling/downwelling and associated coastal jets are directly related to the wind forcing [7], numerous open sea fronts [8] and mesoscale eddies are generated by the internal non-linear ocean dynamics. Unfortunately there are no observational subsurface data available to perform full mesoscale data assimilation and/or initialization of models; therefore location and phases of the fronts and eddies may quite often be modeled with significant shifts. It means that assimilation of current observations at single points does not necessarily improve the predictions in a distance larger than the mesoscale correlation scale, usually a few times the Rossby radius.

The surface currents that are primarily caused by direct wind forcing can be predicted quite well [9]. Comparisons of subsurface current predictions are quite rare and they mainly come from the strait areas where the flow has essential topographic constrictions [10]. They have shown that in order to improve the quality of predictions, adjustment of the model topography may be helpful.

This paper is aimed at comparison of subsurface current measurements with the predictions of two different setups of the operational HIROMB model. After the description of observation sites, wind conditions and the models used, the current roses are compared. It was reasonable to split the analysis of time series of currents into low-frequency and high-frequency bands. The vertical structure of currents is also analyzed using the EOF method.

OBSERVATION SITES AND WIND CONDITIONS

Current velocity measurements were carried out at four observation sites with different topographic and hydrographic background and in different seasons: Lohusalu (L), Vaindloo1 (V1), Vaindloo2 (V2) and Kunda (K) (Fig. 1). Site L (59.4500 N, 24.1667 E) is located in the western part of the gulf on the southern coastal slope. This site near the Lohusalu Peninsula is 6 km from the coast, where the depth is 50 m. The data were gathered during the spring and early summer period (13.03–30.06.2009).

Sites V1 (59.8683 N, 26.4300 E) and V2 (59.8500 N, 26.2700) about 9 km apart are located in the central part of the gulf in a deeper passage around the small Vaindloo Island. The sites lie approximately 30 km from the southern coast of the gulf, where the depths are 68 m (V1) and 75 m (V2). The measurements were performed in late fall (29.10–25.11.2009). Site K (59.7017 N, 26.4033 E) is located about 15 km southward from sites V1 and V2 in the deep basin southeastward extension towards the Kunda Bay. The depth of the site is 66 m; the data were collected in winter and early spring (12.01–27.04.2010).

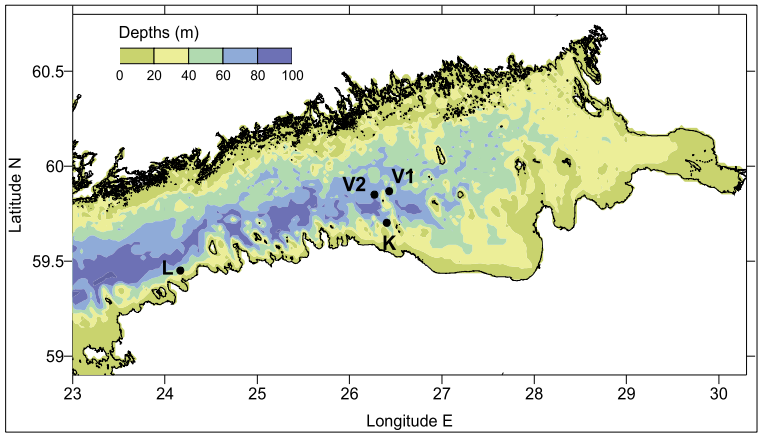

Fig. 1. Map of the Gulf of Finland. Locations of ADCP measurements are given by dots and corresponding labels.

At all sites bottom-mounted 307.2 kHz broad-band ADCP (RDInstruments) were used. The instruments measured current velocities over 2-m depth bins with the sampling interval of 10 minutes (average of 50 pings). Due to surface side lobe effect the data of two bins from the surface were contaminated and therefore not used, i.e. the upper reliable bin was centered at a depth of 5 m. The first bin available above the instrument was centered at 5 m from the bottom. The quality of the data series at each depth bin was checked using the procedure which is based on certain criteria for the internal control parameters (signal correlation, percentage good and error velocity) of the ADCP [11]. Relying on this analysis, bad data were replaced using linear interpolation of the series.

Hourly wind data for the observation periods were available from the Estonian Meteorological and Hydrological Institute (EMHI) coastal meteostations Pakri (10 km from site L) and Kunda (30 km from sites V1 and V2, and 15 km from site K). All observation periods were characterized by relatively low wind speeds, which may be to some extent underestimated because of the dominance of landward wind measured at the coast. During the observations at site L the mean wind speed was 3.9 m/s. The proportion of weak (up to 5 m/s) and moderate winds (6–10 m/s) was 71% and 28%, respectively. The NE–E and S–SSW winds dominated, being moderately strong at the same time. Other winds were relatively changeable by direction with a virtual absence of NW and SE winds. The measurement period at sites V1 and V2 was mainly characterized by weak winds (93%). The mean wind speed was 3.5 m/s and even during stronger events speeds did not exceed 10 m/s. It can be mentioned at this point that such weak background winds are unusual for fall in the northern Baltic region. Winds blew mostly from the SSE–SSW, and the W–NW winds were practically absent. Wind conditions during the observations at site K were very similar considering the share of weak winds, wind strength (mean speed 3.0 m/s), as well as dominant wind directions. The speed of wind exceeded 10 m/s only during two short-time events.

MODELS

Two state-of-the-art circulation models were compared against ADCP current velocity measurements: one model with a 1 nm (nautical mile) horizontal grid step and another model with a 0.5 nm horizontal grid step. Both models use the same code called HIROMB (High Resolution Operational Model for the Baltic Sea) [12,13] but different setups, i.e. different computational domains, meteorological forcing, bathymetry, boundary conditions and river inflows. During the observation period the model code was updated from version 3.3 to version 4.0. Therefore comparisons at observation sites L, V1 and V2 were performed with version 3.3 and at site K with version 4.0.

The model with the 1 nm horizontal resolution (also referenced as HIROMB-BS01) is run at the Swedish Meteorological and Hydrological Institute (SMHI). Its domain has 752×735 horizontal grid points and it covers the entire Baltic Sea. This 1 nm model is also the cornerstone for the Baltic-wide oil pollution forecast system Seatrack-Web on the sea surface [14] and it has proved to have a very good sea level prediction capability [15,16]. In version 3.3 it has 16 vertical layers with a resolution of 4 m between surface and 12 m, 6 m between 12 m and 30 m, 10 m between 30 m and 60 m, and 15 m between 60 m and 90 m. Further down the vertical grid steps increase. Such a surface-refined grid is acceptable for the Baltic Proper and the shallow Danish straits, but it is too coarse for the deeper regions with variable stratification like the Gulf of Finland. Therefore in version 4.0 the vertical resolution of the 1 nm model setup was increased. Altogether it has 50 vertical layers in which the upper 20 layers are 4 m thick (0–80 m), 5 layers are 5 m thick (80–105 m), 4 layers are 6 m thick (105–123 m), and further down the model layers are thicker. Thus version 4.0 covers the Gulf of Finland (max depth ~100 m) with a much higher vertical resolution than version 3.3. The HIRLAM (High Resolution Limited Area Model) weather model with a 22 km horizontal resolution which is run at the SMHI is used for atmospheric forcing.

The model with the 0.5 nm horizontal resolution (also referenced as HIROMB-EST) is run by the Marine Systems Institute (MSI) in Estonia. It has 529×455 horizontal grid points and it covers mostly Estonian coastal waters, including the entire Gulf of Finland and the Gulf of Riga. The vertical resolution of the model is 3 m from surface down to 90 m, and 5 m between 90 m and 135 m. Atmospheric forcing is taken from the HIRLAM model with an 11 km horizontal resolution which is run at the EMHI. Open sea boundary conditions along the western boundary (21.55 E) of the region are taken from the 1 nm model. The 0.5 nm model has been in operational use since the 1st of May 2009.

RESULTS AND DISCUSSION

Current Roses

Current roses were drawn to investigate the dominating speeds and directions of the currents at the depths where maximum current speeds were observed in the measurement series (Fig. 2). At observation site L the maximum current speeds were found in the surface layers and therefore currents at a depth of 10 m were more closely investigated. The measurements revealed a prevalence of westward alongshore currents. Both models showed more pronounced westward alongshore flow than measurements. The speed of dominating currents (20–25 cm/s in the 0.5 nm model and 10–15 cm/s in the 1 nm model) was overestimated and direction (230º–250º and 235º–255º, respectively) was more unidirectional following the recent general circulation scheme of the Gulf of Finland [17]. It must be noted that some earlier studies have suggested an opposite, eastward mean flow along the Estonian coast. Observations showed a more varied distribution of current directions obviously due to switching between upwelling and downwelling regimes that was not modeled so well.

At sites V1 and V2 the maximum current speeds were found at a depth of about 50 m, in the halocline in a layer of maximum vertical density gradients. The flow directions appeared strongly constrained in specific sectors, both in the measurements and the model results. There were significant differences between the 1 nm and 0.5 nm model results at V1, obviously due to the differences in resolution and gridded bathymetry of the models. Vaindloo Island, located close to the observation sites, is relatively small and it is poorly described by the 1 nm model (it is actually absent in the surface layer). Therefore the 1 nm model predicted an eastward flow spread more widely at site V1 with dominating current speeds of 5–10 cm/s. The results of the 0.5 nm model showed dominating current speeds exceeding 20 cm/s directed mainly south. The observations revealed a southeastward flow but the dominating current speeds were nearly the same. The differences in dominating directions between the 0.5 nm model and the observations may have been caused by the problems of bathymetry in the model domain, namely the unrealistic gridded presentation of the island slopes, submarine hills and deep passages. Some transformation analysis of current directions was made and the results will be discussed later.

At site V2 the 1 nm model predicted again an almost eastward flow with dominating current speeds of 5–10 cm/s, as at V1. The 0.5 nm model showed dominating north-northeastward currents with speeds of 5–10 cm/s, which is in reasonable accordance with the observations. The currents from the 0.5 nm model were more unidirectional than the observed currents, but the mean directions coincided well.

Sites V1 and V2 are located on the opposite slopes surrounding Vaindloo Island. The mean flow at V1 was directed southeast and at V2 almost north. Thus, one can conclude that in the deeper layers (within the halocline) there is a dominant clockwise current curved along the deeper passage in the vicinity of Vaindloo Island. On the larger scale of the Gulf of Finland, it is in agreement with the concept of the eastward estuarine flow of saltier waters. The speed of this flow was essentially higher than the speed of the inversely directed current in the surface layer; it must be remembered that the current roses in Fig.2 are presented at the depth where the speed of current was highest. The westward counter-clockwise curved flow in the surface layer (not shown) near the southern coast moves in opposition to the general circulation scheme of the Gulf of Finland and it can be explained by at least two reasons. Firstly, the time scale of observation is only one month, in which the flow might not be in accordance with the mean circulation; instead it could present a temporary flow anomaly caused by large scale forcing events. Secondly, the general circulation schemes are quite uncertain in details; one such scheme [17] is based on the 1 nm model (the same as in the present study) that failed to predict the flow observed near Vaindloo Island.

The current roses at observation site K showed mainly northwestward currents at a depth of 10 m where the speeds were highest. The distribution of current directions in the 1 nm model was in accordance with the one shown by measurements, although the speed was strongly underestimated. Dominant speeds of the currents in both models were 5–10 cm/s, while the observations contained a considerable amount of current speeds exceeding 20 cm/s. While the currents at a depth of 10 m are still influenced by the wind drift stress, one might speculate that the high current speeds observed could be caused by local small scale stronger wind events, which were not included in atmospheric forcing of the models. However, this is probably not the case, because the observations were performed mainly in winter when the sea at site K was mostly covered with ice. Thus, the high current speeds are probably due to the moving ice on the surface, as will be discussed later. It can be added here that compared to other observation sites the prediction of the 0.5 nm model at site K was less accurate, but the currents obtained from the 1 nm model were in better accordance with the observed currents. The latter fact is related to the improved vertical resolution introduced into the new model version. The 1 nm model also applies daily data assimilation of observational ice charts, which enables better prediction of time spans of free water, drifting ice and compressive ice.

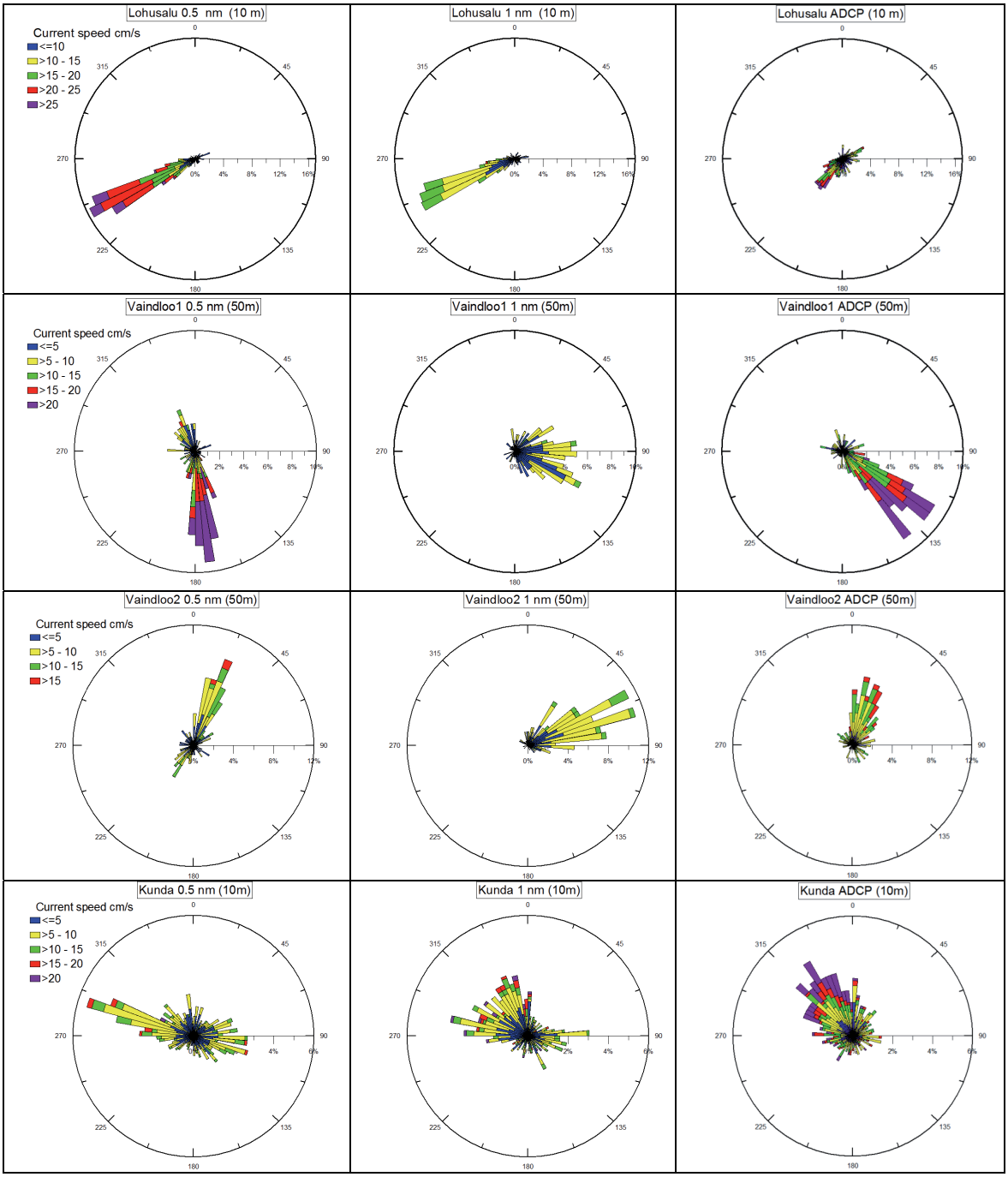

Fig. 2. Current roses of modeled (0.5 nm model – left column, 1 nm model – middle column) and observed currents (right column) in the layers of maximum current speeds at locations L, V1, V2 and K (from top to down). Color scale of current speed for each site is given at roses of 0.5 nm model.

Low-Frequency Currents

Low-frequency time series of horizontal current components were obtained by using the 36 h moving average procedure. The filter length was determined by the spectral analysis of the observational data. The main statistical characteristics of the observed and modeled low-frequency series and the correlations between them are presented in Table 1. At all sites the observed variability of the low-frequency current was dominantly higher than the variability predicted by either model. On average the 0.5 nm model produced 60% and the 1 nm model only 40–50% of the standard deviation observed. The predicted mean flow was often much more biased in the surface layer than in deeper horizons. That was probably caused by the salinity forecast bias in the Gulf of Finland (too strong horizontal salinity gradients, too small vertical gradients [16]) and by the absence of assimilation of mesoscale dynamic patterns into the models. Surprisingly, the correlations of currents predicted by the 0.5 nm model with the observed currents were evidently not higher than those calculated by the 1 nm model, as might be assumed on the basis of the model resolutions. In the following passages, these general findings will be detailed separately for different observation sites.

At the near-coastal site L the observed low-frequency current variability was in surface layers at a depth of 10 m mostly higher than at other sites at the same depth, evidencing the presence of coastal jets. The phase of mainly alongshore current oscillations was well predicted by both models as reflected in high correlation coefficients (up to 0.82). However, the mean alongshore current component was strongly biased (–8.1 cm/s) for the 0.5 nm model, resulting in a more westward flow than observed. This could be partly explained by the adjustment phase of the 0.5 nm model after initialization of temperature and salinity fields interpolated from the 1 nm model: the 0.5 nm model started just at the beginning of the analysis period, and it may take several weeks or months before stratification and mean currents accommodate to the new grid configuration and mixing coefficients. Considering that phase (by correlation) and amplitude (by standard deviation) of the modeled time series were in reasonable accordance with the measurements but the mean flow was quite biased, the coastal currents are probably influenced by some poorly predictable large scale oceanographic events (like transient baroclinic coastally trapped waves) generated in a distance from the specific observation site. In the bottom layer the observed variability was smaller but the models still underestimated it. It was noticed that with a range of only one to a few grid steps to the near-coastal depth contours and the coastline, the models tend to suppress the cross-shore currents.

Low-frequency current variability at sites V1 and V2 was compared at the depths of 10 m and 55 m. In upper layers both models failed to predict the observed currents in a satisfactory manner. The directions of the mean flow were significantly biased at both sites: by +85º and +99º at site V1 and by –123º and –154º at site V2 for the 0.5 nm and 1 nm models, respectively. The speed bias did not exceed 3 cm/s. The models did not simulate the density gradients and associated circulation branches quite properly (there is no data assimilation for the sub-surface temperature and salinity fields). By the CTD observations (not shown), the layer of maximum density gradients within the halocline lied at both sites at a depth of about 50 m, but at V2 the density profile was stretched: above 50 m the isopycnals were lifted by 10–15 m compared with site V1, and below 50 m they were lowered by the same amount. Such baroclinic structures were not found in the model results. At the same time the model results were quite similar to each other and mutual correlations between the 0.5 nm and 1 nm currents were within a range from 0.26 (meridional component at site V2) to 0.63 (zonal component at site V1). Regarding the considerably higher standard deviations of measured currents compared to the ones estimated from modeled currents, both model performances were equally poor at site V1. Considering that the current components in the 1 nm model were better correlated (in phase) with the observed components, one can say that this model performed better in the surface layer at V1. On the other hand, the 0.5 nm model had a smaller bias, which actually is a more important parameter for the comparison of currents. At site V2 the 0.5 nm model gave quite reasonable estimates for the amplitude variations and the mean bias. Since sites V1 and V2 were relatively close to each other, the atmospheric wind forcing is similar for both sites. Also, the influence of large scale wind events on sea level changes is similar. Thus, noting the fact that at site V1 the meridional current component is underestimated and at site V2 it is overestimated (Table

TABLE 1
STATISTICAL CHARACTERISTICS OF LOW-FREQUENCY CURRENTS

site_depth	ADCP				0.5 nm model						1 nm model					
	mean(u)	mean(v)	std(u)	std(v)	bias(u)	std(u)	bias(v)	std(v)	$R(u)$	$R(v)$	bias(u)	std(u)	bias(v)	std(v)	$R(u)$	$R(v)$
L_10	-2.5	-4.9	7.9	6.1	-8.1	8.5	-0.7	4.2	0.64	0.75	-4.0	6.1	2.2	2.5	0.69	0.82
L_35	1.6	0.6	6.3	3.7	-2.6	2.5	-1.4	1.5	0.39	0.09	-1.8	1.9	-	-	0.45	-
V1_10	-3.0	6.2	5.0	5.3	6.1	2.5	-4.3	2.2	0.25	0.08	8.4	2.3	-4.6	1.7	0.66	0.47
V1_55	5.8	-6.0	4.8	4.1	-2.3	3.2	1.9	3.3	0.78	0.73	-3.0	1.3	5.4	1.3	0.62	0.37
V2_10	-1.1	-3.4	5.1	4.1	1.7	3.1	3.5	4.2	0.24	0.42	6.7	2.3	7.6	2.7	0.72	0.14
V2_55	1.9	3.7	3.4	3.4	-0.8	1.4	0.3	3.8	0.06	0.77	2.3	1.9	-2.2	1.1	0.33	0.16
K_10	-3.2	4.1	5.3	6.9	2.6	4.1	-3.5	1.9	0.17	0.20	2.1	3.6	-2.6	4.2	0.34	0.65
K_46	0.8	0.6	1.3	2.9	0.2	0.9	-1.1	1.3	0.37	0.39	0.4	0.8	-0.7	1.0	0.31	0.35

std( ) – standard deviation, bias() – mean bias relative to ADCP mean, R( ) – correlation with the ADCP, u – zonal current component, v – meridional current component, L_10 – depth 10 m at site L.

1), the poor prediction of the meridional current component cannot be caused by wrong wind forcing; instead it is in all probability related to the problems in simulation of the density gradients.

In the deeper layer (55 m) at site V1 where the strongest currents were observed, the performance of both models was better than at a depth of 10 m. The 0.5 nm model obviously provided better results because of better vertical resolution above the bottom yielding more accurate bathymetry. Correlation coefficients (ADCP versus the 0.5 nm model) for zonal and meridional components of the current were 0.78 and 0.73, respectively. Also, the biases between mean currents and standard deviations were small resulting in good RMSE [18]. The zonal current component of the 1 nm model was also in moderate correlation with measurements, but there was no significant correlation for the meridional component. The standard deviations of the 1 nm model results comprised only 30% of the observed values.

In bottom layers of V2 the 0.5 nm model performance was also better, as at V1. The overall mean current bias was nearly zero and the difference in standard deviations was also reasonably small. As at V1, the 1 nm model results were too "flat" (Fig. 3), obviously due to the low vertical resolution, resulting in low standard deviation compared with the observations. Correlation rates were also too low. Despite a good visual match with the observations in the 0.5 nm model zonal component time series, the correlation with the observations was still low. The best match with measurements in bottom layers was discovered for the 0.5 nm meridional components, giving a mean bias of 0.3 cm/s, a bias in standard deviation of 0.4 cm/s, and a correlation coefficient of 0.77.

When comparing the time series of current components one has to remember that good correlation is not the most important parameter. The biased mean current components could cause much bigger problems because of possible change of the direction of the mean current, often resulting in the opposite flow in models compared to observations. Since the modeled low-frequency current time series were often strongly biased, an attempt was made to interpret the model results by possible biases in model bathymetry. The bottom layers at site V1 characterized by well constrained current roses (Fig. 2) were chosen for such an analysis. The current rose of the 0.5 nm model clearly indicates that the dominant flow direction is deflected by approximately 40º clockwise from the dominant direction of the ADCP current. As argued before, this could easily be due to the biased bathymetry in the model domain. To follow the direction of local isobaths on the slope of deep passage better, the modeled current vectors were rotated (using classical axis rotation) 40º counter-clockwise to match the direction of the observed current (presumably along-slope). Next, since the depth of the sea at site V1 was deeper than the local depth of the model bathymetry, the model depth was scaled accordingly. This means that the data from 55 m horizon in the model domain were compared with ADCP measurements at a depth of 63 m (both nearest to the bottom). The results of such transformation are presented in Fig. 3. It is evident that the model results can be significantly improved by a simple transformation when knowing the actual bottom topography at a certain location. It also indicates that the flow in bottom layers is highly dependent on topography.

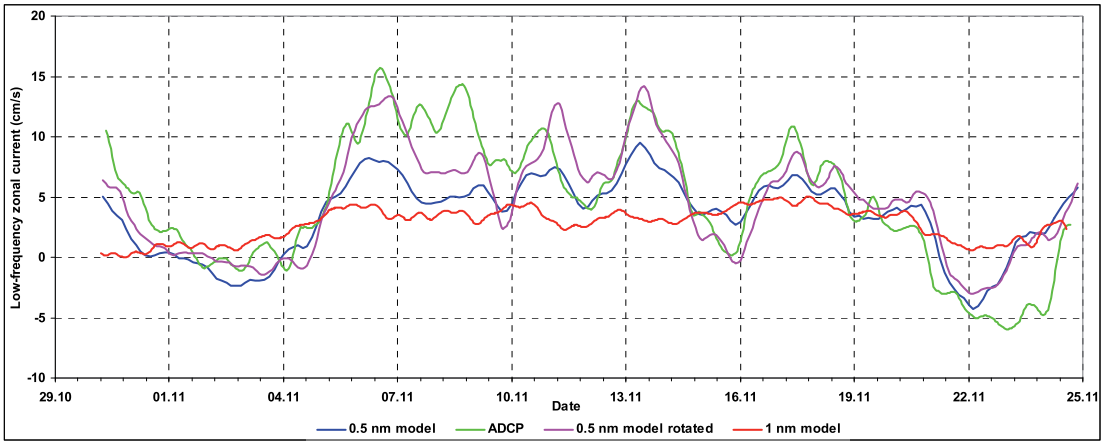

Fig. 3. Low-frequency zonal current component time series in V1 bottom layers. ADCP – at a depth of 63 m, 1 nm model – at 55 m, and 0.5 nm model – at 55 m (i.e. all at depths nearest to the bottom). Note that rotation of 0.5 nm model currents by 40º gives a better match with measurements.

The structure of near-surface (10 m) low-frequency currents was different at observation site K compared to the other sites. The measured time series of both current components contained sharp peaks indicating rapid changes in currents (not shown). Such short-term high-speed currents were observed mainly from the 28th of January until the 11th of March. Later the currents had variations similar to those at other observation sites. During the wintertime observation period, variable ice cover occurred in the Gulf of Finland. Depending on the dominating winds, the pack ice field is quite often drifted across the gulf towards either the northern or the southern shore, leaving the opposite shore temporarily with open water. Compared with the satellite images of ice

conditions (Liis Sipelgas, personal communication), the current peaks can be mostly explained by moving ice passing the observation site. Since the drag coefficient between ice and sea is larger than for air and water, the ice movements had a stronger influence on the sub-surface currents. The models did not match the actual ice conditions very well, espessially the 0.5 nm model where the assimilation of observational ice charts was not done. In the 0.5 nm model ice existed at site K already at the beginning of the measuring period. In the 1 nm model (with ice data assimilation), observation site K was ice-free until the 12th of February and the Gulf of Finland was mostly covered with ice north from the location K as also shown by the remote sensing charts. The first high speed burst in measured currents appeared around the 28th of January. This burst appeared probably due to the drifting ice before the site was covered with more static compressive ice. Another stronger peak of currents observed and modeled from 20th to 21st of February corresponds to the formation of open water due to the drifting of ice towards the northern shore. Consistent with the ice remote sensing results, on the 19th of February site K was totally covered with ice in both models but on the 22nd of February the ice disappeared in both of the models. Around the 1st of April the entire Gulf of Finland became totally ice free due to the melting process.

However, the models had some problems with predicting ice related low-frequency current peaks, although there was some match in prediction of the ice fields. The overall standard deviation of the measurements was up to 6.9 cm/s, while in the models it was only up to 4.2 cm/s. The correlation was quite good (0.65) for the meridional component of the 1 nm model. Other correlation coefficients were lower. Due to the low mean bias between models and measurements the results can be considered satisfactory. The mean currents were with the same sign in the predictions of both models and in the observations (in both current components). This means that the overall movement of the water was in the same direction, which was not always the case at other observation points. In deeper layers the influence of the ice movement decreased and therefore the standard deviation of the observations was up to 2.9 cm/s at a depth of 46 m. The bias of the mean meridional current component was only –1.1 cm/s in the 0.5 nm model. For the 1 nm model the bias of the mean current was even smaller (up to –0.7), which demonstrates well the improvements of the model version 4.0. Note that at other observation sites the bottom layers in the 1 nm model had too low current variability and therefore described mainly the mean flow. In the new version, with significantly improved vertical resolution, the bottom layer of the 1 nm model simulated properly the measurement results. The difference in standard deviations was only up to –1.8 compared to the measurements, which is approximately the same as for the 0.5 nm model.

High-frequency Currents

High-frequency current components were obtained by subtracting the corresponding low-frequency series from the raw series. The comparison of high-frequency currents revealed in some sense qualitatively better results than low-frequency currents. This was surprising since usually the high-frequency currents contain a high fraction of inertial motions (in the Baltic with periods of about 14 h) that can be either barotropic inertial waves radiated from the coasts or baroclinic inertial waves generated when barotropic waves pass the sloping stratified bottom [19]. Switching between these two regimes is quite delicate and baroclinic inertial waves usually yield opposite oscillation phases in the surface and bottom layers. Exact modeling is difficult to achieve due to the low resolutions of the models. Also, there is no real possibility for assimilating such small scale processes. At the same time the high-frequency motions that are forced by the well-predictable sea level variations could be modeled better. This will be considered below. The main statistical characteristics are given in Table 2.

At the offshore observation site V1 the dominating periods of high-frequency variations were above 22 h at all depths, referring to regular seiches with some tidal component. Both models predicted high-frequency currents qualitatively well although the magnitude of variability was underestimated. The standard deviation of the observed current was 4–5 cm/s at most depths compared to the 2–3 cm/s modeled. The correlations gave better results in the near-surface layers, up to 0.44 equally for the 1 nm and 0.5 nm model. Like the low-frequency currents, the high-frequency current time series were too flat (too small variability) in the bottom layers of the 1 nm model. At site V2 the statistics were better although quite similar to V1. All correlations with the observations were higher for both models; the correlation of the zonal component of the current was 0.52 in the 1 nm model. The performance of the 1 nm model was significantly better at V2, giving almost as good quality statistics as the 0.5 nm model.

At the near-coast observation site L the correlation between the time series of the models and the measurements was better for the meridional (almost cross-shore) components of the near-surface current (0.34 for both models) than for the zonal components. In bottom layers better correlation was found in the zonal component.

TABLE 2
STATISTICAL CHARACTERISTICS OF HIGH-FREQUENCY CURRENTS

site_depth	ADCP		0.5 nm model				1 nm model			
	std(u)	std(v)	std(u)	std(v)	$R(u)$	$R(v)$	std(u)	std(v)	$R(u)$	$R(v)$
L_10	4.9	4.6	3.6	2.4	0.36	0.34	2.7	1.8	0.25	0.34
L_35	4.2	3.6	2.7	1.5	0.49	0.25	2.5	-	0.53	-
V1_10	4.9	4.2	3.6	2.7	0.44	0.39	3.0	1.9	0.44	0.22
V1_55	4.2	3.8	3.0	2.4	0.22	0.32	2.0	1.8	0.17	-0.05
V2_10	5.2	3.1	4.1	1.9	0.45	0.22	3.6	2.4	0.52	0.28
V2_55	2.2	3.2	2.9	4.9	0.29	0.54	2.4	1.5	0.28	0.31
K_10	4.9	5.1	4.0	2.7	0.32	0.15	3.9	2.9	0.39	0.41
K_46	2.6	2.6	1.7	1.9	0.42	-0.43	2.1	1.3	0.14	-0.19

std( ) – standard deviation, R( ) – correlation with the ADCP, u – zonal current component, v – meridional current component, L_10 – depth 10 m at site L.

High-frequency currents at observation site K were modified by the existence of sea ice (see also the above description of low-frequency variations). In the time series graphs of the high-frequency current (Fig. 4) some amplitude increase episodes like around 28th of January and 20th of February can be attributed to the ice drift events as described above for the low-frequency currents. While in the low-frequency domain the influence of moving ice was not so clearly visible in bottom layers, the high-frequency currents seem to be influenced by ice from the surface down to the bottom. However, there are also some smaller bursts in currents in other time spans indicating some other source of high-frequency variability. These bursts appear at the same time when rapid sea level changes occur (over 20 cm per day). Therefore the local currents are also influenced by large scale wind events, sometimes in remote areas, resulting in sea level changes. Such sea level related bursts (e.g. from 18th to 27th February; combined with the ice drift events, and from 17th to 21st April) are better simulated by the models than the bursts related to ice movement. Considering that ice movement is also partially related to a rapid change of sea level gradients, one can assume that the bursts seen in high-frequency current time series of model results may be caused by the sea level changes.

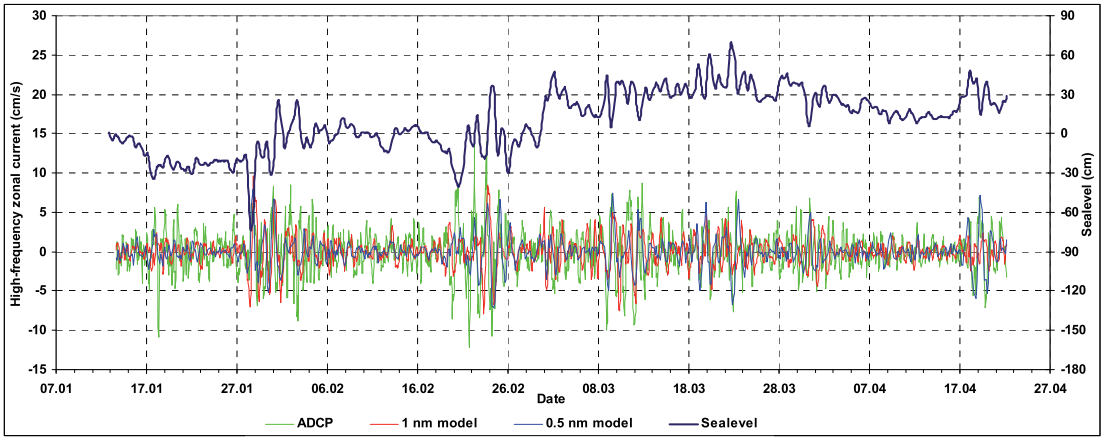

Fig. 4. High-frequency zonal current components at a depth of 46 m and sea level time series at site K.

Regarding the statistics at site K, the correlation of the observed high-frequency current components was in near-surface layers slightly better for the 1 nm model (up to 0.41 for the meridional component) and in near-bottom layers significantly better for the 0.5 nm model (up to 0.42 for the zonal component). An interesting point is that both models had a negative correlation coefficient in the bottom layers with the meridional component of the observed current. For the 0.5 nm model it was up to –0.43, indicating some serious problems with phasing. Note that inertial oscillations that may have vertical phasing options as described above were not visually dominating in any of the time series graphs.

Vertical Structure of Currents

Time series of currents at selected depths showed in several cases a layered flow with opposite current components. An analysis of vertical correlations relative to the level of maximum current variability revealed significant negative values (corresponding to opposite current fluctuations in surface and deeper layers over the whole time interval) for the meridional components at site K (measurements and both models), with the flow separation depth at 20–30 m. The 1 nm model gave a better estimation of vertical correlations at site K than the 0.5 nm model. At sites V1 and V2 such negative correlations were found only in the meridional component of the 1 nm model data, evidencing the model resolution problems in simulating the stratified flows in the regions of complicated topography. At site L both models yielded a perfect match with the observational correlation functions. Nearly barotropic flow regimes with significant positive correlations over the depth range were not found at any of the sites and usually the surface and bottom flows are uncorrelated or negatively correlated (site K). The length of positive vertical correlation of current components is about 20–30 m as estimated on the basis of the data from the measurements and both models.

The vertical correlative structure of currents was further studied by the EOF method by finding the eigenvalues and eigenfunctions of the correlation matrix of joint zonal and meridional current profiles. The techniques described in a recent study of current patterns was used [17]. Of the four sites, V1 had very interesting halocline-centered high-speed currents, as described earlier. The first EOF eigenvectors calculated from the data of observations and the 0.5 nm model are quite similar (Fig. 5a, b). They described 37% and 50% of the variance of currents, respectively. Both the observational and modeled modes are nearly unidirectional with maximum currents at a depth of about 50 m. The direction of maximum currents estimated from the model data is slightly shifted, obviously due to the model topography problems, as discussed earlier. From the depth of maximum currents further down to the bottom, both the observational and model data reveal counterclockwise vector rotation and

magnitude decay, characteristic of the near-bottom Ekman veering. The amplitude time series of the first EOF mode of the model data matches quite well the observational counterpart (Fig. 5c), with a correlation of 0.61.

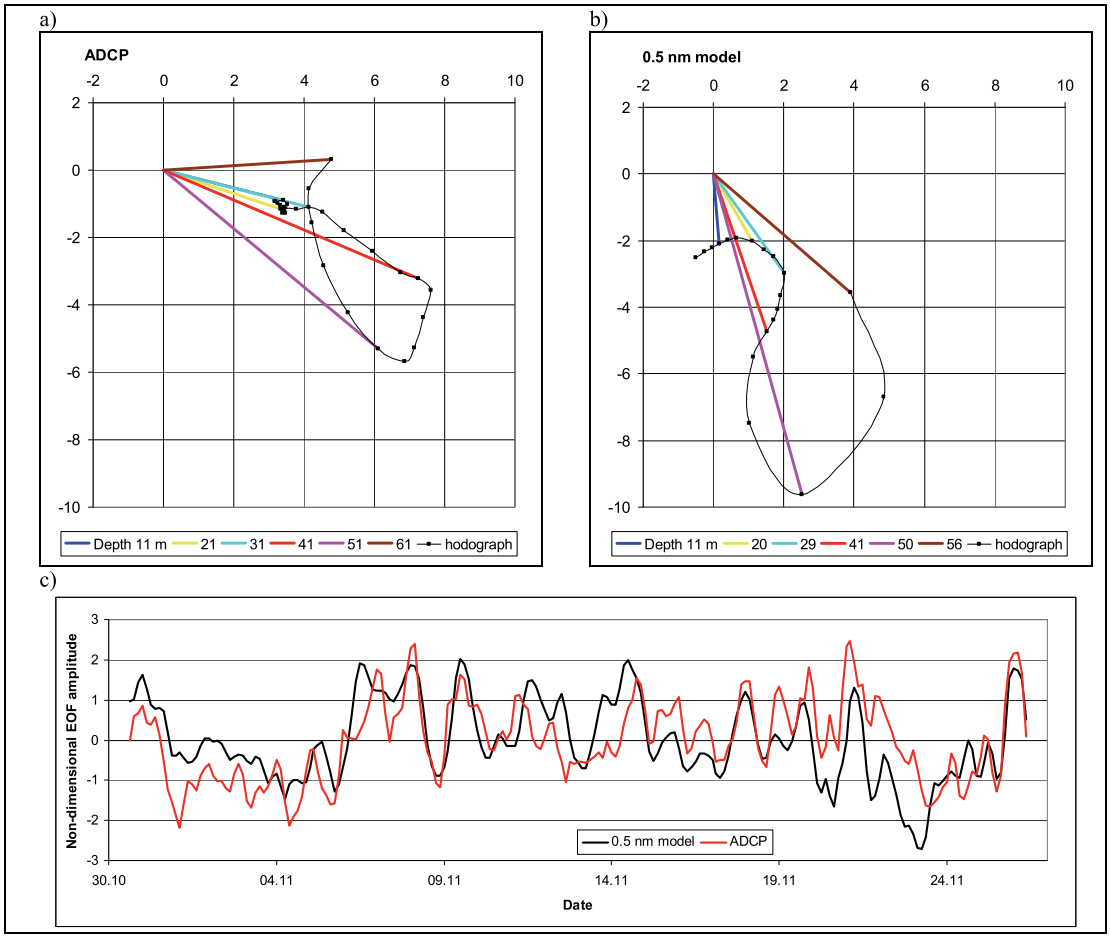

Fig. 5. First EOF eigenvector of currents at site V1 on the basis of the data from ADCP measurements (a) and 0.5 nm model (b), and comparison of the first EOF amplitude time series (c). The eigenvectors are dimensional (cm/s), to yield by scalar product the variance described by a given EOF mode. The EOF amplitudes are non-dimensional with the variance equal to 1.

CONCLUSIONS

Both the 0.5 nm model and the 1 nm model predict a reasonable match with the observed subsurface currents in most of the cases, although there are no data available for carrying out the assimilation of mesoscale oceanographic features. The correlations of the modeled currents with the observed counterparts yield quite often values above 0.5, both in the low-frequency and high-frequency range. In general, the models tend to generate less current variability (smaller standard deviations) than observed. There is also some site-specific bias of mean currents.

In general, the 0.5 nm model predicted a more unidirectional flow than observed. The variability of low-frequency currents is mostly underestimated. In the eastern part of the central Gulf of Finland the mean current speed through the whole water column is underestimated and correlation with measurements is higher in the bottom layers. In contrast, in the entrance part of the gulf the mean current speed is overestimated and the correlation values are better in the near-surface layers. The variability of high-frequency currents is slightly underestimated all over the gulf and some phasing problems were identified.

Current variability in the 1 nm model was even more underestimated than in the 0.5 nm model, compared to the measurements at all observation sites. Significant improvements of bottom layer currents were found in the new version of the model code. The variability of high-frequency currents is mostly underestimated.

Both models were not perfect to predict currents under moving sea ice conditions in all frequency domains. However, high-frequency variations caused by rapid mean sea level variations are well predicted. The rapid mean sea level variations influence the currents in the whole water column from the surface down to the bottom.

Near-bottom and coastal currents are highly constrained by topography. High current speeds (above 20 cm/s) were measured in the deep layers of the rough-bottom area around a small island. Such currents were in general well simulated by the 0.5 nm model, only slightly biased by the dominating direction. When knowing the actual bottom topography, the modeled near-bottom currents can be simply transformed to present more realistic results. Both the observations and the 0.5 nm model results revealed similar halocline-intensified EOF modes of vertical current structure, amplitudes of which were correlated quite well.

ACKNOWLEDGMENT

Thanks to SMHI for sharing the model data and code. Special thanks to Lars Axell for friendly communication concerning the model code details. Liis Sipelgas kindly made the ice remote sensing results available. The study was supported by the contract with the Estonian Meteorological and Hydrological Institute and by the grant No. 7328 of the Estonian Science Foundation.

REFERENCES

[1] K. Eilola, B.G. Gustafson, R. Hordoir, A. Höglund, I. Kuznetsov, H.E. M. Meier, et al., "Quality assessment of state-of-the-art coupled physical-biogeochemical models in hind cast simulations 1970–2005." *SMHI Oceanografi*, nr. 01, 2010, 21 pp.

[2] K. Myrberg, V. Ryabchenko, A. Isaev, R. Vankevich, O. Andrejev, J. Bendtsen, et al., "Validation of three-dimensional hydrodynamic models of the Gulf of Finland." *Boreal Env. Res.*, in press.

[3] T. Koivurova, and I. Pölvnen, "Transboundary environmental impact assessment in the case of the Baltic Sea gas pipeline." *Intern. J. Mar. Coast. Law*, vol. 25, pp. 151–181, 2010.

[4] Z. Otremba, and E. Andrulewicz, "Environmental Concerns Related to Existing and Planned Technical Installations in the Baltic Sea." *Polish J. Env. Studies*, vol. 17, pp. 173–179, 2008.

[5] The Nord Stream Project. "Nord Stream environmental impact assessment documentation for consultation under the Espoo Convention. Key Issue Paper, Seabed Intervention: Works and Anchor Handling." February 2009, 53 pp.

[6] P. Alenius, A. Nekrasov, and K. Myrberg, "Variability of the baroclinic Rossby radius in the Gulf of Finland." *Cont. Shelf Res*., vol. 23, pp. 563–573, 2003.

[7] J. Laanemets, V. Zhurbas, J. Elken, and E. Vahtera, "Dependence of upwelling mediated nutrient transport on wind forcing, bottom topography and stratification in the Gulf of Finland: Model experiments." *Boreal Env. Res*., vol. 14, pp. 213–225, 2009.

[8] J. Pavelson, J. Laanemets, K. Kononen, and S. Nõmmann, "Quasi-permanent density front at the entrance to the Gulf of Finland: response to wind forcing." *Cont. Shelf Res*., vol. 17, pp. 253–265, 1996.

[9] M. Gästgifvars, H. Lauri, A. Sarkanen, K. Myrberg, O. Andrejev, and C. Ambjörn, "Modeling surface drifting of buoys during a rapidly-moving weather front in the Gulf of Finland, Baltic Sea." *Estuar. Coast. Shelf Sci*., vol. 70, pp. 567–576, 2006.

[10] H. Burchard, F. Janssen, K. Bolding, L. Umlauf, and H. Rennau, "Model simulations of dense bottom currents in the Western Baltic Sea." *Cont. Shelf Res*., vol. 29, pp. 205–220, 2009.

[11] J.W. Book, H. Perkins, R.P. Signell, and M. Wimbush, "The Adriatic Circulation Experiment winter 2002/2003 mooring data report: A case study in ADCP data processing." *Memo. Rep. NRL/MR/7330-07-8999*, U.S. Naval Res. Lab., Stennis Space Center, Miss., 2007, 50 pp.

[12] L. Funkquist, "HIROMB, an operational eddy-resolving model for the Baltic Sea." *Bull. Maritime Inst. Gdansk*, vol. 28, pp. 7–16, 2001.

[13] L. Funkquist, and E. Kleine, "An introduction to HIROMB, an operational baroclinic model for the Baltic Sea." *SMHI Rep. Oceanogr*., RO37, 2007, 36 pp.

[14] C. Ambjörn, "Seatrack Web, forecasts of oil spills, a new version." *Env. Res., Eng. Manag.*, vol. 41, pp. 60–66, 2007.

[15] M. Gästgifvars, S. Müller-Navarra, L. Funkquist, and V. Huess, "Performance of operational systems with respect to water level forecasts in the Gulf of Finland." *Ocean Dyn*., vol. 58, pp. 139–153, 2008.

[16] J. Elken, T. Kõuts, P. Lagemaa, U. Lips, U. Raudsepp, and G. Väli, "Sub-regional observing and forecast system for the NE Baltic: Needs and first results." in *IEEE Conf. Proc*., *US/EU-Baltic Symposium "Ocean Observations, Ecosystem-Based Management & Forecasting*", Tallinn, 27–29 May, 2008, 9 pp.

[17] J. Elken, M. Nõmm, and P. Lagemaa, "Circulation patterns in the Gulf of Finland based on EOF analysis of model results." *Boreal Env. Res*., in press.

[18] K.E. Taylor, "Summarizing multiple aspects of model performance in a single diagram." *J. Geophys. Res*., vol. 106, pp. 7183-7192, 2001.

[19] J.H. Reissmann, H. Burchard, R. Feistel, E. Hagen, H.U. Lass, V. Mohrholz, et al., "Vertical mixing in the Baltic Sea and consequences for eutrophication – A review*." Progr. Oceanogr.*, vol. 82, pp. 47–80, 2009.

Paper III

Elken, J., Nõmm, M. and Lagemaa, P. 2011. Circulation patterns in the Gulf of Finland derived from the EOF analysis of model results. *Boreal Environment Research*, 16 (suppl. A), 84–102.

BOREAL ENVIRONMENT RESEARCH 16 (suppl. A): 84–102
ISSN 1239-6095 (print) ISSN 1797-2469 (online)

Helsinki 31 March 2011

Circulation patterns in the Gulf of Finland derived from the EOF analysis of model results

Jüri Elken, Marden Nõmm and Priidik Lagemaa

Marine Systems Institute at Tallinn University of Technology, Akadeemia tee 21, EE-12618 Tallinn, Estonia

Received 7 Dec. 2009, accepted 27 Aug. 2010 (Editor in charge of this article: Kai Myrberg)

Elken, J., Nõmm, M. & Lagemaa, P. 2011: Circulation patterns in the Gulf of Finland derived from the EOF analysis of model results. *Boreal Env. Res.* 16 (suppl. A): 84–102.

For the Gulf of Finland, we carried out the EOF (empirical orthogonal functions) analysis of hourly forecasts from the Baltic Sea operational HIROMB-SMHI model for the period 2006–2008. It is possible to distinguish two regions with a specific regime of circulation variability. The western region behaves like a wide channel. Dominant EOF modes at different sections have similar patterns and their time-dependent amplitudes are well correlated. A prevailing mode of currents (23%–42% of the variance) is barotropic (unidirectional over the whole section) and its oscillation (spectral peak at 24 h) is related to the water storage variation of the Gulf. A two-layer flow pattern (surface Ekman transport with deeper compensation flow, 19%–22%) reveals both inertial and lower frequencies. Highest outflow of surface waters occurs during north-easterly winds. The eastern wider region has more complex flow dynamics and only patterns that are nearly uniform over the whole Gulf were detected here. On the sea surface, quasi-uniform drift currents are deflected on the average by 40° to the right from the wind direction and they cover 60% of the circulation variance. Sea level variability is heavily (98%) dominated by nearly uniform changes which are caused by the water storage variations of the Gulf. Sea level gradients contain the main axis (23%) and transverse (17%) components, forced by winds of the same direction. The flows below the surface are decomposed also into the main axis (24%–40%) and transverse (13%–16%) components that are correlated with the sea level gradients according to the geostrophic relations.

Introduction

Large estuarine basins exhibit general cyclonic circulation in the northern hemisphere. Along-basin density gradients, created by the freshwater discharge at the head and deeper inflow of more saline waters on the ocean boundary, are modified by the transverse flows and diapycnal mixing (Chant *et al*. 2007). However, the circulation is highly variable due to the wide range of involved processes. Variable circulation patterns of the marginal seas are not so well established as compared with the atmospheric circulation patterns.

The Baltic Sea is a multi-basin estuarine sea with multidude scales of oceanographic variability. The mean surface circulation in the subbasins is cyclonic (Palmén 1930). On the shorter time scales (less than a few months) currents and stratification are modified by the variable forcing, such as moving weather patterns and fluctuat-

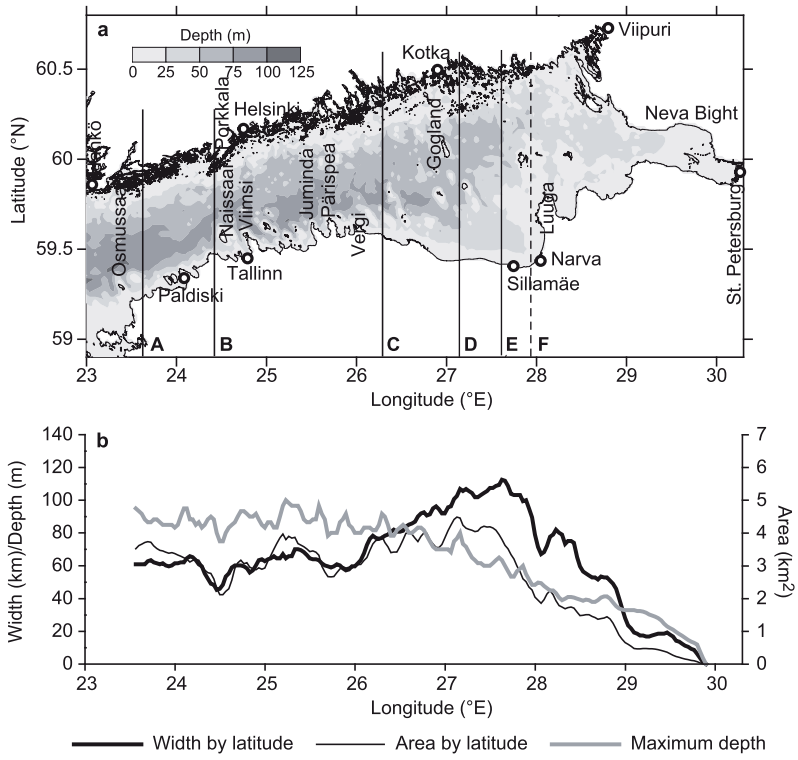

Fig. 1. Topography of the Gulf of Finland: (**a**) a map with depth contours, (**b**) longitudinal distributions of transverse width and area of the offshore regions with depth more than 10 m, and maximum depth. Letters A to E denote the sections for cross-channel analysis, A to F is the region of horizontal pattern analysis.

ing water exchange on the outer boundary of the basin (Matthäus and Schinke 1999). Unsteady circulation components may include propagation of long gravity waves of tidal and/or storm surge origin (Jönsson *et al*. 2008), Ekman transport of the upper layer and compensating deeper flows (Krauss and Brügge 1991), their evolution into upwelling/downwelling patterns (Lehmann and Myrberg 2008) and/or quasi-steady wind circulation patterns characteristic to the lakes and channels without lateral density gradients. Adjustment to the changed forcing is governed by the generation and decay of inertial waves (Nerheim 2004) and barotropic/baroclinic Kelvin waves (Lass and Talpsepp 1993). There is also a mesoscale component not always directly related to the forcing fields, comprised mainly of mesoscale fronts and eddies (Reissmann *et al*. 2009).

The Gulf of Finland is an elongated estuarine basin of the Baltic Sea (Fig. 1a), located east from the Hankö–Osmussaar line, that has the highest specific freshwater discharge (per unit area and unit volume of the basin) among other Baltic Sea sub-basins (e.g. Bergström and Carlsson 1994). With the reference to the estuarine terminology, the head is located in the east where the Neva River, entering through St. Petersburg, discharges 2400 $m^3 s^{-1}$ of freshwater (66% of the Gulf of Finland runoff), the largest amount among Baltic rivers. In the west, there is a free connection of the Gulf to the Baltic Proper without a topographical constriction and/or sill. Overall length of the Gulf from west to east is about 400 km. Despite the channel-like general shape, the width of the Gulf is quite variable. The western part, extending from the entrance at about 23.5°E to 26°E near the Vergi Peninsula, has quite uniform meridional width (Fig. 1b) of about 60–70 km, counted by depths greater than 10 m. Maximum depth by latitude is from 80 to 100 m. In this part, the Gulf has contractions near 24.5°E–24.8°E (from Naissaar and Viimsi to Porkkala) and 25.6°E–25.9°E (near the Juminda and Pärispea Peninsulas), where the width decreases by 20%–30% and the cross-section area by 40%–50%. East from 26°E, the central basin widens up to 110 km (excluding the shallow areas) at 27.6°E near Sillamäe. Maximum depth decreases to 60 m. Further to the east from Narva towards the Neva Bight, the Gulf

gets more narrow and shallow.

Salinity and density fields in the Gulf of Finland exhibit some features of a partially mixed estuary. The mean horizontal circulation is cyclonic — with average inflow of the more saline water close to the southern, Estonian coast and outflow of the less saline water along the northern, Finnish coast. Speeds of the mean circulation have been estimated a few cm s^{-1}. However, the circulation is modified by several factors, as described above. Instantaneous currents may reach 20–30 cm s^{-1} or even more (Alenius *et al*. 1998).

Over the seasons, changes of stratification and wind forcing create different mean patterns of circulation in the Gulf of Finland, as described already by Witting (1912) and Palmén (1930) (*see* the review by Alenius *at al*. 1998). Instrumental observations give reliable estimates of the variability of currents, but unfortunately they are limited either in time or space to give estimates of the current patterns and their variations. Therefore, the present circulation estimates are based, to a large extent, on the model results.

Multiannual model studies (Lehmann *et al*. 2002, Andrejev *et al*. 2004, Meier 2005) have reconfirmed the observational arguments of the mean cyclonic circulation. The results gave further insight into the problem of persistency of the current direction, i.e. fraction of the vector-mean current speed to the scalar-mean speed (Palmén 1930). Within the limits of model performance, the earlier observation-based indications were renewed by the concepts of high-stability current belts, where persistency above 0.5 (Andrejev *et al*. 2004) is concentrated in the outflow region, to the north from the central axis of the Gulf.

The present paper is aimed to study the unsteady circulation patterns of the Gulf of Finland, using the available hourly model results from the operational HIROMB-SMHI model system for the period 2006–2008. Using the empirical orthogonal functions (EOF) method, we decompose the large-scale circulation variability into dominating, objectively determined patterns/modes of the temporally variable amplitude. When possible, we draw out the relations of the EOF amplitude variations to the variations in external forcing. This way we contribute to the existing circulation knowledge both in the statistical and physical (oceanographic) sense.

Material and methods

Model data

We used the results from the operational HIROMB-SMHI model system (Funkquist 2001, Gästgifvars *et al*. 2008) for the period 2006–2008. The model domain covers the whole Baltic Sea and its extension to the North Sea (9.375°E–30.236°E, 53.658°N–65.892°N) with a grid step 5/3´E by 1´N (about 1 nautical mile) yielding 752 × 735 horizontal grid points. The model presents the Baltic Sea by 16 vertical layers, with a grid step of 4 m from the surface down to 12 m, 6 m further down to 30 m, 10 m down to 60 m and increasing further below. The model has mixing modules based on the κ-ω approach (Umlauf *et al*. 2003) for vertical mixing and Smagorinski formulation for horizontal mixing. It has also an extensive ice mechanics and thermodynamics module. The model is forced by the atmospheric forecasts from the HIRLAM-SMHI model system, with a grid step of 22 km, and river forecasts from the HBV surface water modeling system. Lateral open sea conditions are derived from larger domain models using the nesting technique. Tidal forcing is introduced along the North Sea outer boundary of the largest three-dimensional domain (grid step 12 nautical miles). The system performs data assimilation, based on the different data: remote sensing data of sea surface temperature and sea ice, *in situ* observations at MARNET buoys and from ships, including vertical profiles from the HELCOM stations and daily FerryBox surface section (Tallinn–Helsinki, Lips *et al*. 2008b) data for salinity and temperature.

We have assembled the daily forecasts from two upgrades of the model into one time series. Version 3.0 had been running since 15 Nov. 2005. The next version 3.1 (Axell 2006) started on 19 Sep. 2007. It introduced the variable wind stress coefficient and included effects of the surface waves. Specific to the present study, the sea

surface wind stress components τ_λ, τ_φ along the longitude λ and latitude φ are calculated with a common quadratic formula from the corresponding wind speed components W_λ and W_φ at the height of 10 m as

$$\tau_\lambda = \rho_a c_D W_\lambda \sqrt{W_\lambda^2 + W_\varphi^2} \text{ and}$$

$$\tau_\varphi = \rho_a c_D W_\varphi \sqrt{W_\lambda^2 + W_\varphi^2},$$

where ρ_a is the air density. Until 18 Sep. 2007, the drag coefficient c_D was defined as

$$c_D = 10^{-3}(0.7 + aW)$$

where $W = \sqrt{W_\lambda^2 + W_\varphi^2}$, and $a = 0.09$ (m s^{-1})$^{-1}$.

In order to correct the modeled too high surface current velocities during stronger winds and too low velocities during weaker winds as compared to the observations, the dependence on neutral-stability winds W_N was introduced in version 3.1, $c_D = 1.3 \times 10^{-3}$ at $W_N < 8$ m s^{-1} and $c_D = 10^{-3}(0.84 + a_N W_N)$, $a_N = 0.058$ (m s^{-1})$^{-1}$. Depending on the atmospheric stability (difference of temperature of air and water), the drag coefficient varies at wind speeds below 10 m s^{-1} from 0.9×10^{-3} (most stable) to 1.95×10^{-3} (most unstable).

Recent validation study of six three-dimensional models against more than 300 vertical profiles of temperature and salinity measured in the Gulf of Finland (Myrberg *et al*. 2010) concluded that the best model was HIROMB, although no model was the best/worst in all cases. Another study (Elken *et al*. 2008) showed that on the average, during the warm season HIROMB produces too high surface salinity gradients and too low vertical stratification as compared with the observational data. Sea level validation (Gästgifvars *et al*. 2008, Elken *et al*. 2008) revealed that root mean square errors of 1–24 h sea level forecasts at different coastal stations of the Gulf of Finland are 5–10 cm. Unfortunately, model comparisons with current observations are quite rare. Gästgifvars *et al*. (2006) concluded that during the rapidly changing weather conditions drift trajectories, calculated using the HIROMB-based system Seatrack Web, followed well the observed drifter trajectories in the central part of the Gulf of Finland.

Application of the EOF method

We shall analyze the circulation patterns on the basis of hourly data from the operational HIROMB model system for the period 2006–2008: altogether 25 968 sets of grid data. Within the statistical procedures, we consider the deviations of currents, density, sea level and wind from the 3-year mean fields. The deviation fields are decomposed into spatial modes (fixed over the time period) with time-dependent amplitudes, using the well-known EOF method (e.g. von Storch and Zwiers 1999), which is a Principal Component Analysis. This technique allows for estimating the variance ("energy") contribution of individual spatial modes to the overall variability. The time-dependent amplitudes show, how in specific events different spatial patterns are amplified or damped.

The EOF method is particularly useful when variability of studied fields is *a priori* known to be governed by standing patterns. In the complex range of ocean variability, such cases occur, for example in basin-wide horizontal patterns (Schrum *et al*. 2006), and vertical profiles or sections dominated by low-frequency waves (Lass and Talpsepp 1993, Pizzaro and Shaffer 1998) or flows in a channel (Thomson *et al*. 2007).

For the specific application, let us analyze the set of spatio-temporal data $\psi(i,j,k,n)$, where i, j and k are the indices of space coordinates and n is the time step index. The EOF method is based on the analysis of one-dimensional sets of variables. For this purpose we transform the multi-dimensional data set of the size M at each time step n into a one-dimensional array of index $m = m(i,j,k)$, where m is the data counter in the multi-dimensional data sequencing loop. The reverse transformations of coordinates are $i = i(m)$, $j = j(m)$, $k = k(m)$, which perform remapping of the found EOF features back to the original space. If the time-averaged mean is

$$\overline{{}^{n}\psi(m)} = \frac{1}{N}\sum_{n=1}^{N}\psi(m,n)$$

then the fluctuation is

$$\psi'(m,n) = \psi(m,n) - \overline{{}^{n}\psi(m)}\ .$$

The fluctuations can be presented by a superposition

$$\psi'(m,n) = \sum_{l=1}^{L} A_l(n) F_l(m)$$

where the number of modes L equals the number of spatial data points M. Here $F_l(m)$ is a normalized orthogonal spatial structure function (mode) and $A_l(n)$ is the time-dependent amplitude of the mode l. The modes $F_l(m)$ are found as eigenvectors of the (spatial) covariance matrix of $\psi'(m,n)$. Different modes p, q are orthogonal in terms of condition

$$\sum_{m=1}^{M} F_p(m) F_q(m) = 0 \text{ if } p \neq q.$$

Then the amplitudes of EOF modes are found in the form

$$A_l(n) = \sum_{m=1}^{M} \psi'(m,n) F_l(m).$$

The variance (energy) contained in a particular mode l is determined as the ratio of the corresponding eigenvalue λ_l to the sum of all eigenvalues over L. The modes are usually numbered by the decreasing variance, with the 1st mode containing the largest fraction of the overall variance. Note, that the analyzed dataset $\psi(m,n)$ may also contain components of physical vectors such as currents and winds.

Analysis of EOF mode patterns and amplitudes

Classical EOF method uses normalized non-dimensional modes

$$\sum_{m=1}^{M} F_l^2(m) = 1$$

and dimensional amplitudes $A_l(n)$. However, the interpretation of the numerical results of such a presentation depends on the number of selected spatial data points M. As an alternative (e.g. von Storch and Zwiers 1999), we use the dimensional spatial modes

$$\sum_{m=1}^{M} \tilde{F}_l^2(m) = \lambda_l$$

and the non-dimensional amplitudes $\tilde{A}_l(n)$ scaled to yield their standard deviation equal to 1. Therefore, if we consider $\tilde{A}_l(n) = 1$ as a typical event then graph of the individual mode $\tilde{F}_l(m)$ presents the physical values of the spatial pattern of this event.

We chose to study the EOF modes at selected fixed levels (horizontal patterns) and in selected meridional (nearly cross-gulf, deflection angle up to 15°) sections. Although we also performed some analysis of the monthly and tri-monthly data sub-sets over 3 years, the final selection was one data set over the whole period since the mode patterns turned out to be quite similar. Transects (Fig. 1) were selected along longitudes 23.65°E (section A), 24.38°E (B), 26.26°E (C), 27.13°E (D) and 27.60°E (E). The area for the horizontal pattern analysis was confined between 23.65°E (A) and 27.93°E (F). Sections contained up to 250 active grid points (section B) and horizontal patterns up to 3714 points (surface analysis).

We seek the physical interpretation of the formal EOF patterns and their relation to forcing by analyzing the time series of EOF amplitudes of different modes, using correlation analysis and power spectra analysis. The overall length of hourly amplitudes was 25 968 points. Due to this large sample size, correlations were statistically highly significant even for low correlation values. However, for oceanographic reasons (low-frequency events may be quite rare within a few years) we did not consider the relations, whose coefficients of determination (R^2) were below 0.4. Spectral analysis was done using the Welch averaged periodogram method built in the MATLAB. The data was divided into about 100 overlapping segments by setting the Hamming filter window length equal to 512, with the overlap length equal to 256 (50% of the window). Power spectral densities were calculated then as the average of the periodograms of individual segments.

The vector fields, like winds and currents over a horizontal area, were analyzed by mapping the vector components at different grid points into the one-dimensional array and remapping the derived modes $\tilde{F}_l(m)$ back to the original vector components and grid points. Many of the vector patterns appeared to be quite non-divergent. For the visualization of vectors, we used the streamfunction approach (Watterson 2001) if R^2 for the correlations between the origi-

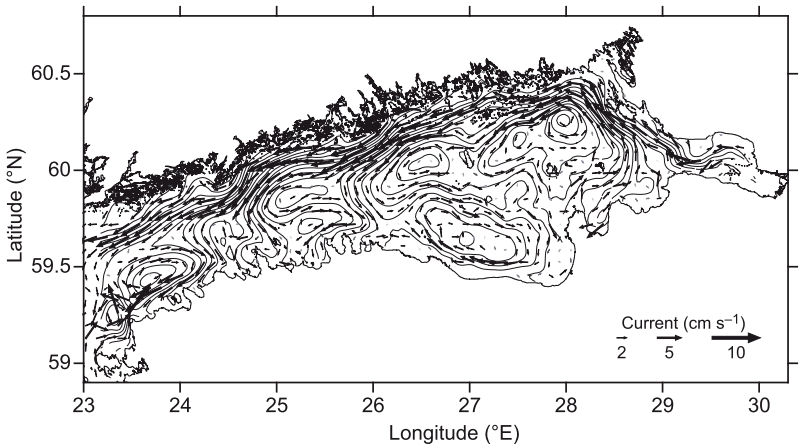

Fig. 2. Mean circulation of period 2006–2008 in the most stable layer (4–8 m) of the Gulf of Finland. The currents are presented by every 4th vector superimposed by the streamfunction contours.

nal vectors and the vectors calculated from the streamfunction exceeded 0.6.

Mean circulation

The period 2006–2008 was characterized by mild to moderate winters and normal wind regime. The mean wind vector, based on the forcing data in the central part of the Gulf, was about 2 m s^{-1} from 240°–250° as within the longer period. However, several significant meteorological and oceanographic events occurred. Intensive upwelling occurred along the southern coast in July–August 2006 (Lips *et al*. 2008a), due to the unusually persistent easterly winds. Stormy periods in October–November 2006 and in January 2007 caused high sea levels in the Gulf due to the southwesterly winds (Elken *et al*. 2008).

The mean current fields (Fig. 2) reveal the known cyclonic circulation. The currents in the most stable layer of 4–8 m, just below the drift-influenced surface layer, reveal the maximum outflow of less saline water near the Finnish coast in the Finnish Coastal Current (Stipa 2004). As compared with the earlier results, Andrejev *et al*. (2004) — who used the OAAS model — obtained the mean outflow in 1987–1992 closer to the main axis of the Gulf. The shift can be explained by the differences of the specific forcing events during different periods (although the mean wind vectors were the same), and the specific features in the response of the two models under the same forcing (Myrberg *et al*. 2010). Both the HIROMB-SMHI model (present study) and the OAAS model (Andrejev *et al*. 2004) reveal some other interesting circulation features. The southward recirculation loop, detaching from the Finnish Coastal Current and feeding the southern eastward currents, is located just east from the Tallinn–Helsinki connection line. We also note the second southward loop of the Finnish Coastal Current near 26°E (Fig. 2). In the eastern part of the Gulf, from 26.5°E to 27.7°E, the currents near the southern coast are oriented in reverse, westward direction. An unexplained circulation feature appears in the western part of the southern coast, west from 24.4°E (Fig. 2). Namely, the coastal currents are directed westwards and the inflow of more saline open Baltic Sea waters takes place offshore, in the deepest parts of the Gulf.

Vertical structure of the mean currents in section B (Fig. 3) exhibits the outflow on the northern slopes of the Gulf, some 10–15 km offshore, at the depths of 10–20 m. Inflow takes place in the deepest part of the Gulf in two depth ranges, close to the surface and in the halocline within the depths from 40 to 60 m. The mean sea level drops by 2–3 cm from north to south, forcing the outflow of surface waters in accordance with the geostrophic relations. Towards greater depths, the density gradients oppose the sea level drop, resulting in the decrease of pressure gradients and along-channel flow.

Note that all the further pattern variation analysis is based on the deviations (anomalies) from the mean fields given in this section.

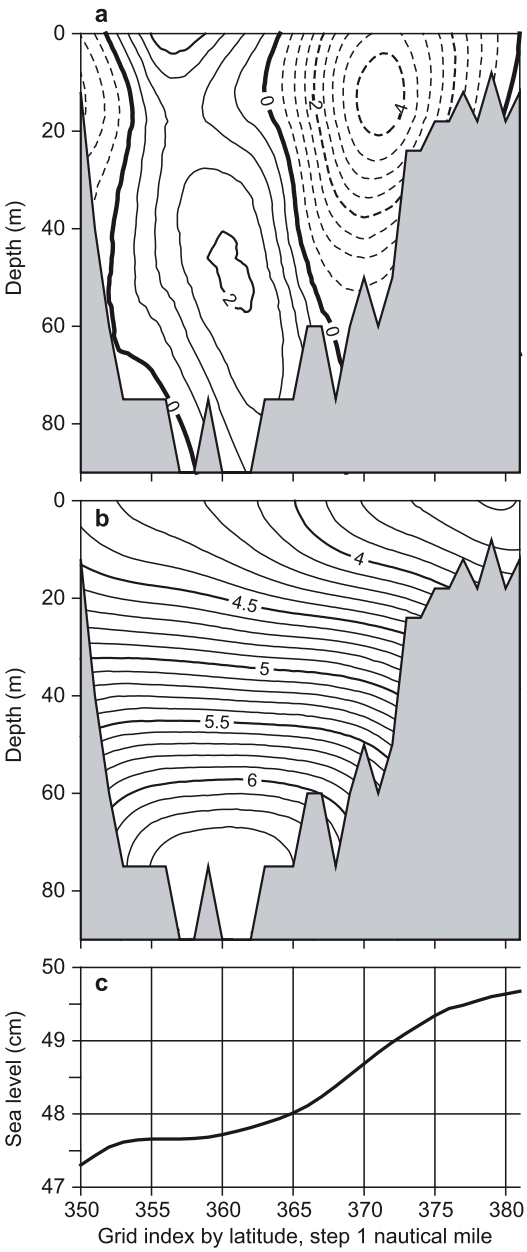

Fig. 3. Mean (**a**) east-west currents, (**b**) density , and (**c**) sea level in section B of the period 2006–2008. The contours for currents and density anomalies are cm s^{-1} and kg m^{-3}, respectively.

EOF modes of circulation variables

Horizontal fixed level modes

We started the analysis of horizontal modes in a region from A to F (the wide part of the Gulf, Fig. 1b) from wind vectors, considering as usual deviations from the mean fields. The two first wind vector modes comprise 93% of the wind field variance. Horizontally the modes are almost uniform: the relative standard deviation of vector magnitudes is only 3%; therefore, we may also calculate standard deviation of directions and conclude that it is less than 2° (for the small relative vector magnitudes the direction is quite uncertain, but this is not the case here). It means that on the average "physical" wind vectors of the two first EOF modes are geometrically almost orthogonal (perpendicular) at each horizontal grid point. Note, that individual modes are exactly orthogonal in terms of EOF eigenvector scalar product over the whole domain, not necessarily the "physical" vectors at each grid point. Within this analysis, 53% of the wind variance (1st mode) is oriented along direction 226° (SW–NE) or 46° (according to the EOF sign determination options) and 40% (2nd mode) along 316° (NW–SE) or 136°. This result justifies common usage of the horizontally uniform, only time-dependent wind field in modeling studies of sub-regions, which extent is much smaller than baroclinic Rossby radius of the atmosphere (about 1000 km, Gill 1982).

Wind-driven surface currents are generally known to follow the wind stress, but they are deflected from the wind direction due to the Earth's rotation. The two first current modes (deviations from the mean fields, Fig. 4) comprise together 60% of the variance. They also exhibit horizontally quasi-uniform patterns like the wind modes, but the spatial variability of the vector magnitudes is somewhat higher. Still, the directional variation study is justified and the standard deviation is 18°–20°. Main variations of the surface current direction take place in the coastal areas and between the western and eastern parts of the calculation area. Within the sign determination freedom of EOF modes, the mean direction is 104° or 284° for the 1st mode and 16° or 196° for the 2nd mode. It means that on the average the 1st and 2nd surface current modes are geometrically perpendicular within ±2° accuracy. As shown in Fig. 4, the 3rd and 4th modes of surface currents do not comprise horizontally uniform drift patterns. Instead, they

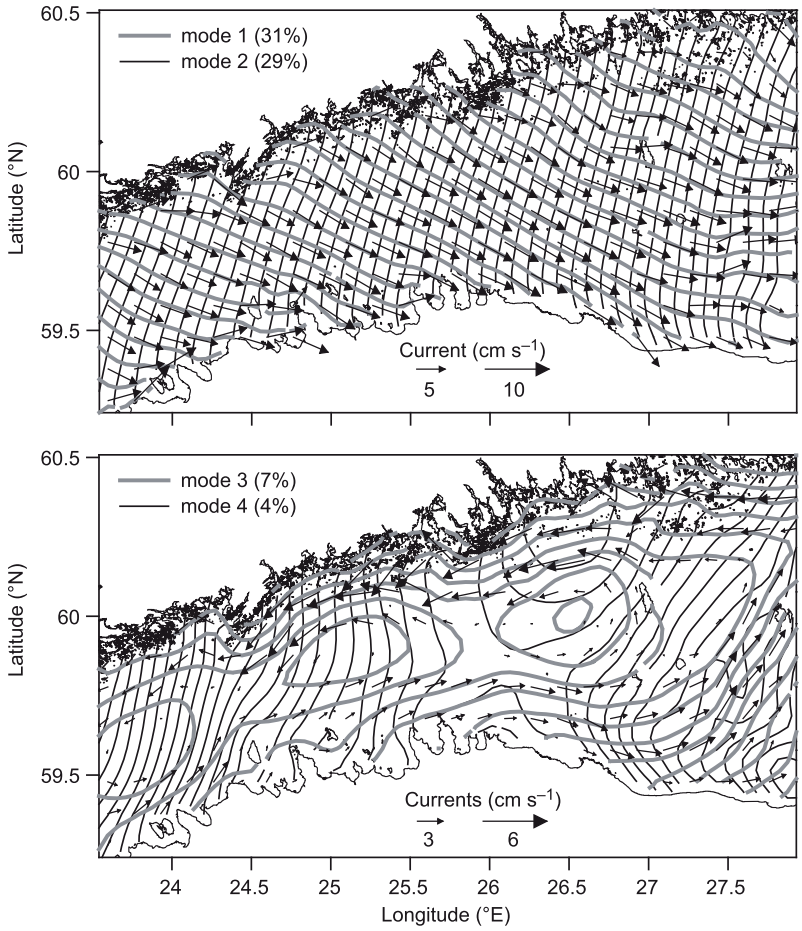

Fig. 4. Horizontal EOF mode patterns of surface current, 1st and 2nd mode (top panel), 3rd and 4th mode (bottom panel). The vector patterns of modes are visualized by the streamfunction method. For comparison, actual vectors of the 1st and 3rd mode are also drawn.

reveal a number of circulation cells where the mean direction does not make sense. A characteristic feature of the 3rd mode (7% of variance) is opposite currents along the southern and northern coasts of the channel, and partial circulation closures at longitudes 24.5°E–24.8°E and 25.6°E–25.9°E, where the cross-channel geometry shows contractions.

Further, we studied how the amplitudes of the two first modes of surface currents A_{u1} and A_{u2} are related to the amplitudes of wind modes A_{W1} and A_{W2}. Since the surface currents have notable energy near the inertial period of 14 h as obtained from the spectral analysis of A_{u1} and A_{u2}, we used for their suppression a 3-point filter:

$$\tilde{\psi}(t) = 0.25\left[\psi(t - T/2) + 2\psi(t) + \psi(t + T/2)\right]$$

(here ψ and $\tilde{\psi}$ are original and filtered variables, T is the period to be damped). We found that amplitudes A_{u1} and A_{u2} of the two first current modes correlate well with the wind stress functions $A_{W1}\sqrt{A_{W1}^2 + A_{W2}^2}$ and $A_{W2}\sqrt{A_{W1}^2 + A_{W2}^2}$ of the amplitudes of the two first wind modes A_{W1} and A_{W2}, if the physical vectors of wind stress amplitudes are projected to a proper angle. The best correlations (R^2 = 0.71) with both A_{u1} and A_{u2} were obtained when wind amplitudes A_{W1} and A_{W2} were rotated as horizontal vector components (with respect to EOF mode directions 46° and 136°, respectively) clockwise by 20°. This means that current component A_{u1} towards 104° correlates with the wind stress towards 66° (i.e. 46° + 20°) and component A_{u2} towards 196° correlates with the wind stress towards 156° (136° + 20°). From the above we conclude that 60% of the surface current variance is explained by the relation: speed of the surface currents is proportional to the wind stress (wind speed squared) and the currents are deflected

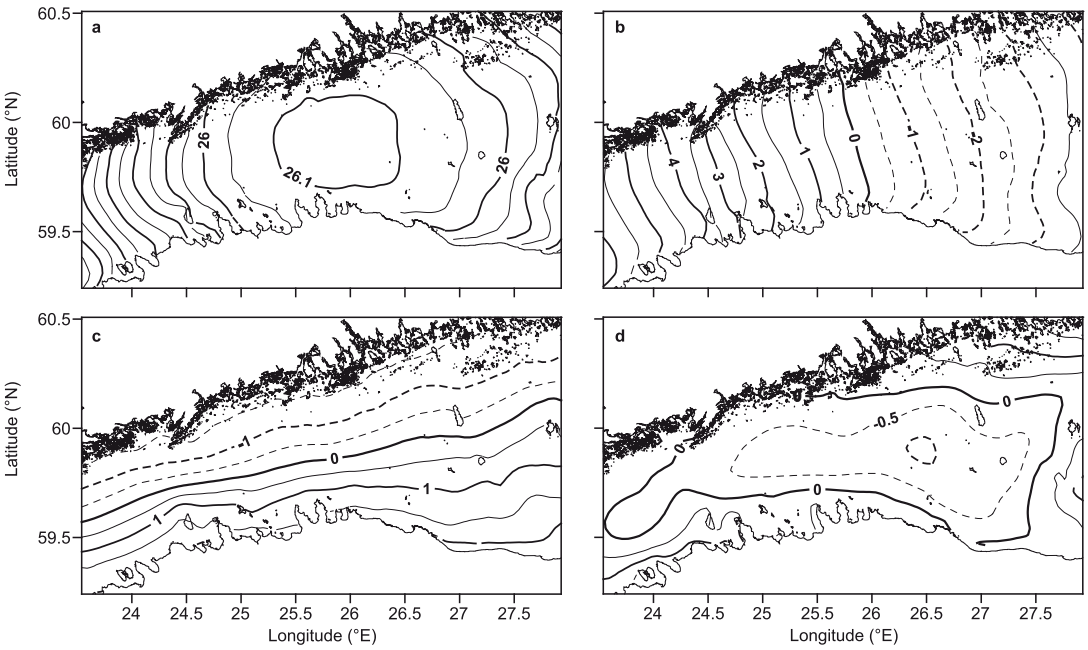

Fig. 5. Horizontal EOF mode patterns of the sea level, modes: (**a**) mode 1 (98.6%), CI = 0.05 cm; (**b**) mode 2 (1.0%), CI = 0.5 cm; (**c**) mode 3 (0.2%), CI = 0.5 cm; and (**d**) mode 4 (0.03%), CI = 0.5 cm;. The mode patterns are dimensional (cm), scaled by the square root of the variance of each mode. Note the smaller contour interval for the flat 1st mode.

on the average 40° to the right from the wind direction. Although several observational studies revealed linear dependence between the wind speed and the surface current speed (*see* the review by Alenius *at al*. 1998), we found in case of prevailing EOF modes a better correlation match between current speed and quadratic wind stress. It is interesting to note that scatter plots of amplitudes of wind stress functions and surface currents revealed two distinct clusters during the whole period 2006–2008. These clusters correspond to the older model version 3.0 with linear drag coefficient dependence on the wind speed, and to the new version 3.1 with stability-dependent wind stress drag coefficient. The values of R^2 were 0.84–0.86 for the old version and 0.77 for the new version. From old to new version, the wind-to-current transfer coefficient decreased by about 2 times. We note that these relation changes reflect only the revision of model features, not the circulation physics. The 40° deflection angle of the current anomalies (from the mean fields) relative to the wind anomalies is the same for both model versions. From the earlier studies, based on observations at specific locations, the deflection angle (including the mean fields) could be up to 60° (Gästgifvars *et al*. 2006).

Sea level variability is heavily (98.6% of variance) dominated by the flat 1st mode, where difference of the minimal and maximal values is only 2% of the mean value of the mode (Fig. 5). This mode thus presents storage variations (filling and emptying) of the whole gulf, with negligible spatial gradients. Quite expectedly, the amplitudes of this mode are not correlated with the local wind amplitudes, since the storage variations of the particular gulf depend on the mean sea level of the whole Baltic Sea and the large-scale air pressure and wind fields over the whole sea area (Lehmann and Hinrichsen 2001, Lehmann *et al*. 2002). Spatial gradients of the sea level are dominated by the along-channel (2nd mode, 1.0%) and cross-channel (3rd mode, 0.2%) variations. The 4th mode (0.03%) reveals high levels in the central part of the Gulf and low levels near the coast, or vice versa, depending on the sign of the amplitude. This mode therefore represents amplification or decay of the mean cyclonic circulation.

Sea level gradients have significant dependence on wind direction. Along-channel gradients (2nd mode) are amplified by wind stress projected to 275° (R^2 = 0.77) and cross-channel gradients (3rd mode) by wind stress projected to 195° (R^2 = 0.49). In other words, sea level rises in the eastern end of the Gulf by the westerly wind stress component and on the northern shore by the southerly (slightly south-westerly) wind stress component. The 4th mode of the sea level gradients is excited by the westerly wind stress component (direction 285°, R^2 = 0.39) and the amplitudes correlate with the 3rd "circulation" mode of the surface currents (R^2 = 0.55).

The currents below the surface Ekman layer are forced by the sea level gradients and dynamically adjusted baroclinic pressure gradients. In order to suppress the possible distortions from the highly dominating almost uniform first sea level mode, the sea level gradients were decomposed into EOF modes separately. The along- and cross-channel gradient modes yield 23% and 17% of the total gradient variance, respectively. The amplitude correlation with the original sea level is high (R^2 = 0.92) for the cross-channel components and lower (R^2 = 0.73) for the along-channel components. On both analyzed current depth levels, 24–30 m (thermocline) and 50–60 m (halocline), the two first dominating current modes are quite homogeneous. The flow components are oriented along the main axis of the Gulf (24% of variance in the thermocline and 40% in the halocline) and along the transverse cross-channel direction (13% and 16%, respectively). The along-channel flow (1st current mode) is related to the cross-channel sea level gradients (2nd mode) in the thermocline with R^2 = 0.71 and in the halocline R^2 = 0.46. The transverse flow (2nd current mode) is correlated with the along-channel sea level gradients (1st mode), a bit more (R^2 = 0.64) in the halocline than in the thermocline (R^2 = 0.50). Therefore, we conclude that an evident geostrophic relation exists between the dominating sea level gradients and the flows below the surface Ekman layer.

In the frequency domain, the amplitudes of the wind modes have dominating energy in the synoptic range with a peak from 80 to 110 h. Most energetic, 1st sea level mode exhibits spectral maximum on the period of 31 h. Higher sea level modes are dominated by 24 h oscillations. We note that energetic diurnal tidal oscillations have been found also by the spectral analysis of observational data at selected sites in the Gulf of Finland (Johansson *et al*. 2001). Currents on the fixed levels are dominated either by the 24 h oscillations (1st mode) or inertial oscillations (higher modes). However, the 2nd ("cross-channel") and 3rd ("circulation") modes have maxima also in the low-frequency range, on the periods about 66 h and 30 days, respectively. During the strong upwelling event on the southern (Estonian) coast in July–August 2006 (Lips *et al*. 2008a), the amplitude of the 3rd surface current mode revealed distinct anomaly throughout the whole period.

Section modes

Further we studied the details of circulation patterns on selected meridional (cross-channel) sections. Since the horizontal analysis of the wind fields, presented above, showed quasi-uniform patterns, then (not surprisingly) correlations of the wind amplitudes between individual sections yield R^2 above 0.9. The same is valid for the 1st mode of the sea level variations.

First four modes of the east-west current anomalies cover 74% of the variance in section B (Fig. 6). In other sections of the western and central areas (A and C), both the geometry of patterns and the fractions of explained variance are similar. The amplitudes of the current modes are well correlated ($R^2 > 0.8$).in the western part between A and B, and less correlated ($0.4 < R^2 < 0.6$) in the eastern part of the central area between B and C. Further to the east, in the wider area of the Gulf (sections D and E) the similarity of the mode geometry and the correlations are lost.

The modes of density anomalies in the section B are depicted in Fig. 7. Three first modes cover 88% of the variance. In different sections, the most energetic 1st mode (52%–55%) presents mainly the seasonal density variations (Haapala and Alenius 1994) — strengthening of stratification during summer and weakening during winter — and is therefore highly coherent between all the different sections. Higher density

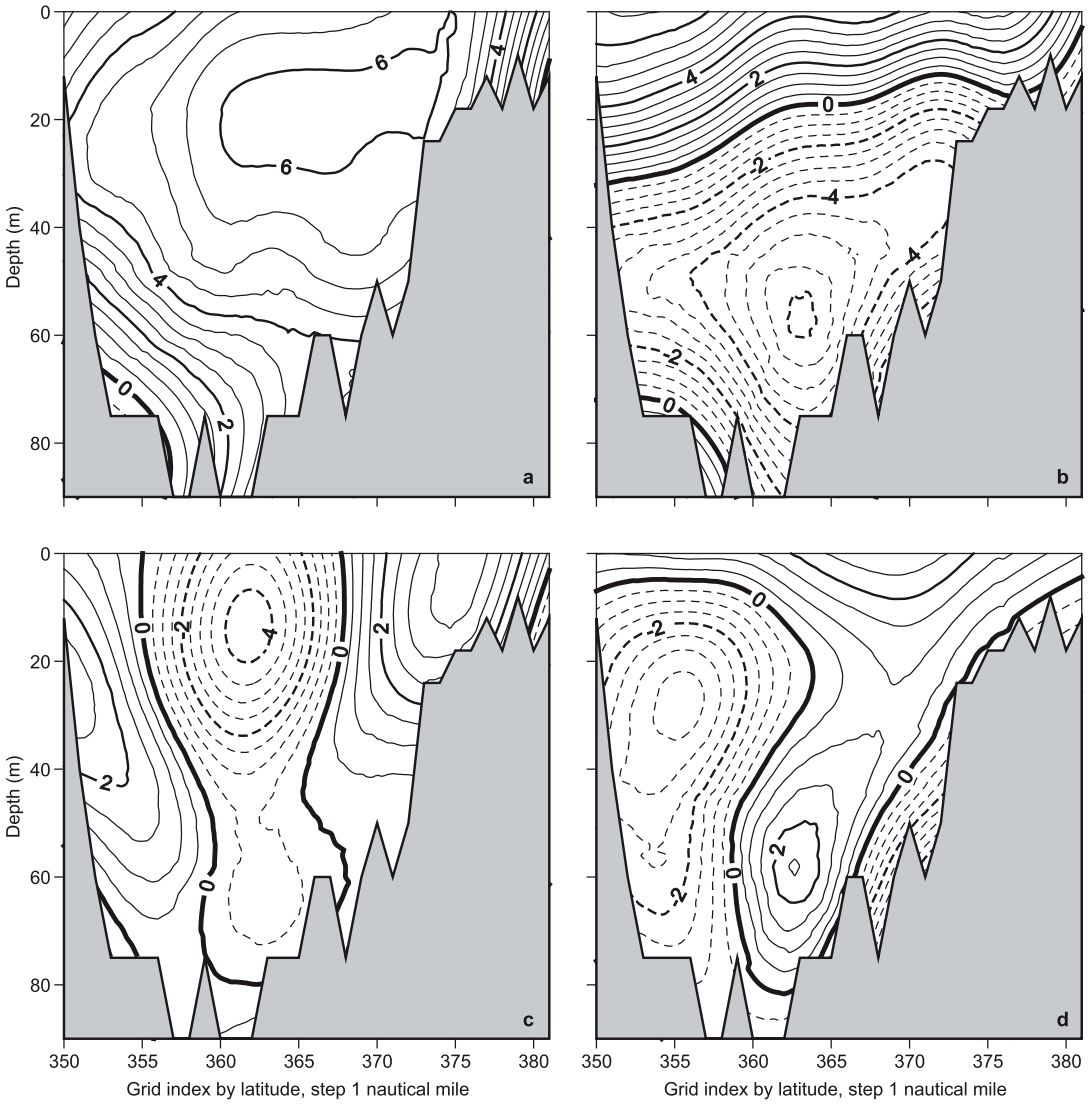

Fig. 6. Patterns of EOF modes of the east-west currents in the section B: (**a**) current U mode 1 (42%), (**b**) current U mode 2 (18%), (**c**) current U mode 3 (7%), and (**d**) current U mode 4 (6%). The mode patterns are dimensional (cm s^{-1}), scaled by the square root of the variance of each mode.

modes describe stratification disturbances due to the circulation variability. The geometrical similarity of these modes is apparent only from section A to C. Change of mean over section density is governed by the 2nd almost flat mode (22%–27%).

EOF analysis gives some physically meaningful modes. The 1st current EOF (23%–42%) is a flat ("barotropic") mode, characterized by unidirectional flow through the whole section. By amplitude variability it is related to the short-term (hours to days, spectral peak at 24 h) water storage variations in the Gulf, since correlation with the time derivative of the sea level 1st mode amplitude is acceptable ($R^2 \approx 0.4$).

The 2nd current EOF (19%–22%) is an "Ekman" mode (surface Ekman transport with deeper compensation flow). The flows are opposite in the surface and deeper layers but unidirectional within a layer. In the frequency space the amplitudes are dominated by the inertial (14 h) and low-frequency (days to a few tens of days)

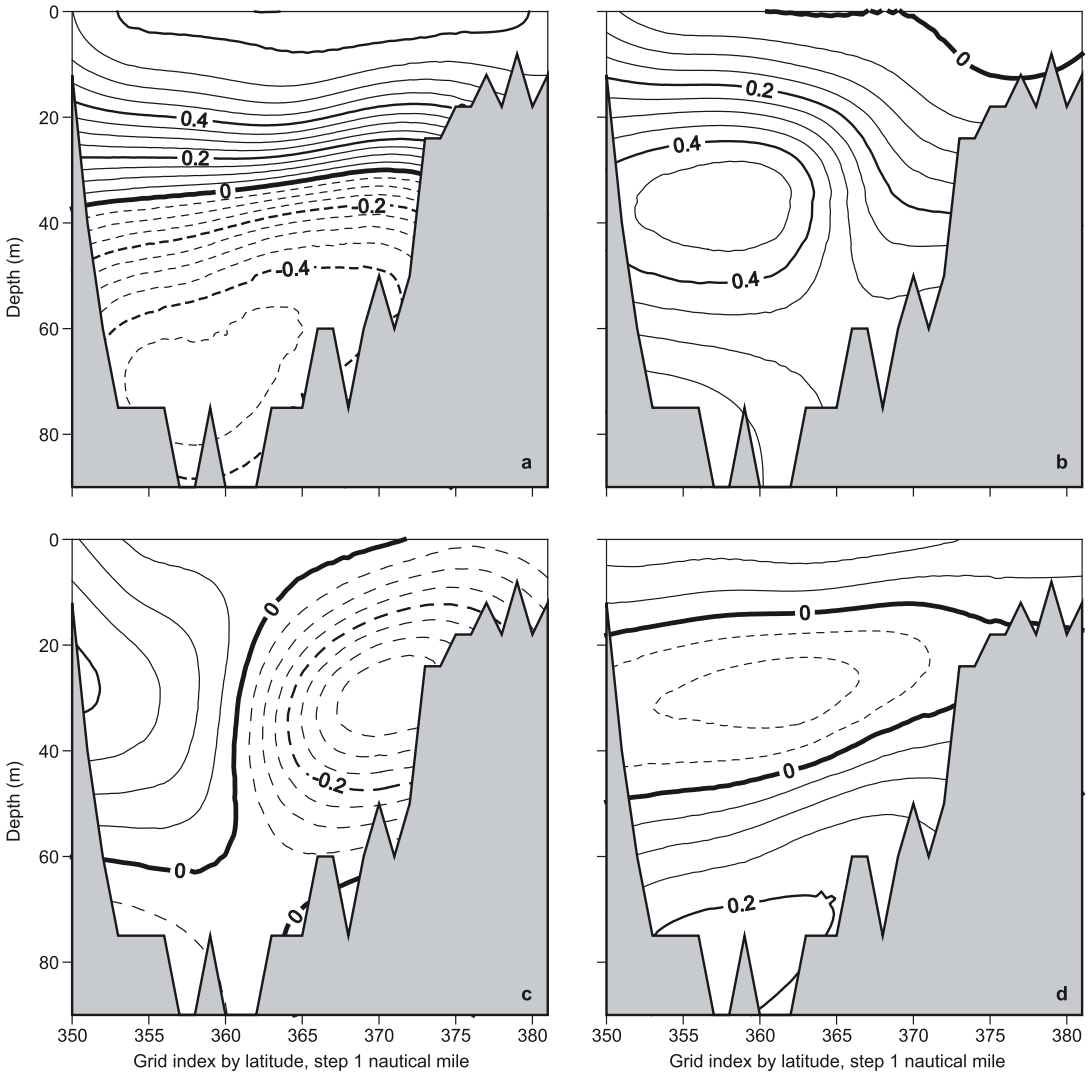

Fig. 7. Patterns of EOF modes of density in section B: (**a**) density mode 1 (55%), (**b**) density mode 2 (22%), (**c**) density mode 3 (10%), and (**d**) density mode 4 (4%). The mode patterns are dimensional (kg m^{-3}), scaled by the square root of the variance of each mode.

oscillations. By correlation analysis with the wind stress, highest surface layer outflow and deeper water inflow occur during north-easterly winds ($R^2 \approx 0.6$). Elken *et al*. (2003) obtained the same angle of wind stress projection, which provided the best correlation with the deep water outflow. We also made EOF detection of the joint east–west and north–south vector components. The joint 1st mode (32%) is "barotropic" for both of the current components. By the amplitudes, it is highly correlated ($R^2 > 0.9$) with the east–west component. The joint 2nd mode (15% of the variance) has similar geometry for the east–west component as the one-component mode (Fig. 6) and is well correlated with the latter ($R^2 \approx 0.8$). The north–south component of the joint mode has quite similar pattern geometry as the east-west component. It means that cross-channel flow components cause dynamical tilting of isopycnals.

The 3rd density EOF (15%–20%) is a thermocline "upwelling" mode that presents opposite density anomalies near the northern and southern coasts, concentrated in the mean (over

the seasons and years) pycnocline (≈ thermocline), located at depths of 35–40 m. The amplitudes of this mode did not show any correlations with wind stress projections. However, this density mode is acceptably ($R^2 \approx 0.4$) correlated with the 2nd "Ekman" mode of currents, which is furthermore correlated with the north-easterly wind stress projection. Unfortunately, analysis of the reasons for such a loss (or in some instances, gain) during correlation transfer is out of the scope of the present study.

The 3rd current EOF (6%–9%) presents a quite interesting structure of the "Bennett-Csanady" mode. In the long channels closed at least at one end, the steady flow is characterized by along-wind coastal jets and a compensation flow in the middle (deep part) of the channel with its maximum below the surface, since there is a competition between along-wind drift component and the return flow forced by the sea-level gradients established in a channel (Bennett 1974, Krauss and Brügge 1991). One might expect that this mode is amplified during the periods of persistent along-channel winds. We check this in the next sub-chapter.

Examples from EOF amplitude time series

Although the amplitudes of individual modes of the same data sets are uncorrelated over the whole period of determination, during specific events a joint excitement of different modes may occur.

One example of the amplitude time series behavior is given by a snapshot from July to September 2006 (Fig. 8), that covers the period of intense upwelling, observed near the southern coast of the Gulf from the end of July to the middle of August (Lips *et al*. 2009). Using the shipboard CTD measurements, the "normal" situation observed on 25 July was replaced on 8 August by upward displacement of the boundary of the upper mixed layer near the southern coast. The isotherm 10 °C was during the first survey everywhere at 10–20 m depths, but lifted by the second survey to the surface and shifted from the southern coast some 15–20 km offshore. The isohaline 6 psu, located during the first section at 10–30 m depths, also surfaced and shifted offshore by the same distance. Minimum surface salinities, that should be present in the water masses of the Finnish Coastal Current, were found on 8 August in the central part of the cross-gulf section. On 15–16 August and 22 August, further sections revealed relaxation of the upwelling process, i.e. warming of colder waters transported formerly to the surface from the deeper layers. The whole upwelling event was accompanied by the increase of salinity of deep layers.

The upwelling was created by the dominating easterly winds (Fig. 8a) that occurred from 29 July to 29 August. Sea level in Tallinn (both observed and modeled, Fig. 8b) was below the long-term average throughout the whole period. Standard deviations of model errors in respect to the sea level observations were 3.5 cm. Within this period, the model produced smaller amplitudes of the 25–28 h period seiches than observed. We can present the modeled sea levels in Tallinn (Fig. 8b) by the horizontal EOF modes, multiplying the sea level mode values in this location (Fig. 5) to the time series values of the amplitudes (Fig. 8d). The 1st flat mode gave maximum error 10 cm, but counting all the first 4 modes the maximum error reduced to 4 cm (Fig. 8c). Larger errors occurred on 15 August after sudden wind change from easterly to southerly and westerly directions. Such rapid wind changes occurred also later on 29 August and on 4 September. The amplitude of the 1st horizontal sea level mode (Fig. 8d) showed a negative value, corresponding to the lower than average sea level in the Gulf. The 2nd sea level mode (*see* the pattern in Fig. 5) was of positive amplitude (i.e. the sea level was lower in the eastern part of the Gulf than in the western part) and the 3rd mode was of negative amplitude (higher sea levels occurred near the northern coast due to the Ekman transport of easterly winds). Stronger easterly wind pulses took place from 29 July to 3 August and from 12 to 15 August. An interesting sea level feature is the amplification of the 4th horizontal "circulation" mode after 3 August. The amplitude value –3 (scaled to the standard deviation) corresponds to the cyclonic sea level doming with elevation about 3 cm in the central part of the Gulf.

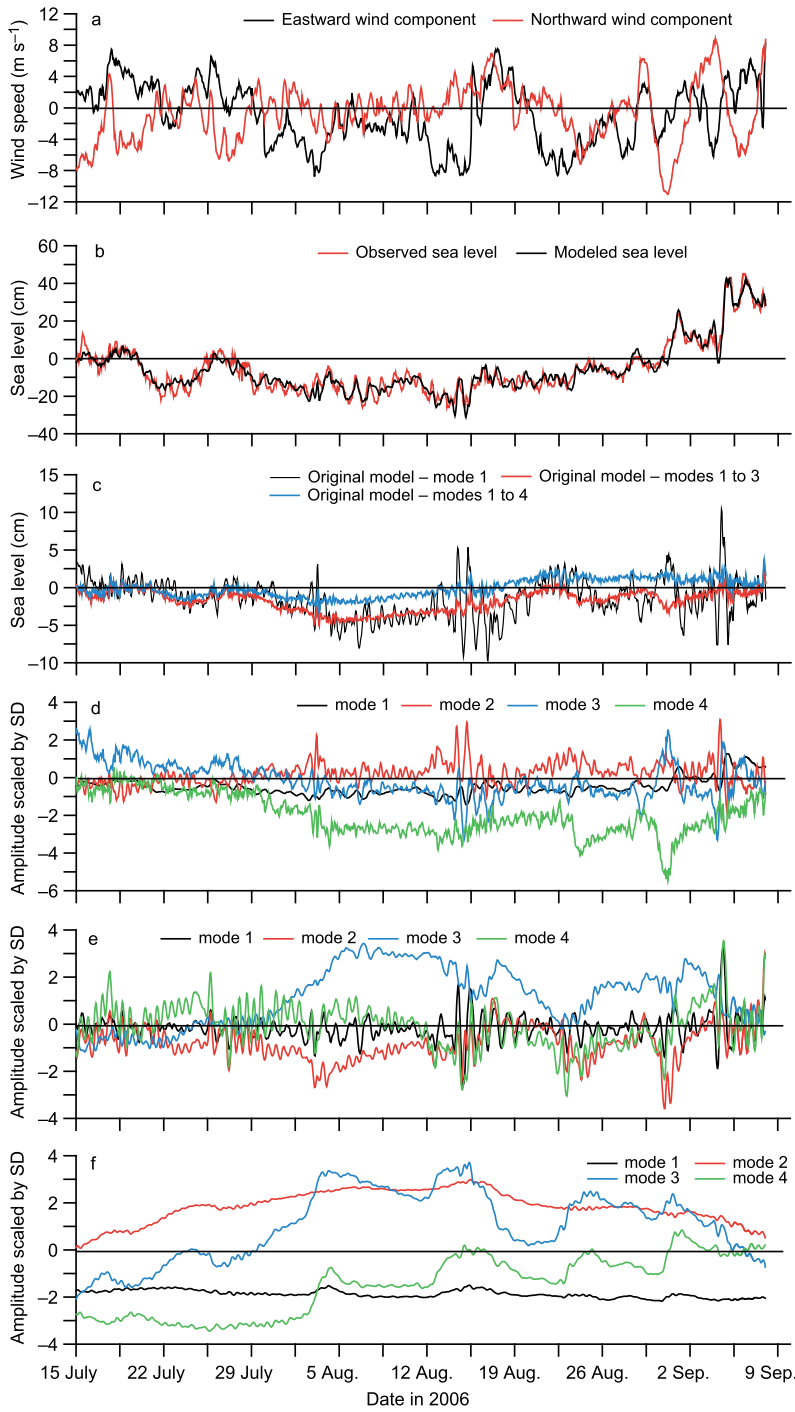

Fig. 8. Time series snapshot in July–September 2006: (**a**) wind components in the central gulf derived from the model forcing data; (**b**) observed and modeled sea level in Tallinn (*see* Fig. 1); (**c**) errors of sea level presentation in Tallinn by horizontal EOF modes (*see* Fig. 5) compared with the original modeled data, mode 1 and cumulatively the modes 1 to 3 and 1 to 4; (**d**) amplitudes of the first four EOF horizontal modes of sea level (*see* Fig. 5); (**e**) amplitudes of the first four EOF section modes of the east-west currents in section B (*see* Fig. 6); (**f**) amplitudes of the first four EOF section modes of density in section B (*see* Fig. 7). The EOF amplitudes (**d**–**f**) are non-dimensional, scaled by the condition that the standard deviation of each amplitude over the period of 2006–2008 is equal to 1.

The patterns of currents revealed 24 h to 30 h period oscillations of the amplitude (Fig. 8e) of the 1st barotropic mode around the value –0.28, that gives the mean westward speed up to 1.8 cm s^{-1}. The 2nd "Ekman" mode had an amplitude of –1.3 from 29 July to 15 August. This corresponds to the maximum of 12 cm s^{-1} westward flow in the surface layer (as can be

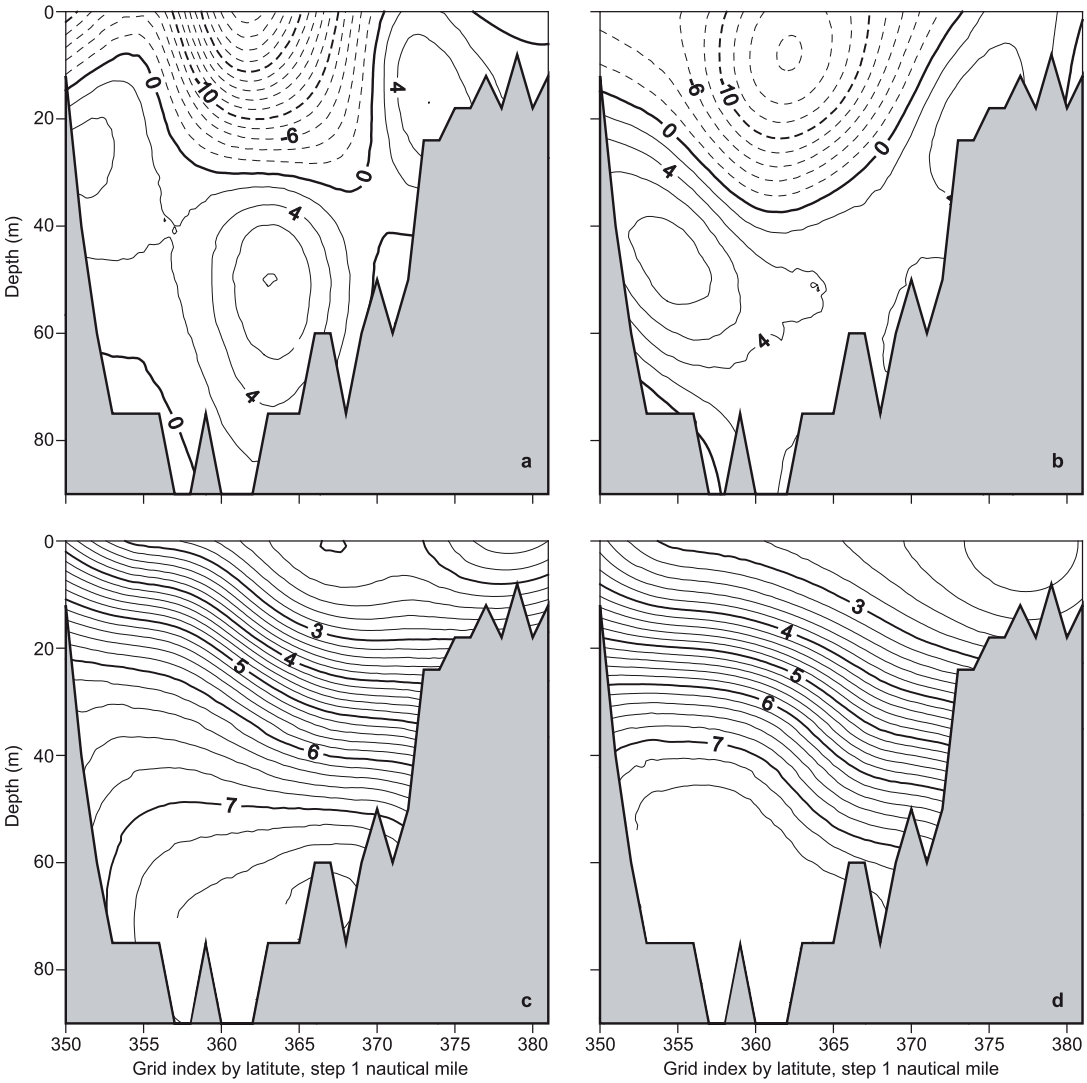

Fig. 9. Mean east–west currents (**a**, **b**) and density (**c**, **d**) in section B of period 9–12 August 2006, calculated from the model data (**a**, **c**) and as a sum of the four first EOF modes with the mean amplitudes over the period.

expected from the wind direction) and up to 8 cm s^{-1} eastward flow in deeper layers. The highest amplitude value — up to 3.4 standard deviations — had the 3rd ("Bennett-Csanady") section mode of currents (*see* the pattern in Fig. 6), that was persistent throughout the whole upwelling period. However, since the mode amplitude was positive, its presence has no direct physical explanation because the flow component due to this mode was against the wind direction in the more shallow coastal zones. By looking at the mean flow during the shorter period from 9 to 12 July (Fig. 9a, the mean wind was 3.9 m s^{-1} from 92°), the Finnish Coastal Current had shifted to the central axis of the Gulf. This feature is quite well reproduced by the superposition of the four first EOF modes, plus the mean flow over the longer period (Fig. 9b). Therefore the high amplitude of the 3rd mode was just a mathematical result of the EOF analysis to shift the Finnish Coastal Current southwards.

Amplitudes of density modes (Fig. 8f) revealed ordinary stronger summer stratification (negative amplitudes of the 1st mode, *see*

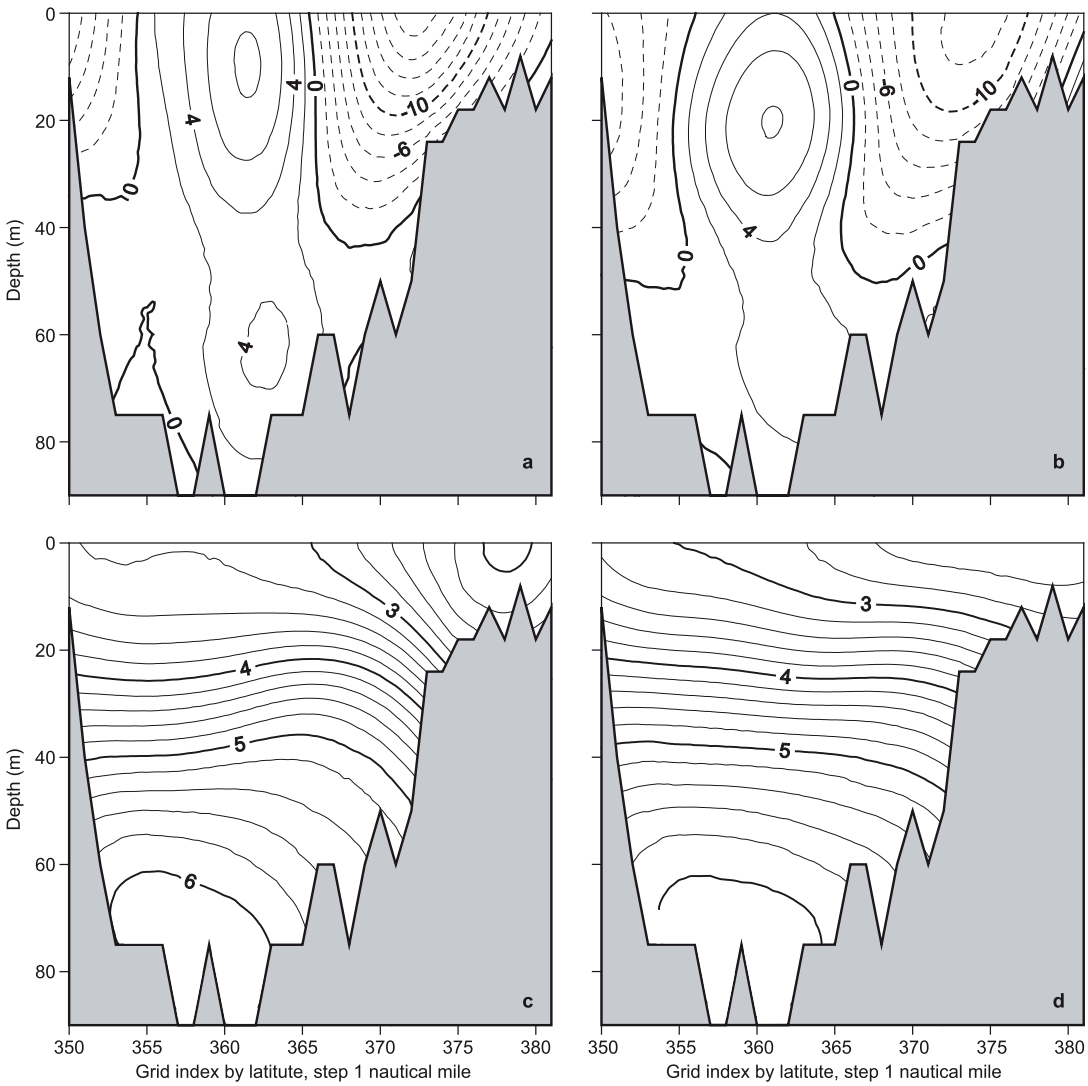

Fig. 10. Same as Fig. 9, but for the period 9–12 August 2007.

the pattern in Fig. 7), higher than usual mean density over the whole water column (positive amplitudes of the 2nd mode), and increase of density in the thermocline of the southern coast and its reduction near the northern coast (positive amplitudes of the 3rd mode from 29 July to 15 August). The amplitude time series of the 3rd "upwelling" density mode reflects the behavior of the 2nd "Ekman" mode of currents. Let us remind, that during the longer period the correlation of these modes was $R^2 = 0.4$. The modeled short-period mean density (Fig. 9d) with sloping isopycnals is close to the observed stratification during the upwelling (Lips *et al*. 2009). Again, as for the currents, the main characteristics of the density distribution are reproduced by the superposition of the four first EOF modes (Fig. 9d).

To compare the upwelling event in August 2006 with other periods of persistent winds, we present the mean currents and density in section B for the same dates as in 2006, but in 2007 (i.e. from 9 to 12 August 2007, Fig. 10). The mean wind in the central gulf was also 3.9 m s^{-1} but from 121°, still with easterly component as for 2006. The shorter period mean current (Fig. 10a) reveals the Finnish Coastal Current near

its long-term location on the northern slope of the Gulf. The mean amplitudes of the 1st and 2nd current modes were about 3 times smaller than in 2006. Among the EOF amplitudes during the period, the highest share — 1.9 times the standard deviation — had the amplitude of the 3rd "Bennett-Csanady" mode, whose sign was consistent with the channel flow theory. The resulting flow field, both in original model data and in superposition of the first four EOF modes (Fig. 10b), shows upwind compensation flow in the deeper part of the section. Mean flow is geostrophically consistent with the tilting of modeled isopycnals (Fig. 10c). Although the mean slopes are reproduced by the EOF modes well (Fig. 10d), the counter-flow in the deeper area is not in agreement with the monotonic tilting of EOF-derived isopycnals. The stratification in 2007 was considerably weaker than in 2006. Despite the similar short-term wind forcing during both years, the distributions of currents and density were quite different due to the different history of forcing.

Conclusions

Variance of the studied circulation and forcing fields, explained by the four first EOF modes, is high for the wind (96%) and sea level (99%). Horizontal modes of currents explain 71% of the variance on the surface and 67% in the halocline. On the meridional (about cross-gulf) sections of the western and central parts of the Gulf, three first density modes cover 86%–89% of the variance. Since the 1st density mode includes regular seasonal variations of the stratification, the explained "circulation" variability part of the leading density modes is lower than the above numbers. Indeed, the four first modes of east-west currents explained only 65%–73% of the variance. This moderate explanation rate (about 2/3) is not surprising, since the Gulf of Finland has intensive mesoscale and small-scale processes like eddies, frontal meanders, filaments, inertial waves etc., which cannot be presented by the basin scale coherent patterns.

Time series of EOF mode amplitudes contain interesting information. In several cases they allow quantitative estimation of qualitatively known cause-effect relationships within the complex ocean dynamics. Furthermore, the amplitude time series reflect well the main events in the basin scale circulation. Since EOF method is based on the products from the correlation matrix, we expect that extensions of EOF analysis, both by regions and studied variables, may contribute to the better assimilation schemes implemented in the operational models.

By the analysis of non-steady circulation patterns of the Gulf of Finland, we can distinguish two regions with a specific regime of variability.

Firstly, a western (near-mouth) wide channel that connects the entrance area to the central part of the Gulf. The topography is characterized by quasi-uniform width and cross-section area. Time-dependent wind forcing (the wind fields are quite homogeneous over the whole gulf, the flat modes cover 93% of the variance) creates similar along-channel current patterns on the cross-sections of the channel, as shown by the EOF modes. Time-dependent EOF amplitudes of the dominant modes correlate well between the sections.

Secondly, the eastern (near-head) wide basin that extends from the central part to the narrow estuary head. The flow dynamics here is more complex due to the topographical features and the vicinity of large freshwater source. We were not able to discover simple meridional patterns of circulation variability in this region, except for the patterns that are quasi-uniform over the whole gulf.

In the western, wide channel region, the dominating current variation (23%–42%) is barotropic (unidirectional flow over the whole section) oscillation (spectral peak at 24 h), that is related to the water storage variation of the Gulf. Two-layer flow (surface Ekman transport with deeper compensation flow, 19%–22%) has both the inertial and lower frequencies. In respect to the wind forcing, highest outflow of surface waters occurs during north-easterly winds. Third by energy (6%–9%) current pattern presents a quite interesting structure of the "Bennett-Csanady" mode: coastal jets and a compensation flow in the middle (deep part) of the channel, with a maximum below the surface. This mode in actual conditions usually appears in combination with other modes.

On the sea surface, quasi-uniform drift currents are deflected on the average by 40° to the right from the wind direction and they cover 60% of the circulation variance. Sea level variability is heavily (98%) dominated by almost uniform changes due to the water storage variations of the Gulf. Dominating sea level gradients are described by the main axis (23%) and the transverse (17%) components, forced by the winds of the same direction. Namely, the sea level rises in the eastern part of the Gulf during westerly winds and near the northern coast during southerly winds. The flows below the surface are also decomposed into the main axis (24%–40%) and the transverse (13%–16%) components, which are correlated with the sea level gradients according to the geostrophic relations.

Acknowledgements: The model data were kindly provided by the Swedish Meteorological and Hydrological Institute under the cooperation within BOOS (Baltic Operational Oceanographic System) and HIROMB (High Resolution Operational Model of the Baltic Sea). Friendly contribution by Lars Axell is highly appreciated. The analysis part of the study was supported by the grant no. 7328 of the Estonian Science Foundation.

References

Alenius P., Myrberg K. & Nekrasov A. 1998. The physical oceanography of the Gulf of Finland: a review. *Boreal Env. Res*. 3: 97–125.

Andrejev O., Myrberg K., Alenius P. & Lundberg P.A. 2004. Mean circulation and water exchange in the Gulf of Finland — a study based on three-dimensional modelling. *Boreal Env. Res*. 9: 1–16.

Axell L. 2006. *Weaker surface currents in HIROMB 3.1*. 9th HIROMB Scientific Workshop 28–31 August 2006, SMHI, Gothenburg, available at http://www.environment.fi/download.asp?contentid=56290&lan=en.

Bennett J.R. 1974. On the dynamics of wind-driven lake currents. *J. Phys. Oceanogr.* 4: 400–414.

Bergström S. & Carlsson B. 1994. River runoff to the Baltic Sea. *Ambio* 23: 280–287.

Chant R.J., Geyer W.R., Houghton R., Hunter E. & Lerczak J. 2007. Estuarine boundary layer mixing processes: insights from dye experiments. *J. Phys. Oceanogr.* 37: 1859–1877.

Elken J., Raudsepp U. & Lips U. 2003. On the estuarine transport reversal in deep layers of the Gulf of Finland. *J. Sea Res*. 49: 267–274.

Elken J., Kõuts T., Lagemaa P., Lips U., Raudsepp U. & Väli G. 2008. Sub-regional observing and forecast system for the NE Baltic: needs and first results. In: *US/EU Baltic Symposium "Ocean Observations, Ecosystem-Based Management & Forecasting", Tallinn, 27–29 May, 2008*, IEEE Conference Proceedings, doi:10.1109/BALTIC.2008.4625551.

Funkquist L. 2001. HIROMB, an operational eddy-resolving model for the Baltic Sea. *Bulletin of the Maritime Institute in Gdansk* 28: 7–16.

Gästgifvars M., Lauri H., Sarkanen A., Myrberg K., Andrejev O. & Ambjörn C. 2006. Modelling surface drifting of buoys during a rapidly-moving weather front in the Gulf of Finland, Baltic Sea. *Estuarine, Coastal and Shelf Science* 70: 567–576.

Gästgifvars M., Müller-Navarra S., Funkquist L. & Huess V. 2008. Performance of operational systems with respect to water level forecasts in the Gulf of Finland. *Ocean Dynamics* 58: 139–153

Gill A. 1982. *Atmosphere–ocean dynamics*. Academic Press.

Haapala J. & Alenius P. 1994. Temperature and salinity statistics for the Northern Baltic Sea 1961–1990. *Finnish Mar. Res*. 262: 51–121.

Johansson M., Boman H., Kahma K.K. & Launiainen J. 2001. Trends in sea level variability in the Baltic Sea. *Boreal Env. Res*. 6: 159–179.

Jönsson B., Döös K., Nycander J. & Lundberg P. 2008. Standing waves in the Gulf of Finland and their relationship to the basin-wide Baltic seiches. *J. Geophys. Res*. 113: C03004, doi:10.1029/2006JC003862

Krauss W. & Brügge B. 1991. Wind-produced water exchange between the deep basins of the Baltic Sea. *J. Phys. Oceanogr.* 21: 373–384.

Lass H.U. & Talpsepp L. 1993. Observations of coastal jets in the Southern Baltic. *Cont. Shelf Res*. 13: 2–3: 189–203.

Lehmann A. & Hinrichsen H.H. 2001. The importance of water storage variations for water balance studies of the Baltic Sea. *Phys. Chem. Earth B* 26: 383–389.

Lehmann A., Krauss W. & Hinrichsen H.H. 2002. Effects of remote and local atmospheric forcing on circulation and upwelling in the Baltic Sea. *Tellus* 54A: 299–316.

Lehmann A. & Myrberg K. 2008. Upwelling in the Baltic Sea — a review. *J. Mar. Systems* 74: S3–S12

Lips U., Lips I., Liblik T. & Elken J. 2008a. Estuarine transport *versus* vertical movement and mixing of water masses in the Gulf of Finland (Baltic Sea). In: *US/EU Baltic Symposium "Ocean Observations, Ecosystem-Based Management & Forecasting", Tallinn, 27–29 May, 2008*, IEEE Conference Proceedings, doi:10.1109/BALTIC.2008.4625535.

Lips U., Lips I., Kikas V. & Kuvaldina N. 2008b. Ferrybox measurements: a tool to study meso-scale processes in the Gulf of Finland (Baltic Sea). In: *US/EU Baltic Symposium "Ocean Observations, Ecosystem-Based Management & Forecasting", Tallinn, 27–29 May, 2008*, IEEE Conference Proceedings, doi:10.1109/BALTIC.2008.4625536.

Lips I., Lips U. & Liblik T. 2009. Consequences of coastal upwelling events on physical and chemical patterns in the central Gulf of Finland (Baltic Sea). *Cont. Shelf Res*. 29: 1836–1847.

Matthäus W. & Schinke H. 1999. The influence of river runoff on deep water conditions of the Baltic Sea. *Hyd-*

robiologia 393: 1–10.

Meier H.E.M. 2005. Modeling the age of Baltic Sea water masses: quantification and steady state sensitivity experiments. *J. Geophys. Res.* 110: C02006 doi: 101029/2004JC002607

Myrberg K., Ryabchenko V., Isaev A., Vankevich R., Andrejev O., Bendtsen J., Erichsen A., Funkquist L., Inkala A., Neelov I., Rasmus K., Rodriguez Medina M., Raudsepp U., Passenko J., Söderkvist J., Sokolov A., Kuosa H., Anderson T.R., Lehmann A. & Skogen M. D. 2010: Validation of three-dimensional hydrodynamic models of the Gulf of Finland. *Boreal Env. Res.* 15: 453–479.

Nerheim S. 2004. Shear-generating motions at various length scales and frequencies in the Baltic Sea — an attempt to narrow down the problem of horizontal dispersion. *Oceanologia* 46: 477–503.

Palmén E. 1930. Untersuchungen über die Strömungen in den Finnland umgebenden Meeren. *Soc. Sci. Fenn., Comm. Phys.-Math.* 12: 1–94.

Pizarro O. & Shaffer G. 1998. Wind-driven, coastal-trapped waves off the Island of Gotland, Baltic Sea. *J. Phys. Oceanogr.* 28: 2117–2129.

Reissmann J.H., Burchard H., Feistel R., Hagen E., Lass H.U., Mohrholtz V., Nausch G., Umlauf L. & Wieczorek G. 2009. Vertical mixing in the Baltic Sea and consequences for eutrophication — a review. *Progr. Oceanogr.* 82: 47–80.

Schrum C., St. John M. & Alekseeva I. 2006. ECOSMO, a coupled ecosystem model of the North Sea and Baltic Sea: Part II. Spatial-seasonal characteristics in the North Sea as revealed by EOF analysis. *J. Mar. Syst.* 61: 100–113.

Stipa T. 2004. Baroclinic adjustment in the Finnish coastal current. *Tellus* 56A: 79–87.

Thomson R.E., Mihály S.F. & Kulikov E.A. 2007. Estuarine *versus* transient flow regimes in Juan de Fuca Strait. *J. Geophys. Res.* 112: C09022, doi: 10.1029/2006JC003925.

Umlauf L., Burchard H. & Hutter K. 2003. Extending the κ-ω turbulence model towards oceanic applications. *Ocean Modelling* 5: 195–218.

von Storch H. & Zwiers F.W. 1999. *Statistical analysis in climate research*. Cambridge University Press, Cambridge.

Watterson I.G. 2001. Decomposition of global ocean currents using a simple iterative method. *J. Atmos. Oceanic Technol.* 18: 691–703.

Witting R. 1912. *Zusammenfassende Übersicht der Hydrographie des Bottnischen und Finnischen Meerbusens und der nördlichen Ostsee nach den Untersuchungen bis Ende 1910*. Finnländische hydrographisch-biologische Untersuchungen 7.

DISSERTATIONS DEFENDED AT TALLINN UNIVERSITY OF TECHNOLOGY ON *NATURAL AND EXACT SCIENCES*

1. **Olav Kongas**. Nonlinear Dynamics in Modeling Cardiac Arrhytmias. 1998.

2. **Kalju Vanatalu**. Optimization of Processes of Microbial Biosynthesis of Isotopically Labeled Biomolecules and Their Complexes. 1999.

3. **Ahto Buldas**. An Algebraic Approach to the Structure of Graphs. 1999.

4. **Monika Drews**. A Metabolic Study of Insect Cells in Batch and Continuous Culture: Application of Chemostat and Turbidostat to the Production of Recombinant Proteins. 1999.

5. **Eola Valdre**. Endothelial-Specific Regulation of Vessel Formation: Role of Receptor Tyrosine Kinases. 2000.

6. **Kalju Lott**. Doping and Defect Thermodynamic Equilibrium in ZnS. 2000.

7. **Reet Koljak**. Novel Fatty Acid Dioxygenases from the Corals *Plexaura homomalla* and *Gersemia fruticosa.* 2001.

8. **Anne Paju**. Asymmetric oxidation of Prochiral and Racemic Ketones by Using Sharpless Catalyst. 2001.

9. **Marko Vendelin**. Cardiac Mechanoenergetics *in silico*. 2001.

10. **Pearu Peterson**. Multi-Soliton Interactions and the Inverse Problem of Wave Crest. 2001.

11. **Anne Menert**. Microcalorimetry of Anaerobic Digestion. 2001.

12. **Toomas Tiivel**. The Role of the Mitochondrial Outer Membrane in *in vivo* Regulation of Respiration in Normal Heart and Skeletal Muscle Cell. 2002.

13. **Olle Hints**. Ordovician Scolecodonts of Estonia and Neighbouring Areas: Taxonomy, Distribution, Palaeoecology, and Application. 2002.

14. **Jaak Nõlvak**. Chitinozoan Biostratigrapy in the Ordovician of Baltoscandia. 2002.

15. **Liivi Kluge**. On Algebraic Structure of Pre-Operad. 2002.

16. **Jaanus Lass**. Biosignal Interpretation: Study of Cardiac Arrhytmias and Electromagnetic Field Effects on Human Nervous System. 2002.

17. **Janek Peterson**. Synthesis, Structural Characterization and Modification of PAMAM Dendrimers. 2002.

18. **Merike Vaher**. Room Temperature Ionic Liquids as Background Electrolyte Additives in Capillary Electrophoresis. 2002.

19. **Valdek Mikli**. Electron Microscopy and Image Analysis Study of Powdered Hardmetal Materials and Optoelectronic Thin Films. 2003.

20. **Mart Viljus**. The Microstructure and Properties of Fine-Grained Cermets. 2003.

21. **Signe Kask**. Identification and Characterization of Dairy-Related *Lactobacillus.* 2003

22. **Tiiu-Mai Laht**. Influence of Microstructure of the Curd on Enzymatic and Microbiological Processes in Swiss-Type Cheese. 2003.

23. **Anne Kuusksalu**. 2–5A Synthetase in the Marine Sponge *Geodia cydonium*. 2003.

24. **Sergei Bereznev**. Solar Cells Based on Polycristalline Copper-Indium Chalcogenides and Conductive Polymers. 2003.

25. **Kadri Kriis**. Asymmetric Synthesis of C_2-Symmetric Bimorpholines and Their Application as Chiral Ligands in the Transfer Hydrogenation of Aromatic Ketones. 2004.

26. **Jekaterina Reut**. Polypyrrole Coatings on Conducting and Insulating Substracts. 2004.

27. **Sven Nõmm**. Realization and Identification of Discrete-Time Nonlinear Systems. 2004.

28. **Olga Kijatkina**. Deposition of Copper Indium Disulphide Films by Chemical Spray Pyrolysis. 2004.

29. **Gert Tamberg**. On Sampling Operators Defined by Rogosinski, Hann and Blackman Windows. 2004.

30. **Monika Übner**. Interaction of Humic Substances with Metal Cations. 2004.

31. **Kaarel Adamberg**. Growth Characteristics of Non-Starter Lactic Acid Bacteria from Cheese. 2004.

32. **Imre Vallikivi**. Lipase-Catalysed Reactions of Prostaglandins. 2004.

33. **Merike Peld**. Substituted Apatites as Sorbents for Heavy Metals. 2005.

34. **Vitali Syritski**. Study of Synthesis and Redox Switching of Polypyrrole and Poly(3,4-ethylenedioxythiophene) by Using *in-situ* Techniques. 2004.

35. **Lee Põllumaa**. Evaluation of Ecotoxicological Effects Related to Oil Shale Industry. 2004.

36. **Riina Aav**. Synthesis of 9,11-Secosterols Intermediates. 2005.

37. **Andres Braunbrück**. Wave Interaction in Weakly Inhomogeneous Materials. 2005.

38. **Robert Kitt**. Generalised Scale-Invariance in Financial Time Series. 2005.

39. **Juss Pavelson**. Mesoscale Physical Processes and the Related Impact on the Summer Nutrient Fields and Phytoplankton Blooms in the Western Gulf of Finland. 2005.

40. **Olari Ilison**. Solitons and Solitary Waves in Media with Higher Order Dispersive and Nonlinear Effects. 2005.

41. **Maksim Säkki**. Intermittency and Long-Range Structurization of Heart Rate. 2005.

42. **Enli Kiipli**. Modelling Seawater Chemistry of the East Baltic Basin in the Late Ordovician–Early Silurian. 2005.

43. **Igor Golovtsov**. Modification of Conductive Properties and Processability of Polyparaphenylene, Polypyrrole and polyaniline. 2005.

44. **Katrin Laos**. Interaction Between Furcellaran and the Globular Proteins (Bovine Serum Albumin β-Lactoglobulin). 2005.

45. **Arvo Mere**. Structural and Electrical Properties of Spray Deposited Copper Indium Disulphide Films for Solar Cells. 2006.

46. **Sille Ehala**. Development and Application of Various On- and Off-Line Analytical Methods for the Analysis of Bioactive Compounds. 2006.

47. **Maria Kulp**. Capillary Electrophoretic Monitoring of Biochemical Reaction Kinetics. 2006.

48. **Anu Aaspõllu.** Proteinases from *Vipera lebetina* Snake Venom Affecting Hemostasis. 2006.

49. **Lyudmila Chekulayeva**. Photosensitized Inactivation of Tumor Cells by Porphyrins and Chlorins. 2006.

50. **Merle Uudsemaa**. Quantum-Chemical Modeling of Solvated First Row Transition Metal Ions. 2006.

51. **Tagli Pitsi**. Nutrition Situation of Pre-School Children in Estonia from 1995 to 2004. 2006.

52. **Angela Ivask**. Luminescent Recombinant Sensor Bacteria for the Analysis of Bioavailable Heavy Metals. 2006.

53. **Tiina Lõugas**. Study on Physico-Chemical Properties and Some Bioactive Compounds of Sea Buckthorn (*Hippophae rhamnoides* L.). 2006.

54. **Kaja Kasemets**. Effect of Changing Environmental Conditions on the Fermentative Growth of *Saccharomyces cerevisae* S288C: Auxo-accelerostat Study. 2006.

55. **Ildar Nisamedtinov**. Application of ^{13}C and Fluorescence Labeling in Metabolic Studies of *Saccharomyces* spp. 2006.

56. **Alar Leibak**. On Additive Generalisation of Voronoï's Theory of Perfect Forms over Algebraic Number Fields. 2006.

57. **Andri Jagomägi**. Photoluminescence of Chalcopyrite Tellurides. 2006.

58. **Tõnu Martma**. Application of Carbon Isotopes to the Study of the Ordovician and Silurian of the Baltic. 2006.

59. **Marit Kauk**. Chemical Composition of $CuInSe_2$ Monograin Powders for Solar Cell Application. 2006.

60. **Julia Kois**. Electrochemical Deposition of $CuInSe_2$ Thin Films for Photovoltaic Applications. 2006.

61. **Ilona Oja Açik**. Sol-Gel Deposition of Titanium Dioxide Films. 2007.

62. **Tiia Anmann**. Integrated and Organized Cellular Bioenergetic Systems in Heart and Brain. 2007.

63. **Katrin Trummal**. Purification, Characterization and Specificity Studies of Metalloproteinases from *Vipera lebetina* Snake Venom. 2007.

64. **Gennadi Lessin**. Biochemical Definition of Coastal Zone Using Numerical Modeling and Measurement Data. 2007.

65. **Enno Pais**. Inverse problems to determine non-homogeneous degenerate memory kernels in heat flow. 2007.

66. **Maria Borissova**. Capillary Electrophoresis on Alkylimidazolium Salts. 2007.

67. **Karin Valmsen**. Prostaglandin Synthesis in the Coral *Plexaura homomalla*: Control of Prostaglandin Stereochemistry at Carbon 15 by Cyclooxygenases. 2007.

68. **Kristjan Piirimäe**. Long-Term Changes of Nutrient Fluxes in the Drainage Basin of the Gulf of Finland – Application of the PolFlow Model. 2007.

69. **Tatjana Dedova**. Chemical Spray Pyrolysis Deposition of Zinc Sulfide Thin Films and Zinc Oxide Nanostructured Layers. 2007.

70. **Katrin Tomson**. Production of Labelled Recombinant Proteins in Fed-Batch Systems in *Escherichia coli*. 2007.

71. **Cecilia Sarmiento**. Suppressors of RNA Silencing in Plants. 2008.

72. **Vilja Mardla**. Inhibition of Platelet Aggregation with Combination of Antiplatelet Agents. 2008.

73. **Maie Bachmann**. Effect of Modulated Microwave Radiation on Human Resting Electroencephalographic Signal. 2008.

74. **Dan Hüvonen**. Terahertz Spectroscopy of Low-Dimensional Spin Systems. 2008.

75. **Ly Villo**. Stereoselective Chemoenzymatic Synthesis of Deoxy Sugar Esters Involving *Candida antarctica* Lipase B. 2008.

76. **Johan Anton**. Technology of Integrated Photoelasticity for Residual Stress Measurement in Glass Articles of Axisymmetric Shape. 2008.

77. **Olga Volobujeva**. SEM Study of Selenization of Different Thin Metallic Films. 2008.

78. **Artur Jõgi**. Synthesis of 4'-Substituted 2,3'-dideoxynucleoside Analogues. 2008.

79. **Mario Kadastik**. Doubly Charged Higgs Boson Decays and Implications on Neutrino Physics. 2008.

80. **Fernando Pérez-Caballero**. Carbon Aerogels from 5-Methylresorcinol-Formaldehyde Gels. 2008.

81. **Sirje Vaask**. The Comparability, Reproducibility and Validity of Estonian Food Consumption Surveys. 2008.

82. **Anna Menaker**. Electrosynthesized Conducting Polymers, Polypyrrole and Poly(3,4-ethylenedioxythiophene), for Molecular Imprinting. 2009.

83. **Lauri Ilison**. Solitons and Solitary Waves in Hierarchical Korteweg-de Vries Type Systems. 2009.

84. **Kaia Ernits**. Study of In_2S_3 and ZnS Thin Films Deposited by Ultrasonic Spray Pyrolysis and Chemical Deposition. 2009.

85. **Veljo Sinivee**. Portable Spectrometer for Ionizing Radiation "Gammamapper". 2009.

86. **Jüri Virkepu**. On Lagrange Formalism for Lie Theory and Operadic Harmonic Oscillator in Low Dimensions. 2009.

87. **Marko Piirsoo**. Deciphering Molecular Basis of Schwann Cell Development. 2009.

88. **Kati Helmja**. Determination of Phenolic Compounds and Their Antioxidative Capability in Plant Extracts. 2010.

89. **Merike Sõmera**. Sobemoviruses: Genomic Organization, Potential for Recombination and Necessity of P1 in Systemic Infection. 2010.

90. **Kristjan Laes**. Preparation and Impedance Spectroscopy of Hybrid Structures Based on $CuIn_3Se_5$ Photoabsorber. 2010.

91. **Kristin Lippur**. Asymmetric Synthesis of 2,2'-Bimorpholine and its 5,5'-Substituted Derivatives. 2010.

92. **Merike Luman**. Dialysis Dose and Nutrition Assessment by an Optical Method. 2010.

93. **Mihhail Berezovski**. Numerical Simulation of Wave Propagation in Heterogeneous and Microstructured Materials. 2010.

94. **Tamara Aid-Pavlidis**. Structure and Regulation of BDNF Gene. 2010.

95. **Olga Bragina**. The Role of Sonic Hedgehog Pathway in Neuro- and Tumorigenesis. 2010.

96. **Merle Randrüüt**. Wave Propagation in Microstructured Solids: Solitary and Periodic Waves. 2010.

97. **Marju Laars**. Asymmetric Organocatalytic Michael and Aldol Reactions Mediated by Cyclic Amines. 2010.

98. **Maarja Grossberg**. Optical Properties of Multinary Semiconductor Compounds for Photovoltaic Applications. 2010.

99. **Alla Maloverjan**. Vertebrate Homologues of Drosophila Fused Kinase and Their Role in Sonic Hedgehog Signalling Pathway. 2010.

100. **Priit Pruunsild**. Neuronal Activity-Dependent Transcription Factors and Regulation of Human *BDNF* Gene. 2010.

101. **Tatjana Knjazeva**. New Approaches in Capillary Electrophoresis for Separation and Study of Proteins. 2011.

102. **Atanas Katerski**. Chemical Composition of Sprayed Copper Indium Disulfide Films for Nanostructured Solar Cells. 2011.

103. **Kristi Timmo**. Formation of Properties of $CuInSe_2$ and $Cu_2ZnSn(S,Se)_4$ Monograin Powders Synthesized in Molten KI. 2011.

104. **Kert Tamm**. Wave Propagation and Interaction in Mindlin-Type Microstructured Solids: Numerical Simulation. 2011.

105. **Adrian Popp**. Ordovician Proetid Trilobites in Baltoscandia and Germany. 2011.

106. **Ove Pärn**. Sea Ice Deformation Events in the Gulf of Finland and This Impact on Shipping. 2011.

107. **Germo Väli**. Numerical Experiments on Matter Transport in the Baltic Sea. 2011.

108. **Andrus Seiman**. Point-of-Care Analyser Based on Capillary Electrophoresis. 2011.

109. **Olga Katargina**. Tick-Borne Pathogens Circulating in Estonia (Tick-Borne Encephalitis Virus, *Anaplasma phagocytophilum*, *Babesia* Species): Their Prevalence and Genetic Characterization. 2011.

110. **Ingrid Sumeri**. The Study of Probiotic Bacteria in Human Gastrointestinal Tract Simulator. 2011.

111. **Kairit Zovo**. Functional Characterization of Cellular Copper Proteome. 2011.

112. **Natalja Makarytsheva**. Analysis of Organic Species in Sediments and Soil by High Performance Separation Methods. 2011.

113. **Monika Mortimer**. Evaluation of the Biological Effects of Engineered Nanoparticles on Unicellular Pro- and Eukaryotic Organisms. 2011.

114. **Kersti Tepp**. Molecular System Bioenergetics of Cardiac Cells: Quantitative Analysis of Structure-Function Relationship. 2011.

115. **Anna-Liisa Peikolainen**. Organic Aerogels Based on 5-Methylresorcinol. 2011.

116. **Leeli Amon**. Palaeoecological Reconstruction of Late-Glacial Vegetation Dynamics in Eastern Baltic Area: A View Based on Plant Macrofossil Analysis. 2011.

117. **Tanel Peets**. Dispersion Analysis of Wave Motion in Microstructured Solids. 2011.

118. **Liina Kaupmees**. Selenization of Molybdenum as Contact Material in Solar Cells. 2011.

119. **Allan Olspert**. Properties of VPg and Coat Protein of Sobemoviruses. 2011.

120. **Kadri Koppel**. Food Category Appraisal Using Sensory Methods. 2011.

121. **Jelena Gorbatšova**. Development of Methods for CE Analysis of Plant Phenolics and Vitamins. 2011.

122. **Karin Viipsi**. Impact of EDTA and Humic Substances on the Removal of Cd and Zn from Aqueous Solutions by Apatite. 2012.

123. **David Schryer**. Metabolic Flux Analysis of Compartmentalized Systems Using Dynamic Isotopologue Modeling. 2012.

124. **Ardo Illaste**. Analysis of Molecular Movements in Cardiac Myocytes. 2012.

125. **Indrek Reile**. 3-Alkylcyclopentane-1,2-Diones in Asymmetric Oxidation and Alkylation Reactions. 2012.

126. **Tatjana Tamberg**. Some Classes of Finite 2-Groups and Their Endomorphism Semigroups. 2012.

127. **Taavi Liblik**. Variability of Thermohaline Structure in the Gulf of Finland in Summer. 2012.